



**NTNU – Trondheim**  
Norwegian University of  
Science and Technology

# Modelling and Robust Control of Production Force of a Wave Energy Converter

**Mathias Huuse Marley**

Marine Technology

Submission date: June 2014

Supervisor: Roger Skjetne, IMT

Co-supervisor: Jonas Sjolte, Fred. Olsen. Ltd.

Norwegian University of Science and Technology  
Department of Marine Technology



# MASTER THESIS DESCRIPTION SHEET

<b>Name of the candidate:</b>	Mathias Marley
<b>Field of study:</b>	Marine control engineering
<b>Thesis title (Norwegian):</b>	Modellering og robust regulering av produksjonskraft fra bølgekraftverk.
<b>Thesis title (English):</b>	Modelling and robust control of production force of a wave energy converter.

## Background

Fred. Olsen's wave energy converter (WEC) Lifesaver is currently located off the coast of England and producing electricity. The converter works by the point-absorber principle, producing power by heave and pitch motion. It has three independent power-take-off (PTO) units installed, each unit consisting of an electrical generator, a winch, and a mooring line. Failure of the primary mooring lines has been the main operational issue of Lifesaver since it was deployed in April 2012. The aim of this thesis is to develop a control strategy for mitigating maximum power take-off versus line-break safety constraints.

Large force oscillations have been recorded in the mooring line during production. The source of these oscillations is unknown. A better understanding of the mooring line and PTO dynamics is needed in order to suppress the unwanted behavior. A process plant model of Lifesaver including the PTO system is previously developed. This model needs to be further improved, and possibly expanded to include more elements of the production mooring line.

The current control system is velocity-dependent only. Due to inertial forces in the PTO there is a discrepancy between the mooring line tension and the generator torque. We have seen that large accelerations cause both impulse loads and slack in the mooring line. Acceleration feedback can be used to limit the peak forces, but the performance is limited due to signal quality and stability constraints. It is believed that better performance may be obtained by use of more sophisticated control procedures.

## Work description

- Perform a literature review to provide background and relevant references on:
  - Wave energy converters (WECs) and other relevant renewable energy producers.
  - Modelling of mooring lines.
  - Methods for controlling force/torque in mechanical systems.
- Write a list with abbreviations and definitions, and a section explaining particularly relevant terms and concepts related to WECs and renewable energy in an alphabetic order.
- Evaluate the magnitude of the hydrodynamic forces on the mooring line. Expand the process plant model to include excitation forces on the subsea buoy.
- Improve the process plant model developed previously. Verify the model by comparing simulated results with recorded results. Perform a sensitivity analysis on the uncertain parameters of the model, mainly stiffness and material damping of the rope sections and added mass of the subsea buoy.
- Identify the natural frequencies of the system by performing an eigenvalue analysis on a linearized model. Use this information to identify the source of the unwanted force oscillations.
- Propose alterations to the PTO system to physically prevent the unwanted behavior. Discuss how the behavior will change if the WEC is moved to deeper waters.
- Propose control strategies that mitigate the force oscillations and increase the robustness of the system.
- Explore the possibility of increasing energy production by use of more sophisticated control methods.

## Guidelines

The scope of work may prove to be larger than initially anticipated. By the approval from the supervisor, described topics may be deleted or reduced in extent without consequences with regard to grading.

The candidate shall present his personal contribution to the resolution of problems within the scope of work. Theories and conclusions should be based on mathematical derivations and logic reasoning identifying the various steps in the deduction.

The report shall be organized in a rational manner to give a clear exposition of results, assessments, and conclusions. The text should be brief and to the point, with a clear language. The report shall be written in English (preferably US) and contain the following elements: Abstract, acknowledgements, table of contents, main body, conclusions with recommendations for further work, list of symbols and acronyms, references, and (optionally) appendices. All figures, tables, and equations shall be numerated. The original contribution of the candidate and material taken from other sources shall be clearly identified. Work from other sources shall be properly acknowledged using quotations and a Harvard citation style (e.g. *natbib* Latex package). The work is expected to be conducted in an honest and ethical manner, without any sort of plagiarism and misconduct. Such practice is taken very seriously by the university and will have consequences. NTNU can use the results freely in research and teaching by proper referencing, unless otherwise agreed upon.

The thesis shall be submitted with two printed and electronic copies, to 1) the main supervisor and 2) the external examiner, each copy signed by the candidate. The final revised version of this thesis description must be included. The report must appear in a bound volume or a binder according to the NTNU standard template. Computer code and a PDF version of the report shall be included electronically.

**Start date:** 14 January, 2013      **Due date:** As specified by the administration.

**Supervisor:** Roger Skjetne

**Co-advisor(s):** Jonas Sjolte

---

**Roger Skjetne**  
Supervisor

# Abstract

Lifesaver is a point-absorber wave energy converter developed by Fred. Olsen. She is currently deployed off the coast of England for pre-commercial testing. Lifesaver consists of a toroidal floater supporting three Power-Take Off (PTO) units moored separately to the seabed. The mooring lines are kept taut by electrical generators.

Large force oscillations have been encountered in the mooring lines during testing. The source of force oscillations is identified as velocity fluctuations in the PTO drive train due to sudden saturation of generator torque. The unfavorable transient response is a result of low stiffness in the mooring line combined with large inertia in the drive train.

A numerical model of the mooring line and PTO unit is developed for use in control system development. The system dynamics are identified through a frequency analysis of a linearized model. Based on these findings a Kalman filter observer is developed to estimate force and force gradient from the angular velocity of the electrical generator.

Three different controllers are proposed to mitigate the undesirable force oscillations. The first prevents sudden saturation by limiting the generator force gradient, and should be straight-forward to implement. Proportional-derivative (PD) feedback of the rope force is enabled by the Kalman filter, and is shown to effectively mitigate the unwanted behavior. However, PD feedback reduces the stability margin of the controller and must be implemented with care. A control algorithm using hysteresis is explored. The hysteretic controller behaves in a predictable and similar manner independent of the incoming wave, and has the potential of increasing robustness during high sea states.

Real-time optimization of the main control parameter using extremum seeking is explored. The algorithm may be used to track a time-varying optimum due to changes in sea state. The adaptation rate is limited by the high peak-to-average power ratio of Lifesaver.

# Sammendrag

Fred. Olsens bølgekraftverk Lifesaver er for tiden stasjonert utenfor England for pre-kommersiell testing. Lifesaver består av en sirkulær flyter med tre separate enheter som konverterer bølgeenergi til elektrisk energi. Enhetene er stramt forankret til havbunnen.

Kraftvibrasjoner i ankerlinene er blitt målt under testing. Kilden til kraftvibrasjoner er identifisert som hastighetsvibrasjoner i giret som forbinder ankerlinen til en elektrisk generator. Vibrasjonene oppstår som følge av brå saturering av kraften fra generatoren. Den uønskede transiente responsen skyldes lav stivhet i ankerlinen kombinert med høy treghet i giret.

En numerisk modell av ankerlinen og giret utvikles for å bli brukt til å teste ulike kontrollsystemer. En frekvensanalyse av en linearisert modell blir utført for å bedre forståelsen av dynamikken til systemet. Basert på resultatet blir et Kalman-filter utviklet for å overvåke kraften i ankerlinene via hastigheten til generatoren.

Tre ulike regulatorer blir foreslått for å begrense de uønskede vibrasjonene. Den enkleste unngår brå saturering ved å begrense kraftgradienten i generatoren. Kalman-filteret muliggjør bruken av proporsjonal-derivat-regulering på taukraften. Dette viser seg å være svært effektivt i å redusere vibrasjoner. En kontrollalgoritme som benytter seg av hysteresis utforskes. Hystere-regulatoren oppfører seg likt og forutsigbart uavhengig av den innkommende bølgen, og har derfor potensialet til å øke robustheten til systemet.

Til slutt blir sanntidsoptimering ved hjelp av ekstrempunktsøking utforsket. Algoritmen finner den optimale dempningskoeffisienten til generatoren, og kan benyttes til å følge et tidsvarierende optimum som følge av endring i sjøtilstand.

# Preface

I was first introduced to the Fred. Olsen wave energy project during my third year of studies towards becoming a marine engineer. The project immediately caught my attention, and I felt very lucky when they offered me a job the following summer. I spent the summers of 2012 and 2013 working with and on Lifesaver. This helped me gain a new and better understanding of the complex challenges faced when trying to develop a reliable and commercially viable wave energy converter. One of these challenges is related to robust control of the production force, which is the topic of my thesis.

I would like to thank my supervisor Professor Roger Skjetne for letting me choose a topic of my liking, and helping me when needed. Skjetne has guided me in the right direction and provided valuable insight on how control theory can be applied to the topic at interest.

I also wish to thank the team at Fred. Olsen for letting me use Lifesaver in my master thesis and providing me with the resources needed. A special thanks goes to Jonas Sjolte who has been my co-supervisor and main contact at Fred. Olsen.



# Contents

<b>Abstract</b>	<b>i</b>
<b>Sammendrag</b>	<b>ii</b>
<b>Preface</b>	<b>iii</b>
<b>Table of Contents</b>	<b>vii</b>
<b>List of Tables</b>	<b>viii</b>
<b>List of Figures</b>	<b>x</b>
<b>Abbreviations</b>	<b>xi</b>
<b>1 Introduction</b>	<b>1</b>
1.1 Motivation . . . . .	1
1.2 Ocean Wave Energy . . . . .	1
1.2.1 Energy potential . . . . .	3
1.2.2 Common terms . . . . .	4
1.2.3 Conversion principles . . . . .	5
1.2.4 Common challenges . . . . .	5
1.3 The Lifesaver Wave Energy Converter . . . . .	6
1.3.1 System Description . . . . .	6
1.3.2 Operational challenges . . . . .	7
1.4 Objectives . . . . .	8
<b>2 Literature review</b>	<b>10</b>
2.1 Modelling . . . . .	10
2.1.1 Modelling of mooring lines . . . . .	10
2.2 Control . . . . .	11
2.2.1 Optimal control . . . . .	11
2.2.2 Robust Control . . . . .	13

---

<b>3</b>	<b>Theoretical background</b>	<b>15</b>
3.1	Wave theory . . . . .	15
3.1.1	Regular wave theory . . . . .	15
3.1.2	Irregular sea . . . . .	16
3.2	Control theory . . . . .	16
3.2.1	Continuous-time state space model . . . . .	17
3.2.2	Transfer functions . . . . .	18
3.2.3	Discrete-time state space model . . . . .	18
3.2.4	Pulse-transfer functions . . . . .	19
3.2.5	Stability, Controllability and Observability . . . . .	19
<b>4</b>	<b>Model Development</b>	<b>21</b>
4.1	Overview of model . . . . .	22
4.2	Hydrodynamic model of floater . . . . .	22
4.2.1	Hydrostatic and hydrodynamic forces . . . . .	23
4.2.2	Mooring forces . . . . .	23
4.2.3	PTO model . . . . .	24
4.2.4	Generalized PTO model . . . . .	25
4.2.5	Drive train friction . . . . .	26
4.3	Mooring line model . . . . .	27
4.3.1	Assessment of hydrodynamic forces . . . . .	27
4.3.2	Modelling of subsea buoy . . . . .	28
4.3.3	Mooring rope tension . . . . .	30
4.4	Implementation and numerical solver . . . . .	31
4.5	Model verification . . . . .	31
<b>5</b>	<b>System analysis</b>	<b>33</b>
5.1	Linearized model . . . . .	33
5.2	Frequency analysis . . . . .	35
5.3	Sensitivity analysis . . . . .	36
5.4	Control Plant Model . . . . .	37
5.4.1	Simplified Control Plant Model . . . . .	39
5.5	Comparison of models . . . . .	39
<b>6</b>	<b>Control system development</b>	<b>41</b>
6.1	Preliminaries . . . . .	41
6.1.1	Reference table . . . . .	41
6.1.2	Current control system . . . . .	41
6.1.3	Implementation . . . . .	44
6.1.4	Sensors . . . . .	44
6.2	Observers . . . . .	44
6.2.1	Kinematic observer . . . . .	44
6.2.2	Model based observer . . . . .	45
6.3	Discrete time CPM . . . . .	48
6.3.1	Stability of nominal control law . . . . .	50
6.4	Reference model . . . . .	51

---

6.4.1	Stability in z-domain . . . . .	51
6.4.2	Choice of $T$ . . . . .	52
6.5	Feedback control of rope force . . . . .	52
6.5.1	Feedback using kinematic observer . . . . .	53
6.5.2	Feedback using model based observer . . . . .	54
6.6	Hysteretic controller . . . . .	55
6.7	Real-time optimization . . . . .	56
<b>7</b>	<b>Results and discussion</b>	<b>59</b>
7.1	Observer performance . . . . .	59
7.1.1	Comparison of observers . . . . .	59
7.1.2	Additional Kalman filter estimates . . . . .	59
7.2	Controller performance . . . . .	62
7.2.1	Robustness . . . . .	62
7.2.2	Power output . . . . .	64
7.2.3	Hysteretic controller . . . . .	64
7.3	Extremum seeking . . . . .	64
7.4	Recommendations for future design . . . . .	66
<b>8</b>	<b>Conclusion and future work</b>	<b>69</b>
8.1	Conclusion . . . . .	69
8.2	Recommendations for future work . . . . .	70
	<b>Bibliography</b>	<b>70</b>
	<b>Appendix A</b>	<b>75</b>
	<b>Appendix B</b>	<b>80</b>
	<b>Appendix C</b>	<b>83</b>
	<b>Appendix D</b>	<b>85</b>

# List of Tables

1.1	Key parameters of Lifesaver . . . . .	8
4.1	Drag forces on mooring line . . . . .	28
5.1	Parameters of linearized model . . . . .	35
5.2	Natural frequencies . . . . .	36
6.1	Key parameters of control system . . . . .	42
6.2	Kalman filter gains used in final implementation. . . . .	48
6.3	Parameters used in extremum seeking. . . . .	58
7.1	Case study; average power . . . . .	64

# List of Figures

1.1	Global renewable energy . . . . .	2
1.2	Average annual wave power . . . . .	3
1.3	Conversion principles . . . . .	4
1.4	Lifesaver Wave Energy Converter . . . . .	6
1.5	Conceptual sketch of Lifesaver . . . . .	7
1.6	Recorded force oscillations . . . . .	9
3.1	JONSWAP wave spectrum . . . . .	17
4.1	Simulation model . . . . .	21
4.2	PTO model . . . . .	24
4.3	Drive train torque loss found from experiments. . . . .	27
4.4	Recorded velocity oscillations . . . . .	32
4.5	Simulated velocity oscillations . . . . .	32
5.1	Linearized model . . . . .	33
5.2	Sensitivity analysis; stiffness . . . . .	36
5.3	Sensitivity analysis; damping . . . . .	37
5.4	Sensitivity analysis; added mass . . . . .	38
5.5	Control Plant Model . . . . .	38
5.6	Bode magnitude plot . . . . .	40
5.7	Step response plot . . . . .	40
6.1	Generator force . . . . .	42
6.2	Generator efficiency . . . . .	43
6.3	Block diagram of DT CPM . . . . .	48
6.4	Block diagram of CPM . . . . .	49
6.5	Response with reference model . . . . .	53
6.6	Hysteretic controller . . . . .	56
6.7	Extremum seeking . . . . .	57
7.1	Velocity estimates . . . . .	60
7.2	Rope force estimates . . . . .	60
7.3	Floater velocity estimates . . . . .	61

7.4	Force gradient estimate . . . . .	61
7.5	Case study; rope force . . . . .	63
7.6	Case study; generator force . . . . .	63
7.7	Case study; power . . . . .	65
7.8	Hysteretic controller . . . . .	65
7.9	Extremum seeking . . . . .	66
7.10	Extremum seeking . . . . .	67
7.11	Extremum seeking . . . . .	68

# Abbreviations

CT	=	Continuous Time
CPM	=	Control Plant Model
DT	=	Discrete Time
LTI	=	Linear Time Invariant
PD	=	Proportional Derivative
PTO	=	Power-Take Off
WEC	=	Wave Energy Converter
ZOH	=	Zero Order Hold



# Chapter 1

## Introduction

### 1.1 Motivation

It is now widely recognized among researchers that not only is the temperature of the earth's atmosphere rising, but also that human influence is the dominant cause of global warming [2]. Limiting climate change will require substantial reductions of greenhouse gas emissions. The largest source of man-made greenhouse gases is carbon dioxide from the combustion of fossil fuels to produce power and heat. Although some reduction in carbon dioxide emissions may be possible by use of carbon capturing [23], a significant shift towards more use of renewable energy sources is necessary to mitigate climate change [6].

Today, the vast majority of the earth's energy supply, approximately 80%, comes from fossil fuels. However, in recent years there has been a rapid increase in renewable energy, as illustrated in Figure 1.1. In 2009 6% of the global final energy consumption came from sources referred to as modern renewable energy sources [1]. In 2011 this number had risen to 9.7% [4], an increase of more than 60%.

The most important renewable energy sources for production of electricity are hydro power, wind power and solar power. With today's technology, these energy sources can provide 5.9 times the global energy demand [46]. A major challenge with renewable energy is the uncertain and uneven power supply. Dividing the energy supply between several sources yields a steadier supply. In this regard wave power has the potential of becoming a significant supplement to the more established renewable energy sources.

### 1.2 Ocean Wave Energy

The idea of harvesting power from the ocean is not new. The first known patent for a Wave Energy Converter (WEC) was filed in France as early as 1799 [15]. In Europe intensive research and development of wave energy conversion began after the dramatic increase in oil prices in 1973 [15]. Basic theory regarding wave energy conversion is well described in literature, e.g. in the books by McCormick [31] and Falnes [17]. However, wave energy technology is still considered to be very young and a commercial breakthrough is yet to

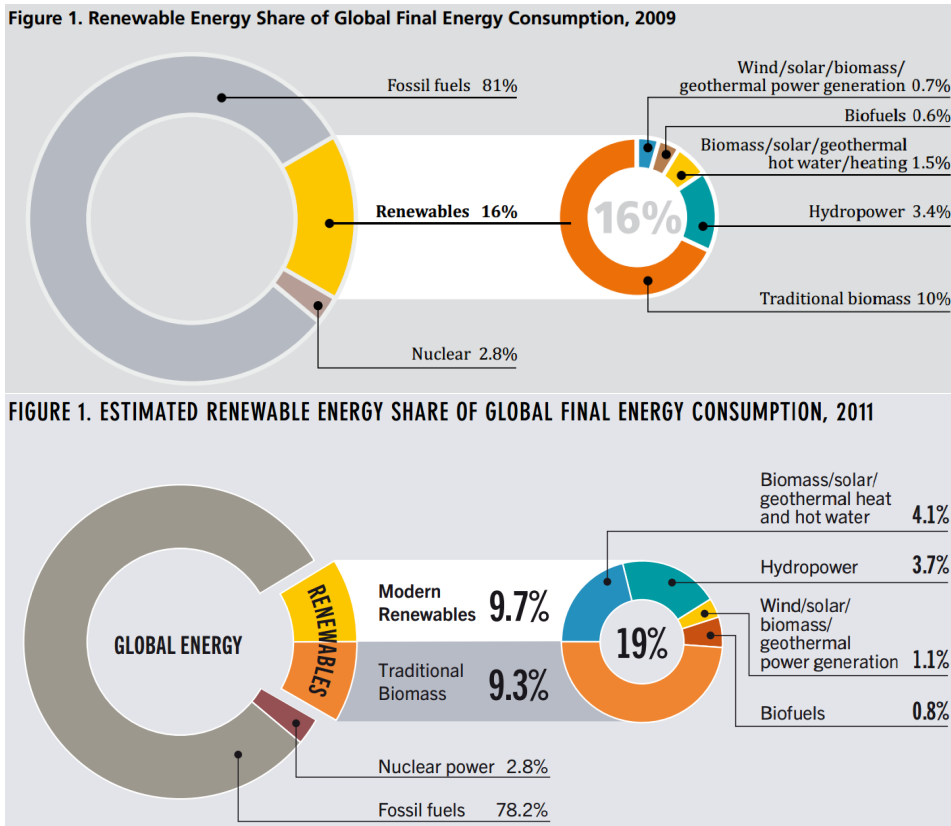


**Figure 1.1:** Estimated renewable energy share of global final energy consumption for 2009 (top) [1] and 2011 (bottom) [4].

come. Only a few megawatt of wave power has been installed world-wide, most of it for demonstration purposes [39]. Today most wave energy research focuses on operational challenges and the practical aspects of producing electricity from ocean waves [21].

### 1.2.1 Energy potential

Fugro OCEANOR has calculated the total annual wave energy that approaches landmasses worldwide to be approximately 17500 TWh [32]. This is slightly less than the world electrical energy consumption (approximately 22000 TWh in 2008 [7]). Fugro OCEANOR further estimate that the exploitable limit is at most 10-25%. This means that wave energy has the potential to provide a significant portion of the worlds electricity needs. Wave power is unevenly distributed across the world. High energy sites, such as some places in the North Atlantic, have an average annual wave power of above 60 [kW/m] (see Figure 1.2).

The power of a wave reduces significantly as one approaches shallower waters [31]. This favors countries with deep coastal waters due to challenges with installing wave energy sites far offshore [31].

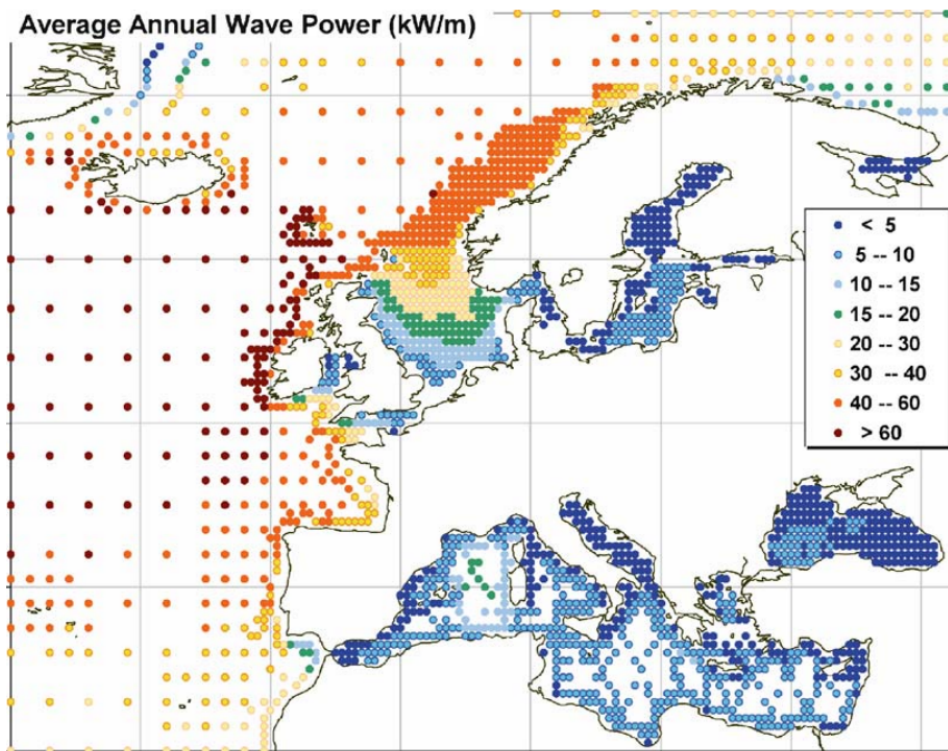


**Figure 1.2:** Average annual wave power [kW/m] in Europe. Reprinted from Fugro OCEANOR [32].

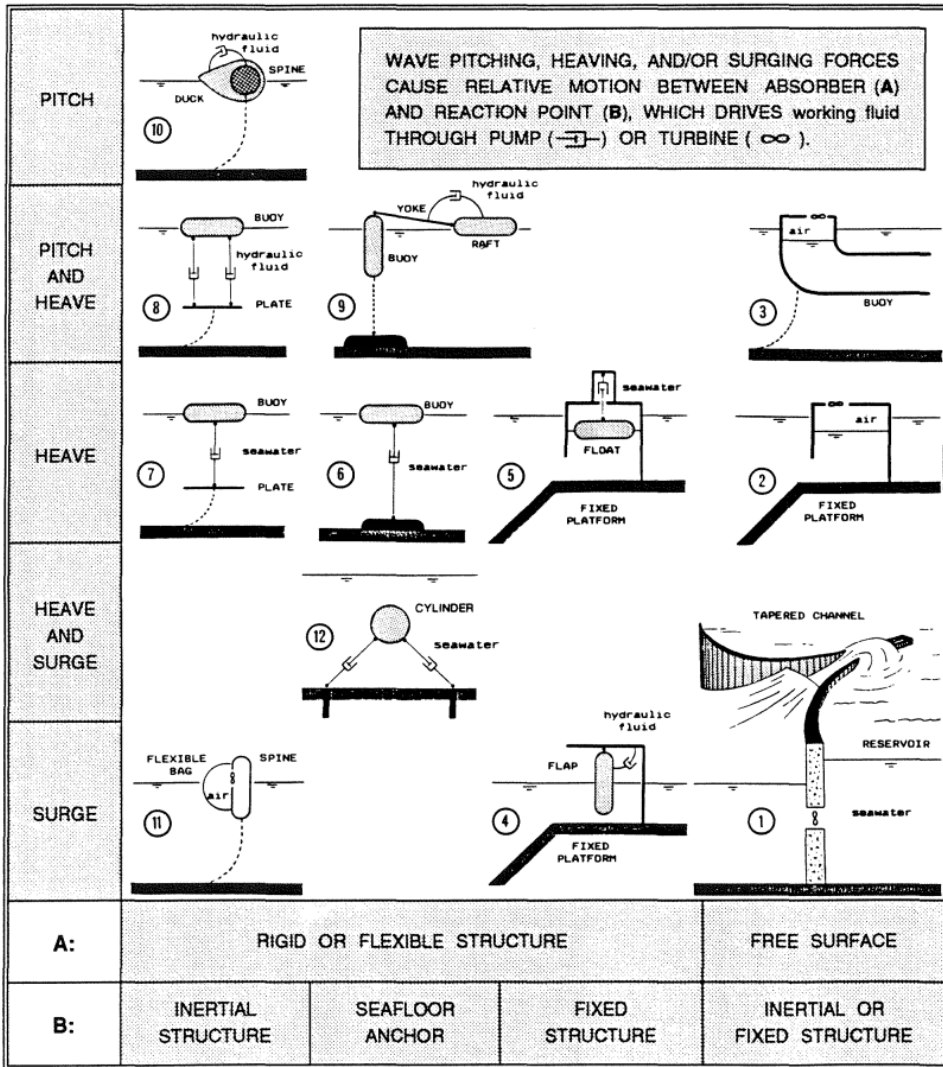


Figure 1.3: Conversion principles as classified by Hagerman [20].

### 1.2.2 Common terms

The following is a list of common terms found in wave energy literature.

**Absorber:** The part of a wave energy converter which is set in motion by the hydrodynamic excitation force.

**Point absorber:** An absorber which is short relative to the incoming wave length, such that the excitation force is evenly distributed along the absorber.

**Reaction point:** Power is extracted by relative motion between the absorber and the reaction point. The reaction point may be a fixed structure, an inertial structure or the seabed.

**PTO:** Power Take-Off, the system which converts the wave power into usable power. May be placed at the absorber, at the reaction point or anywhere between, but must be connected to both.

**Machinery force:** The force from the PTO acting on the absorber. In it's simplest form an absorber is acted upon by two forces; the hydrodynamic force and the machinery force. Note; on the device considered in this thesis the machinery force is the force from the production rope, which is referred to as the production force.

**WEC:** Wave Energy Converter, the full system needed to convert ocean wave energy into mechanical or electrical energy. Includes at minimum the absorber, the PTO and the reaction point. If the reaction point is the seabed a connection between the reaction point and the absorber, i.e. a mooring line, is also needed.

### 1.2.3 Conversion principles

WECs operate on a wide variety of principles. Hagerman [20] has classified the converters according to working principle as shown in Figure 1.3. The converters in the left column utilize the varying surface elevation to drive a turbine, with either air or sea water as the working fluid. The other converters utilize relative motion between bodies to extract energy. Hagerman considers only systems where a hydraulic pump drives a working fluid, but direct mechanical coupling between the absorber and an electrical generator is also possible. The Lifesaver WEC, which will be presented shortly, is a combination of 6 and 8 (see Figure 1.3); pitching and heaving body tightly moored to the seabed.

### 1.2.4 Common challenges

Surviving the harsh ocean environment has been the most common challenge for development of commercially viable wave energy technology. A WEC must obviously be designed to withstand the most severe ocean storms. It must also withstand prolonged exposure to less severe conditions, which may prove just as challenging. In order to be cost-effective the device must be robust and low-maintenance, which is not an easy task for mechanical and hydraulic components in proximity to sea water.

Another common challenge is achieving efficient conversion to usable energy, i.e. electricity. This is a much more challenging task than merely converting into mechanical energy [31]. To use off the shelf electrical generators the slow linear motion of the waves must be converted to high-speed rotational motion. This adds both cost and complexity. The irregular and oscillatory nature of ocean waves leads to a high peak-to-average ratio for both power and forces [15]. This poses a challenge when designing electrical and mechanical components.



**Figure 1.4:** The Lifesaver Wave Energy Converter, pictured outside Falmouth Bay, England, where she was deployed in April 2012. Courtesy Fred. Olsen.

## 1.3 The Lifesaver Wave Energy Converter

Lifesaver, pictured in Figure 1.4, is the latest of several WECs developed by Fred. Olsen. She is currently deployed off the coast of England for pre-commercial testing, where she is installed at a mean depth of 50 m. Lifesaver is a point absorber which produces power from heave and pitch motion.

### 1.3.1 System Description

Lifesaver consists of a floater, the Power Take-Off (PTO) units, the primary mooring lines and the secondary mooring system, in addition to an advanced electrical system not considered in this thesis. A description of the electrical system is found in [42]. A conceptual sketch of the device is shown in Figure 4.2. Key parameters are given in Table 6.1. Power is extracted by increasing the generator torque for positive heave velocities when rope is being pulled out. The minimum generator torque is set to 10 kN to ensure that the rope is kept taut for negative velocities.

**Floater:** For Lifesaver the absorber is referred to as the floater, and is a toroidal steel structure with 16 m. outer diameter, 10 m. inner diameter and a mass of approximately 55 tons. The floater can accommodate up to five PTOs.

**PTO:** Currently three PTOs are installed. Each PTO consists of a winch, a two-step reduction gear and an electrical generator. The generators are connected to a

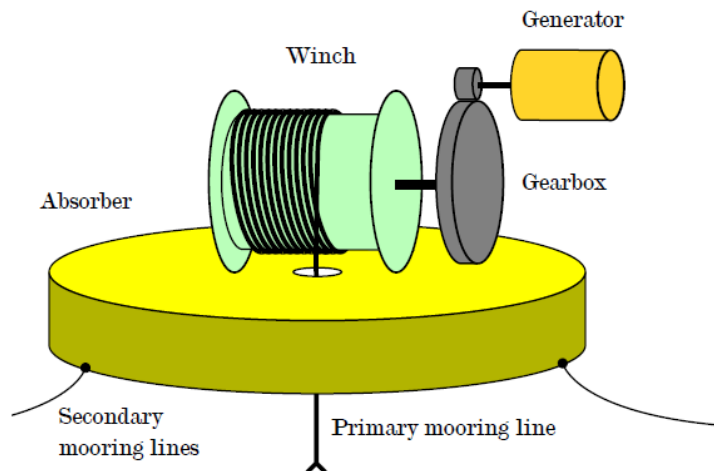


**Figure 1.5:** Conceptual sketch of Lifesaver with the main PTO components; winch, gearbox and generator. Courtesy Fred. Olsen.

common battery bank. The combined linear inertia of the PTO (generator, gearbox and winch) is approximately 3000 kg.

**Primary mooring line:** The PTOs are moored to the seabed separately. Starting from the seabed the primary mooring line consists of; a lower mooring rope of approximately 30 m, a subsea buoy attached to the lower mooring rope, and a production rope running from the subsea buoy to the winch. The subsea buoy is located approximately 15 m. below mean sea level, and has a net positive buoyancy of approximately 4 kN. The primary function of the subsea buoy is to ease maintenance and allow for a shorter production rope.

**Secondary mooring system:** Lifesaver has five catenary moorings referred to as the secondary mooring or storm mooring. The secondary mooring system serves to limit the surge motion and as a safety precaution should the primary mooring lines fail.

### 1.3.2 Operational challenges

Failure of the primary mooring lines has been the main operational issue of Lifesaver since she was deployed in April 2012. The experiences gained during the first year of testing with Lifesaver is presented by Sjolte et al [25]. Further literature on Lifesaver and the Fred. Olsen wave energy project is found in e.g. [40], [12] and [41].

When operated correctly the winch and mooring line concept used on Lifesaver has a high expected lifetime. However, the concept is vulnerable to abnormal loads and wear mechanisms [25]. Force oscillations in the production rope, shown in Figure 1.6, have

**Table 1.1:** Key parameters of Lifesaver. Stiffness parameters are approximate.

<b>WEC</b>	Installation depth	50	m
	Rated export power	70	kW
	Installed generator capacity	400	kW
	Number of PTOs	3	
	Total mass	55	tons
<b>Floater</b>	Outer diameter	16	m
	Inner diameter	10	m
	Height	1	m
<b>PTO</b>	Mechanical force limit	100	kN
	Linear inertia	3010	kg
	Gearbox ratio	39	rad/m
<b>Production rope</b>	Mean length	15	m
	Mean stiffness	1670	kN/m
<b>Lower mooring rope</b>	Length	35	m
	Stiffness	750	kN/m
<b>Subsea buoy</b>	Height	1.0	m
	Diameter	0.7	m
	Volume	0.43	m <sup>3</sup>
	Mass	217	kg

been encountered during testing. In addition, several incidents of slack mooring line has been recorded with the on deck video surveillance. This unwanted behavior is likely to cause additional wear and even mechanical failure. Especially the slack mooring line is of concern, since it may lead to impulse loads or the rope getting tangled. The rope can be kept taut by increasing the minimum force of the generator. Since the generator works as a motor when winding in rope this will result in a decrease in energy output.

It is in place with a quote from the team responsible for developing Lifesaver: "This [unwanted] behaviour is expected to be manageable through active generator compensation, but until such control is in place, conservative control parameters are set for the high wave states" (Sjolte et al [25]).

## 1.4 Objectives

**Model development:** The current numerical model of Lifesaver solves the floater motion considering the mooring line forces as idealized control inputs. Experience acquired during testing of Lifesaver has indicated that the mooring force cannot be considered ideal. Hence it is desirable with a high-fidelity numerical model of the PTO and mooring line, which later can be used to examine different control systems. The model can also be used to assess the energy potential of Lifesaver and as a design tool when upgrading or altering the system. The framework for the expanded model was established during the project thesis *Modelling and control of a wave energy converter* [30]. This model needs to be further improved.

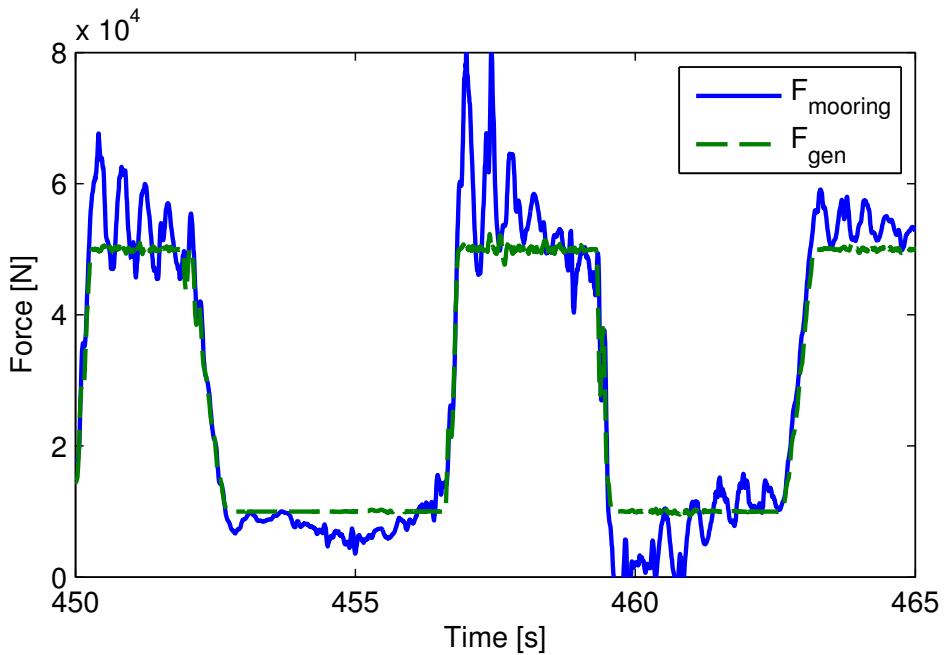


**Figure 1.6:** Force oscillations encountered during testing in rough sea. The oscillations have a frequency of approximately 2 Hz.  $F_{mooring}$  is the tension of the mooring line while  $F_{gen}$  is the force provided by the generator.

**System analysis:** In order to mitigate unwanted behavior a better understanding of the mooring line and PTO dynamics is needed. This includes identification of the source of force oscillations and identifying the resonant frequencies of the full system.

**Control system development:** The previous objectives are merely necessary prerequisites in order to explore different options for robust control of Lifesaver. The aim is to develop a control system that limits the wear of the PTO and mooring line. It is believed that a more sophisticated control system will be able to mitigate the unwanted behavior without reducing the power output. Control strategies that increase power output are also to be explored.

# Chapter 2

## Literature review

### 2.1 Modelling

Realistic models of WECs include several energy domains, usually hydrodynamic, mechanic/hydraulic and electric. Models that consider the whole conversion chain from wave power to electric power are referred to as wave-to-wire models. A time-domain wave-to-wire model of Lifesaver has previously been developed and is described in [36].

Wave-to-wire models may be idealized in one or several of the energy domains. The wave-to-wire model of Lifesaver includes only a very simple model of the mechanical components. The mooring line and the PTO is replaced by an idealized machinery force given by the control input.

#### 2.1.1 Modelling of mooring lines

Hals used bond graph modelling to develop several wave-to-wire models of WECs [21], some of which included mooring lines running from the reaction point to the absorber. The mooring lines were modelled as spring-damper systems. Bond graph modelling is a graphical and systematic approach to modelling of dynamic systems. It is only the modelling procedure which is different from the more common method of formulating the model as differential equations using physical principles. The resulting model will be the same using the two procedures.

To the authors knowledge high-fidelity models of similar PTO and mooring line configurations as found on Lifesaver have not been previously developed. A comparable modelling problem was addressed by Rustad in her doctoral thesis [34]. She modelled top-tensioned risers connected to a semi-submersible using the Finite Element Method (FEM). The obtained model was simple yet realistic and well suited for use in control system development. Rustad considered the platform dynamics uncoupled from the riser dynamics, a simplification which cannot be made when modelling WECs.

FEM was also used by Aamo and Fossen for modelling of moored vessels [8]. They considered mooring lines of constant length. The proposed procedure is well suited for modelling of the secondary mooring system of Lifesaver. The primary mooring, however,

is of variable length, making it challenging to formulate a FEM model of the system. The problem can be circumnavigated by introducing an element of variable length at the coupling between the floater, PTO and mooring line<sup>1</sup>.

## 2.2 Control

The control objective for a WEC is to optimize the power output under constraints imposed by the system, and to ensure the structural integrity of the device. The first objective can be considered optimal control, while the second objective belongs to robust control. This thesis is mainly concerned with robust control.

### 2.2.1 Optimal control

Optimal control of WECs has been a popular research topic for many years. Jørgen Hals covers the topic in detail in his doctoral thesis [21]. Although optimal control is outside the scope of this thesis, knowledge about it is important to understand the challenges faced when designing and controlling WECs. A frequency-domain approach to optimal control is provided by Johannes Falnes in *Ocean Waves and Oscillating Systems* [17]. Hals goes one step further in his thesis by evaluating control procedures in the time domain. The theory in this section is mainly based on his work.

#### Optimal power extraction in frequency-domain

According to Hals the following equation "holds a linear approximation to the dynamic behavior of a rigid body in water":

$$\left( i\omega(M + M_a(\omega)) + R_r(\omega) + \frac{S}{i\omega} \right) v_0 e^{i\phi_u} = F_{e_0} e^{i\phi_e} + F_{m_0} e^{i\phi_m}. \quad (2.2.1)$$

(2.2.1) describes a body oscillating in a single degree of freedom with velocity amplitude  $v_0$  when excited by periodic forces of amplitude  $F_{e_0}$  and  $F_{m_0}$ .  $\omega$  is the oscillation frequency,  $M + M_A$  is the rigid body mass and added mass,  $R_r$  is the radiated resistance (often termed added damping or potential damping), while  $S$  is the hydrostatic stiffness.

$F_e$  is the hydrodynamic excitation force due to incident waves.  $F_m$  is the machinery force, which in the case of Lifesaver is the force from the primary mooring lines. The left parenthesis of (2.2.1) is termed the intrinsic impedance of the body. Further we have that the intrinsic reactance is

$$X(\omega) = \omega(M + M_A(\omega)) - S/\omega, \quad (2.2.2)$$

while the machinery impedance  $Z_m$  is given by the relationship  $F_{m_0} e^{i\phi_m} = Z_m v_0 e^{i\phi_v}$ .

<sup>1</sup>This was done at an early stage of the model development, but the resulting model was computationally intensive and did not add much value compared to the spring-damper approach.

Optimal power extraction is achieved when the absorber is oscillating in phase with the excitation force and with amplitude  $v_0$  such that the radiated power equals half the excitation power [21] [17]. This is obtained if  $Z_m$  equals "the negative complex-conjugate [...] of the intrinsic impedance" [21]. Since  $Z_m$  is complex it follows that the machinery force has components both in-phase and out-of-phase with the velocity.

### Selected control strategies

Optimal control requires knowledge of the future wave excitation, which in the case of irregular waves becomes a non-causal control problem. Such a control system can not be realized in practice. The problem can be made causal by predicting the future wave excitation, e.g. by a Kalman filter or by upstream measurements. Many ingenious control strategies have been devised to remedy the uncertain knowledge of the future, a selection of which are described below.

**Reactive control:** In wave energy control, as opposed to other control theory, reactive control refers to control strategies that require reactive machinery forces. Machinery forces are reactive if the associated power flow is both in and out of the system. The device can be forced to oscillate with optimal phase and amplitude by requiring that the machinery force matches the intrinsic reactance of the oscillating body [21]. Except at the natural frequency, where  $X(\omega)$  is zero, this requires large reactive forces and power flow [21]. For this reason reactive control is very difficult from an engineering point of view.

**Resistive loading:** If the machinery force is restricted to not provide reactive power the machinery force can be written  $F_m = Z_m v$ . The controller becomes purely resistive and the resulting system is called a passive converter [21]. Since the machinery force depends only on the velocity we replace  $Z_m$  with the damping coefficient  $B$ . Hals shows that the optimal machinery damping is frequency-dependent according [21]

$$B(\omega) = -\sqrt{R_r(\omega)^2 + (\omega(M + M_A(\omega)) - S/\omega)^2}. \quad (2.2.3)$$

**Latching/clutching control:** Optimum phase can be achieved without the use of reactive power by stopping the motion during parts of the cycle [21]. This is termed latching control. The main challenge with this control procedure are the large machinery forces required during latching. Determining the latching instant is also a challenge in irregular waves. Another way of achieving optimum phase is to let the body oscillate freely during parts of the cycle [21]. This is termed clutching control since the machinery force is disengaged when the body oscillates freely.

**Tuning of damping:** A third way of achieving optimal phase without the use of reactive power is to tune the damping parameter  $B$  during the wave cycle. This can be considered a combination of clutching and latching, since the machinery force is increased or decreased depending on the desired phase. Schoen, Hals and Moan used fuzzy logic for tuning of  $B$  [37]. For many WECs the saturation limits of  $B$

are very close to each other. If this is the case the optimal is to use a hysteretic "bang-bang" controller which switches only between the maximum and minimum values of  $B$  [24]. If  $B_{min} = 0$  this corresponds to clutching control.

**Phase control:** Control strategies where the desired machinery force depends on the oscillation phase are commonly referred to as phase control. All control strategies above expected the passive converter are considered phase control.

**Extremum seeking:** Extremum seeking is a real-time optimization procedure which can be used in combination with any of the control strategies listed above. Hals used extremum seeking in combination with resistive loading, where he showed that the algorithm can track a time-varying optimum due to changes in sea state [22]. Extremum seeking has also been used to increase power output of wind turbines [47] [14].

Lifesaver is optimised for use as a passive converter, as this is believed to be the most cost-efficient solution [42]. With the exception of very low sea states the PTOs are not able to deliver the machinery force required for more advanced control strategies [41].

## 2.2.2 Robust Control

Hals defines robust control of WECs as "protecting the device and its machinery under severe storm conditions" [21]. In this thesis the definition is expanded to "protection of the device and machinery under all operating conditions", which also includes limiting wear of mechanical components.

Robust control of WECs has not received much attention in literature. This is somewhat peculiar, seeing that robust performance has been one of the main challenges with developing commercially competitive technology. One explanation may be that few devices have made it past an early development stage, in which proof of concept usually receives the most attention.

### Robust fuzzy-logic

Schoen et al ([37],[38]) proposed a procedure to increase the robustness of a fuzzy logic controller. Fuzzy logic was used to maximize short-term energy production through tuning of  $B$ . This required knowledge of the model and the sea state. The robustness to process uncertainty was improved by an optimization algorithm that maximized the stability margin of the fuzzy logic in the s-domain<sup>2</sup>. The main control problem addressed in this thesis is related to actuator dynamics. The hybrid controller proposed by Schoen et al is not considered applicable at this stage of the control system development.

### Similar systems in different applications

Winches used for installation of subsea components or heave compensation of drilling risers both bear resemblance with the PTO concept of Lifesaver. The actuator control

<sup>2</sup>s-domain refers to the Laplace transform of the controller, which will be explained in the subsequent chapter.

objective of a WEC is to track the fast changing desired machinery force. For heave compensation the control objective is to track a desired position [28]. This control objectives differs significantly, such that experience from this field is difficult to benefit from.

A comparable control problem is force control for wire tension during marine crane operations. Skaare and Egeland state that the critical phase is maintaining wire tension when the load goes through the splash zone [43]. During this phase inertial forces from the load results in large oscillations in the wire tension. A parallel force/position control strategy was shown to have best results in maintaining minimum wire tension. The controller tracks a desired position at high-frequency and a desired force at low-frequency. The inner loop position tracking limits accelerations, thus reducing dynamic forces. For this to work a desired position must be available. This is in general not the case for WECs as the absorber motion is given by the excitation force and difficult to predict. The strategy also requires an accurate estimate of the wire tension.

Sagatun, Fossen and Lindegaard propose an impedance control scheme augmented with acceleration feedback to limit dynamic forces of crane operations without requiring other measurements than position and velocity [35]. The procedure, however, requires desired acceleration, velocity and position, neither of which are readily available for Lifesaver.

Pure acceleration feedback has been explored for Lifesaver in [30]. The performance was limited due to poor acceleration estimates which resulted in unstable behavior.

# Chapter 3

## Theoretical background

In this chapter the necessary theoretical background for hydrodynamic modelling and control system development is provided.

### 3.1 Wave theory

The theory in this section regarding ocean waves is extracted from the book *Sealoads* by Faltinsen [18]. Long derivations are omitted since only the results are considered important. For further reading on wave theory (including proofs for several of the equations presented below) *Marine Hydrodynamics* by Newman [33] is recommended.

#### 3.1.1 Regular wave theory

Ocean waves are commonly described by their velocity potential. For simplicity we assume infinite water depth, although the theory is easily extended to finite water depth. The velocity potential of a regular sinusoidal wave propagating in the negative x-direction is

$$\phi = \frac{g\zeta_a}{\omega} e^{kz} \cos(\omega t - kx), \quad (3.1.1)$$

where  $g$  is the acceleration of gravity,  $\zeta_a$  is the wave amplitude,  $\omega$  is the circular frequency,  $k = \omega^2/g$  is the wave propagation number, while  $z$  is the vertical coordinate defined positive upwards. Regular waves are often defined by their height  $H = 2\zeta_a$  and their period  $T = 2\pi/\omega$ .

From the velocity potential we find the dynamic pressure  $p_d$  of the wave as

$$p_d = \frac{d\phi}{dt} = \rho g \zeta_a e^{kz} \sin(\omega t - kx), \quad (3.1.2)$$

where  $\rho$  is the water density. The total pressure in the fluid is according to Bernoulli [18]

$$p = p_d - \rho g z + p_o, \quad (3.1.3)$$

where  $p_o$  is the atmospheric pressure. By requiring that the water pressure is equal to the atmospheric pressure on the surface we find the surface elevation as

$$\begin{aligned} \zeta &= \frac{p_d}{\rho g} = \zeta_a e^{kz} \sin(\omega t - kx) \\ &\approx \zeta_a \sin(\omega t - kx). \end{aligned} \quad (3.1.4)$$

The last approximation is in accordance with linear wave theory, and is exact on the mean surface level  $z = 0$ . The horizontal water particle velocity  $v_x$  and vertical particle velocity  $w_x$  is found from the velocity potential as

$$v_x = \frac{d\phi}{dx} = \omega \zeta_a e^{kz} \sin(\omega t - kx), \quad (3.1.5)$$

$$v_z = \frac{d\phi}{dz} = \omega \zeta_a e^{kz} \cos(\omega t - kx). \quad (3.1.6)$$

The horizontal and vertical water particle acceleration is found by the time derivative of (3.1.5) and (3.1.6), respectively.

### 3.1.2 Irregular sea

A real sea that one encounters at the ocean is referred to as an irregular sea. An irregular sea can be described as a superimposed finite sum of sinusoidal waves of different phase, amplitude and frequency. The surface elevation is then realized as

$$\zeta = \sum_{i=1}^N \sqrt{2S(\omega_i)\Delta\omega} \sin(\omega_i t - k_i x + \epsilon_i), \quad (3.1.7)$$

where  $\sqrt{2S(\omega_i)\Delta\omega}$ ,  $\omega_i$  and  $k_i$  is the amplitude, frequency and wave number of the individual wave components while  $0 < \epsilon_i < 2\pi$  is a random phase angle.  $S(\omega)$  is the energy spectrum, which specifies how the energy is distributed across the frequencies.

The JONSWAP spectrum with values recommended by Faltinsen [18] is used in this thesis. A sea state is then sufficiently defined by its significant wave height  $H_s$  and peak period  $T_p$ .  $H_s$  is (approximately) the average of the one third highest waves, while  $T_p$  is the frequency with the highest energy. Figure 3.1 shows the JONSWAP spectrum for a moderate sea state  $H_s = 2.75$  m.,  $T_p = 10$  s., along with a realization of the given sea state.  $H_s$  and  $T_p$  are often assumed to be constant over a time period of 20 minutes.

## 3.2 Control theory

The theory in this section is taken from the books *Marine Control Systems* by Sørensen [44] and *Computer-Controlled Systems* by Åstrom and Wittenmark [10].

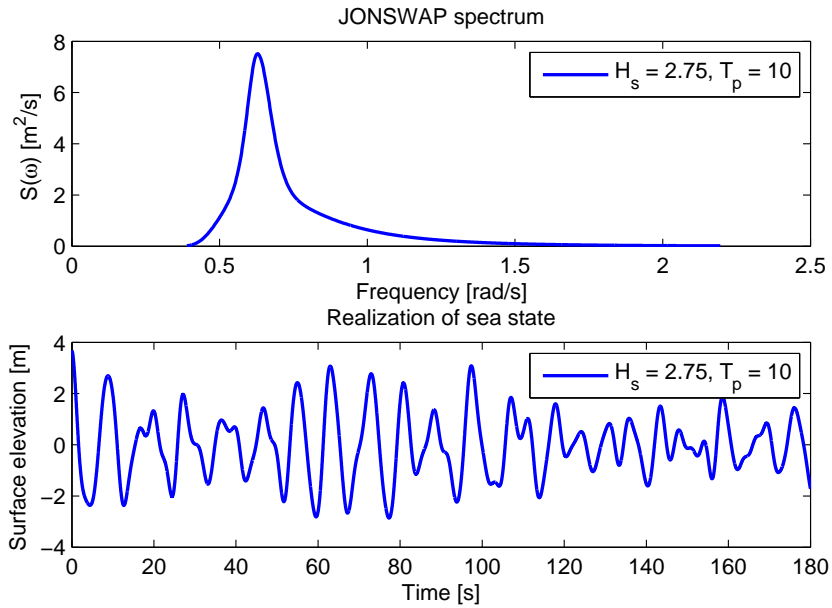


**Figure 3.1:** JONSWAP spectrum with parameters recommended in [18] for  $H_s = 2.75$  m.,  $T_p = 10$  s. A short realization of the sea state below.

### 3.2.1 Continuous-time state space model

In control theory it is common to represent dynamic systems as state space models. In continuous time (CT) a state space model is a set of differential equations,

$$\begin{aligned}\dot{\mathbf{x}} &= \mathbf{f}(\mathbf{t}, \mathbf{x}, \mathbf{u}, \mathbf{w}), \\ \mathbf{y} &= \mathbf{h}(\mathbf{t}, \mathbf{x}, \mathbf{u}, \mathbf{v}),\end{aligned}\tag{3.2.1}$$

where  $\mathbf{x}$  is the state vector,  $\mathbf{u}$  are the control inputs,  $\mathbf{w}$  are the disturbances,  $\mathbf{y}$  is the output vector and  $\mathbf{v}$  is the measurement error. If the system is linear and independent of time (3.2.1) can be written

$$\begin{aligned}\dot{\mathbf{x}} &= \mathbf{A}\mathbf{x} + \mathbf{B}\mathbf{u} + \mathbf{E}\mathbf{w}, \\ \mathbf{y} &= \mathbf{C}\mathbf{x} + \mathbf{D}\mathbf{u} + \mathbf{v}.\end{aligned}\tag{3.2.2}$$

This is known as a linear time invariant (LTI) system.  $\mathbf{A}$  is the system matrix,  $\mathbf{B}$  is the input matrix,  $\mathbf{E}$  is the disturbance matrix, while  $\mathbf{C}$  and  $\mathbf{D}$  are output matrices.

### 3.2.2 Transfer functions

Linear systems can be effectively described and examined by use of transfer functions. The Laplace transform is defined as

$$F(s) = \int_{-\infty}^{\infty} f(t)e^{-st} dt. \quad (3.2.3)$$

Consider the differential equation

$$\dot{x}(t) = ax(t) + bu(t). \quad (3.2.4)$$

Assuming  $x(t = 0) = 0$  the Laplace transform of (3.2.4) is

$$sx(s) = ax(s) + bu(s). \quad (3.2.5)$$

The relationship between input  $u(s)$  and output  $x(s)$  is

$$h(s) = \frac{x(s)}{u(s)} = \frac{b}{s - a}. \quad (3.2.6)$$

$h(s)$  is known as the transfer function, and contains information about the dynamic properties of the system. The transfer function of a LTI system can be found as

$$\mathbf{H}(s) = \mathbf{C}(s\mathbf{I} - \mathbf{A})^{-1}\mathbf{B} + \mathbf{D}. \quad (3.2.7)$$

$\mathbf{H}$  will be an  $n \times m$  matrix of transfer functions,  $n$  being the length of  $\mathbf{y}$  and  $m$  being the length of  $\mathbf{u}$ , providing the relation between each input-output pair. Conversely a state space model can be realized from a transfer function, which is often exploited when designing control systems with desired dynamics.

### 3.2.3 Discrete-time state space model

Whereas real physical processes are continuous in time, a computer operates on Discrete Time (DT) intervals. When designing a computer-controlled system and checking stability we must also consider the DT implementation. The DT equivalent of (3.2.8) is a set of difference equations,

$$\begin{aligned} \mathbf{x}[k + 1] &= \mathbf{\Phi}\mathbf{x}[k] + \mathbf{\Delta}\mathbf{u}[k] + \mathbf{\Gamma}\mathbf{w}[k], \\ \mathbf{y}[k] &= \mathbf{C}\mathbf{x}[k] + \mathbf{D}\mathbf{u}[k] + \mathbf{v}[k], \end{aligned} \quad (3.2.8)$$

where  $k$  denotes the time instant  $t_k$ . It is assumed that the sampling time is constant such that  $t_{k+1} - t_k = h$ , where  $h$  is the sampling time. For sufficiently small sampling time the discrete time matrices can be approximated by  $\mathbf{\Phi} = \mathbf{I} + h\mathbf{A}$  ( $\mathbf{I}$  being the identity matrix),  $\mathbf{\Delta} = h\mathbf{B}$  and  $\mathbf{\Gamma} = h\mathbf{E}$ . However, better approximations exist and are easy to find using e.g. the *c2d*-function included in the Control System Toolbox of MATLAB [3]. In this thesis the trapezoidal *Tustin* method [44] was commonly used.

### 3.2.4 Pulse-transfer functions

The DT equivalent of the transfer function is the pulse-transfer function. Consider the difference equation

$$x[k + 1] = ax[k] + bu[k] \quad (3.2.9)$$

The forward-shift operator  $z$  is defined as  $zx[k] = x[k + 1]$ . This yields

$$zx[k] = ax[k] + bu[k]. \quad (3.2.10)$$

The input-output relation is

$$h(z) = \frac{x[k]}{u[k]} = \frac{b}{z - a}. \quad (3.2.11)$$

$h(z)$  is known as the pulse-transfer function. The pulse-transfer function of a DT LTI system is

$$\mathbf{H}(z) = \mathbf{C}(s\mathbf{I} - \phi)^{-1}\mathbf{\Delta} + \mathbf{D}. \quad (3.2.12)$$

To find the pulse-transfer function of a computer-controlled system, which consists of a CT process and a DT control system, the digital-to-analog converter must also be included. The digital-to-analog converter converts the discrete control signal  $u[k]$  to a continuous signal  $u(t)$ . If  $u(t)$  is constant over one sampling interval the conversion is done using the Zero-Order-Hold (ZOH) method. The transfer function of the ZOH is

$$g(s) = \frac{1 - e^{-sh}}{s} \quad (3.2.13)$$

The pulse-transfer function  $H(z)$  of the cascade  $g(s)h(s)$  can be found by following a procedure described in [10]. For many systems  $H(z)$  can be found in look-up tables, e.g. on page 54 of [10].

### 3.2.5 Stability, Controllability and Observability

Stability, controllability and observability are three important concepts within control theory. The concepts will only be introduced briefly to ensure a common understanding.

**Stability** A system is marginally stable if the states  $|\mathbf{x}(t)| < \infty$  for all times  $t \geq 0$  and all initial conditions  $\mathbf{x}(0)$ . A system is asymptotically stable if  $|\mathbf{x}(t)| \rightarrow 0$  as  $t \rightarrow \infty$ . Marginal stability occurs for only an exact set of parameters and is not relevant in practice [11]. For this reason asymptotic stability is implied when writing only stability. A CT system is asymptotically stable if all poles of the transfer function lie in the left half of the complex plane. A DT system is asymptotically stable if all poles of the pulse-transfer function lie within the unit circle.

**Controllability** A system is controllable if one can find a control input  $\mathbf{u}$  that brings the system from an initial state to a desired state in finite time. A DT LTI system is controllable if the controllability matrix,

$$\mathcal{C} = [\Delta, \Phi\Delta, \dots, \Phi^{n-1}\Delta], \quad (3.2.14)$$

has full column rank, where  $n$  is the number of states.

**Observability** A DT LTI system is observable if the state vector  $\mathbf{x}$  can be reconstructed from the input  $\mathbf{u}$  and output  $\mathbf{y}$ . A DT LTI system is observable if the observability matrix,

$$\mathcal{O} = [\mathbf{C}^T, \Phi^T \mathbf{C}^T, \dots, (\Phi^T)^{n-1} \mathbf{C}^T]^T, \quad (3.2.15)$$

has full column rank, where  $n$  is the number of states.

# Chapter 4

## Model Development

A MATLAB [3] simulation model of Lifesaver has been provided by Fred. Olsen. The provided model consists of the floating body only, with mooring line tension as an idealized control input. The model is expanded to include both the mooring line and PTO. With these changes the generator torque becomes the idealized control input for the simulation.

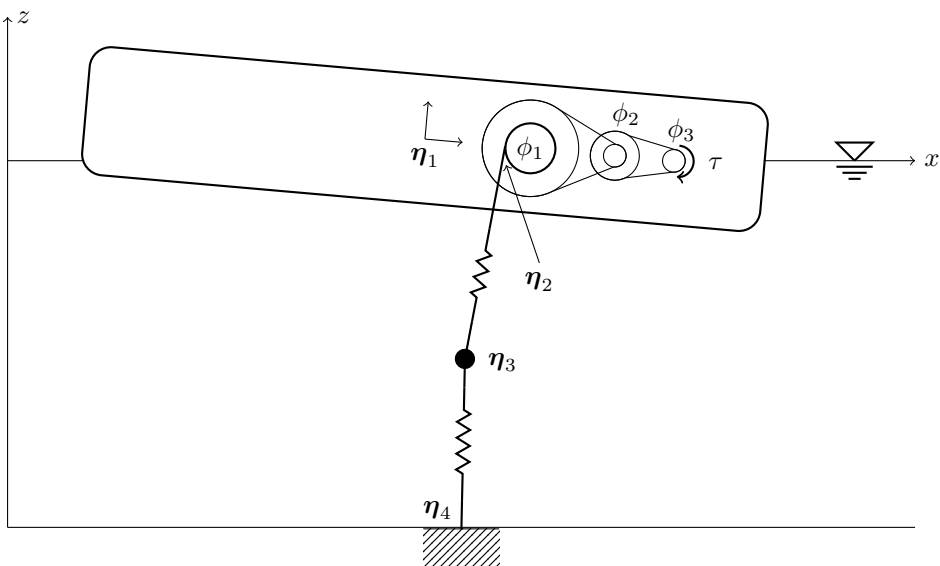


**Figure 4.1:** Illustration of the numerical model with a single PTO and mooring line.

## 4.1 Overview of model

The Degrees Of Freedom (DOFs) included in the final model are shown in Figure 4.1. The model is restricted to the x-z-plane. For simplicity only a single mooring line and PTO is considered when developing the model.

$\boldsymbol{\eta}_1 = [\eta_{1_x} \ \eta_{1_z} \ \theta_1]^T$  is the absorber motion in surge, heave and pitch. Surge is the horizontal motion while heave is the vertical motion. Pitch is the clockwise rotation about the body-fixed origin, which is placed at the volumetric center of the floater.

$\boldsymbol{\eta}_2 = [\eta_{2_x} \ \eta_{2_z}]^T$  is the point where the production rope is connected to the floater, and is referred to as the PTO position.

$\boldsymbol{\eta}_3 = [\eta_{3_x} \ \eta_{3_z}]^T$  is the position of the subsea buoy, which is placed approximately 15 metres below the mean sea level.

$\boldsymbol{\eta}_4 = [\eta_{4_x} \ \eta_{4_z}]^T$  is the position where the lower mooring rope is anchored.

$\boldsymbol{\phi} = [\phi_1 \ \phi_2 \ \phi_3]^T$  is the rotation of each stage of the belt gear.

$\tau$  is the electrical torque of the generator.

The distance from the rotation axis to the PTO is

$$\mathbf{r}_{1/2} = \begin{bmatrix} \eta_{2_x} - \eta_{1_x} \\ \eta_{2_z} - \eta_{1_z} \end{bmatrix}, \quad (4.1.1)$$

Since  $\mathbf{r}_{1/2}$  is a constant body-fixed vector we can write

$$\boldsymbol{\eta}_2 = \begin{bmatrix} \eta_{1_x} \\ \eta_{1_z} \end{bmatrix} + \mathbf{R}(\theta_1)\mathbf{r}_{1/2}. \quad (4.1.2)$$

$\mathbf{R}(\theta_1)$  is the Euler angle rotation matrix [19], which for a rotation in the x-z plane is given by

$$\mathbf{R}(\theta_1) = \begin{bmatrix} \cos(\theta_1) & \sin(\theta_1) \\ -\sin(\theta_1) & \cos(\theta_1) \end{bmatrix}. \quad (4.1.3)$$

We further define the vectors  $\mathbf{r}_{i/j} = \boldsymbol{\eta}_j - \boldsymbol{\eta}_i$  for  $i, j \neq 1$ .

## 4.2 Hydrodynamic model of floater

The provided model solves the force balance equation of the floating body,

$$\mathbf{M}_{RB}\ddot{\boldsymbol{\eta}}_1 = \mathbf{F}_e(t) + \mathbf{F}_s(t) + \mathbf{F}_r(t) + \mathbf{F}_m(t), \quad (4.2.1)$$

where  $\mathbf{M}_{RB}$  is the rigid body mass matrix and  $\mathbf{F}_e$ ,  $\mathbf{F}_s$ ,  $\mathbf{F}_r$  and  $\mathbf{F}_m$  are vectors of external forces and moments. The model is well described in the master thesis of Sandvik [36].

### 4.2.1 Hydrostatic and hydrodynamic forces

$\mathbf{F}_s$  is the hydrostatic force vector given by the displacement from the equilibrium position.  $\mathbf{F}_e$  and  $\mathbf{F}_r$  are the hydrodynamic forces and moments. The excitation force vector  $\mathbf{F}_e$  is due to incident waves. The radiation force vector  $\mathbf{F}_r$  is due to the diffracted wave caused by a body oscillating in water.  $\mathbf{F}_r$  is implemented as a state-space model,

$$\begin{aligned}\dot{\xi}_r &= \mathbf{A}_r \xi_r + \mathbf{B}_r \dot{\eta} \\ \mathbf{F}_r &= \mathbf{C}_r \xi_r + \mathbf{D}_r \dot{\eta}\end{aligned}\quad (4.2.2)$$

$\mathbf{A}_r$ ,  $\mathbf{B}_r$ ,  $\mathbf{C}_r$  and  $\mathbf{D}_r$  are approximated from the frequency-domain solution of the oscillating body, following a procedure proposed by Taghipour, Perez and Moan [45].  $\xi_r$  holds the fluid memory effects that are important when modelling WECs.  $\mathbf{F}_e$  is implemented in a similar way as  $\mathbf{F}_r$ , but with the wave elevation  $\zeta$  as input.

### 4.2.2 Mooring forces

$\mathbf{F}_m$  is the machinery force vector, which in the expanded model becomes the mooring force vector. It is given by the tension, angle and placement of the mooring line. Let  $F$  denote the force in the production rope. Assuming the rope follows a straight line from  $\eta_2$  to  $\eta_3$ , the translational forces become

$$\begin{bmatrix} F_x \\ F_z \end{bmatrix} = F \mathbf{r}_{2/3}^n, \quad (4.2.3)$$

where

$$\mathbf{r}_{2/3}^n = \frac{\mathbf{r}_{2/3}}{\|\mathbf{r}_{2/3}\|}. \quad (4.2.4)$$

$\|\mathbf{r}_{2/3}\|$  is the Euclidean norm of  $\mathbf{r}_{2/3}$  such that  $\mathbf{r}_{2/3}^n$  is a normalized vector. The corresponding pitch moment about the origin is

$$M_y = F_x(\eta_{2z} - \eta_{1z}) - F_z(\eta_{2x} - \eta_{1x}). \quad (4.2.5)$$

$\mathbf{F}_m$  can be written as

$$\mathbf{F}_m = \begin{bmatrix} F_x \\ F_z \\ M_y \end{bmatrix} = F \begin{bmatrix} \mathbf{r}_{2/3}^n \\ \mathcal{R} \end{bmatrix}, \quad (4.2.6)$$

where

$$\mathcal{R} = \left| \begin{bmatrix} \mathbf{r}_{2/3}^n & \mathbf{r}_{1/2} \end{bmatrix} \right| \quad (4.2.7)$$

is the determinant of a matrix with the two vectors in the columns.

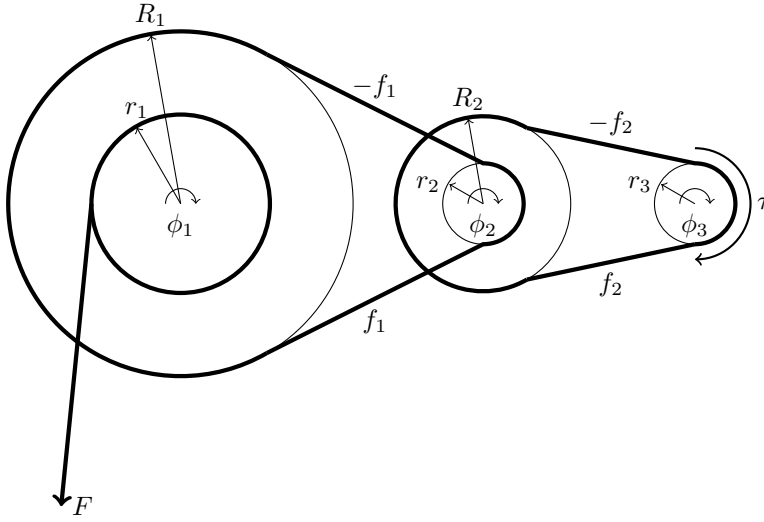


**Figure 4.2:** Schematic diagram of the PTO drive train.  $\phi_1$  represents the winch,  $\phi_2$  represents the middle shaft of the gear and  $\phi_3$  represents the generator.

### 4.2.3 PTO model

The PTO drive train consists of the winch and the generator output shaft connected by a two-stage belt gear, as shown in Figure 4.2.

The belt force has both a static and a dynamic component. The static force is due to pretension and does not create any resulting torque about the DOFs. The dynamic belt force can be both positive and negative, and are sufficiently modelled as linear damper-spring systems,

$$f_1 = \frac{E_1 A_1}{l_1} (\phi_1 R_1 - \phi_2 r_2) + d_1 (\dot{\phi}_1 R_1 - \dot{\phi}_2 r_2), \quad (4.2.8)$$

$$f_2 = \frac{E_2 A_2}{l_2} (\phi_2 R_2 - \phi_3 r_3) + d_2 (\dot{\phi}_2 R_2 - \dot{\phi}_3 r_3). \quad (4.2.9)$$

where tension is defined positive. The first terms of (4.2.8) and (4.2.9) are the spring forces and the second terms are the damping forces.  $E$  is the elastic modulus of each belt,  $A$  is the cross sectional area and  $l$  is the span. The equation of motion for each degree of freedom is

$$I_1 \ddot{\phi}_1 + 2f_1 R_1 = -F r_1, \quad (4.2.10)$$

$$I_2 \ddot{\phi}_2 - 2f_1 r_2 + 2f_2 R_2 = 0, \quad (4.2.11)$$

$$I_3 \ddot{\phi}_3 + 2f_2 r_3 = \tau, \quad (4.2.12)$$

where  $F$  is the rope force,  $\tau$  is the generator torque and  $I_{1-3}$  are the rotational inertias. (4.2.8) - (4.2.12) can be written in matrix form as

$$\mathbf{I}_\phi \ddot{\phi} + \mathbf{D}_\phi \dot{\phi} + \mathbf{K}_\phi \phi = \tau_\phi, \quad (4.2.13)$$

where  $\tau_\phi = [-Fr_1 \ 0 \ \tau]^T$  are the external moments. The system matrices are found as

$$\mathbf{I}_\phi = \begin{bmatrix} I_1 & 0 & 0 \\ 0 & I_2 & 0 \\ 0 & 0 & I_3 \end{bmatrix}, \quad (4.2.14)$$

$$\mathbf{D}_\phi = 2 \begin{bmatrix} d_1 R_1^2 & -d_1 R_1 r_2 & 0 \\ -d_1 r_2 R_1 & d_1 r_2^2 + d_2 R_2^2 & -d_2 R_2 r_3 \\ 0 & -d_2 r_3 R_2 & d_2 r_3^2 \end{bmatrix}, \quad (4.2.15)$$

$$\mathbf{K}_\phi = 2 \begin{bmatrix} \frac{E_1 A_1}{l_1} R_1^2 & -\frac{E_1 A_1}{l_1} R_1 r_2 & 0 \\ -\frac{E_1 A_1}{l_1} r_2 R_1 & \frac{E_1 A_1}{l_1} r_2^2 + \frac{E_2 A_2}{l_2} R_2^2 & -\frac{E_2 A_2}{l_2} R_2 r_3 \\ 0 & -\frac{E_2 A_2}{l_2} r_3 R_2 & \frac{E_2 A_2}{l_2} r_3^2 \end{bmatrix}. \quad (4.2.16)$$

#### 4.2.4 Generalized PTO model

It is desirable to transform the rotational system to an equivalent translational model. By relating all displacements to a common reference it is easier to identify the dominating components of the PTO dynamics. The generalized coordinates are chosen as

$$q_1 = \phi_1 r_1, \quad (4.2.17)$$

$$q_2 = \phi_2 r_2 \frac{r_1}{R_1}, \quad (4.2.18)$$

$$q_3 = \phi_3 r_3 \frac{r_2}{R_2} \frac{r_1}{R_1}. \quad (4.2.19)$$

(4.2.17) - (4.2.19) relate the PTO rotations to the linear motion of the production rope. The generalized displacement vector is defined as  $\mathbf{q} = [q_1 \ q_2 \ q_3]^T$ . The transformation can now be written in matrix form as

$$\mathbf{q} = \mathbf{T}^{-1} \phi, \quad (4.2.20)$$

where

$$\mathbf{T}^{-1} = \begin{bmatrix} r_1 & 0 & 0 \\ 0 & r_2 \frac{r_1}{R_1} & 0 \\ 0 & 0 & r_3 \frac{r_2}{R_2} \frac{r_1}{R_1} \end{bmatrix}. \quad (4.2.21)$$

Since  $\mathbf{T}$  is independent of time it follows that  $\dot{\mathbf{q}} = \mathbf{T}^{-1} \dot{\phi}$ . The equation of motion for the generalized model is written

$$\mathbf{I}_q \ddot{\mathbf{q}} + \mathbf{D}_q \dot{\mathbf{q}} + \mathbf{K}_q \mathbf{q} = \boldsymbol{\tau}_q. \quad (4.2.22)$$

$\mathbf{I}_q$ ,  $\mathbf{D}_q$  and  $\mathbf{K}_q$  are found by requiring conservation of energy. The kinetic energy of the system is

$$E_k = \dot{\phi}^T \mathbf{I}_\phi \dot{\phi} = \dot{\mathbf{q}}^T \mathbf{I}_q \dot{\mathbf{q}}. \quad (4.2.23)$$

Inserting (4.2.20) into (4.2.23) and solving for  $\mathbf{I}_q$  the generalized inertia matrix is found as

$$\mathbf{I}_q = \mathbf{T}^T \mathbf{I}_\phi \mathbf{T}. \quad (4.2.24)$$

$\mathbf{K}_q$  and  $\mathbf{D}_q$  are found in a similar manner from the potential energy and energy dissipation rate, respectively. The generalized force vector is found directly as  $\boldsymbol{\tau}_q = \mathbf{T} \boldsymbol{\tau}_\phi$ . Defining the generalized generator force as

$$u = r_3 \frac{r_2}{R_2} \frac{r_1}{R_1} \tau, \quad (4.2.25)$$

yields  $\boldsymbol{\tau}_q = [-F \ 0 \ u]^T$ .

### 4.2.5 Drive train friction

$\mathbf{D}_q$  is the damping associated with internal displacements in the drive train. Due to torque balance between the pulleys no energy is dissipated through the belts. In addition to the belt damping there is substantial friction in the drive train. The torque loss from generator to winch has been found experimentally for a wide range of generator torques and speeds. The measured values are shown graphically in Figure 4.3.

The drive train torque loss is approximated by a static component, a torque-proportional component and a velocity-proportional component, which in general coordinates can be written

$$f_{loss} = f_0 + d_u u + d_v \dot{q}. \quad (4.2.26)$$

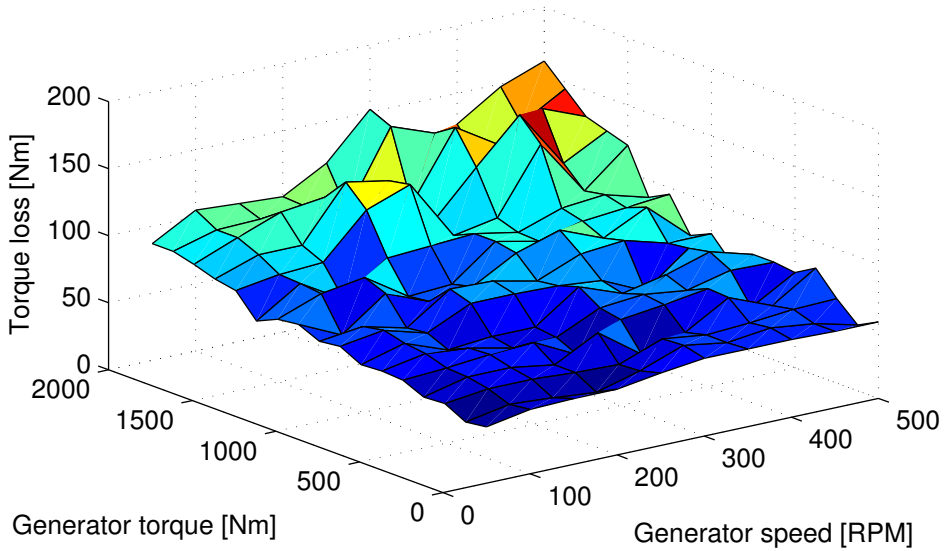


**Figure 4.3:** Drive train torque loss found from experiments.

The coefficients  $d_u$  and  $d_v$  are found by least-squares fitting. The velocity-dependent component is assumed distributed evenly between the gear steps and is included in (4.2.22) as an additional term  $d_v/3$  in the diagonals of  $\mathbf{D}_q$ .

The static and torque-dependent component is implemented as a force loss directly on the control input  $u$ . This can be done using a Coulomb friction model [26], which yields

$$u_{eff} = u - f(u) \tanh(cq_3), \quad (4.2.27)$$

where  $f(u) = f_0 + d_u u$ .  $u_{eff}$  is the effective force acting on the PTO and replaces  $u$  in  $\tau_q$ .  $c$  is set as high as possible without causing instability in the numerical solution.

## 4.3 Mooring line model

The mooring line is modelled as shown in Figure 4.1; two massless springs connected by a point mass. This neglects the hydrodynamic forces acting on the rope sections. This may be an oversimplification of the production rope dynamics, as will be shown by assessing the magnitude of hydrodynamic forces.

### 4.3.1 Assessment of hydrodynamic forces

Morison's equation, as presented by Faltinsen in [18], is a well-known formula for calculating the hydrodynamic forces of submerged cylinders due to incident waves.

The production rope can not be considered a circular cylinder<sup>1</sup>. Instead the equation recommended by DNV-GL (formerly DNV) in RP-C205 will be used [16], where Morison's load formula is presented for slender structural members. The horizontal force on a small longitudinal section  $dl$  of the rope is

$$dF = \rho(1 + C_A)A\dot{v}_x + \frac{1}{2}\rho C_D D v_x |v_x|, \quad (4.3.1)$$

where the added mass coefficient  $C_A$  and drag coefficient  $C_D$  are found in tables.  $A$  is the cross-sectional area and  $D$  is the characteristic cross-sectional dimension (typically the width normal to force direction). The water particle velocity  $v_x$  is found from the velocity potential. The total force is found by integrating along the rope.

Except for very short wave periods the drag force was found to be dominating. Since  $v_x$  reduces exponentially with depth (remember (3.1.5)) the total force on the production rope is approximately the same for different rope lengths. Table 4.1 shows the drag force for different waves.

**Table 4.1:** Maximum drag forces on the upper 15 metres of the production rope for a selection of regular waves.

Wave height [m]	1.0	2.0	4.0	8.0
Wave period [m]	6.0	8.0	10.0	14.0
Drag force [kN]	1.44	2.55	5.53	15.0

Recall that the minimum force of the generator is set to 10 kN. Since the hydrodynamic force is normal to the rope it is probable that the hydrodynamic forces cause significant deflection of the production rope during moderate and rough sea states.

## 4.3.2 Modelling of subsea buoy

### Equation of motion

The subsea buoy is idealized as a point mass and assumed to move in heave and surge only. Since the buoy has the shape of a circular cylinder the hydrodynamic forces acting on the buoy depend on its orientation. This means the hydrodynamic forces must be evaluated in local coordinates. The body-fixed velocity vector  $\boldsymbol{\nu}_3$  is given by the relation

$$\dot{\boldsymbol{\eta}}_3 = \mathbf{R}(\theta_3)\boldsymbol{\nu}_3. \quad (4.3.2)$$

The pitch angle  $\theta_3$  of the buoy is not included as a separate degree of freedom, but approximated as

$$\cos \theta_3 = \frac{\eta_{2z} - \eta_{4z}}{\|\mathbf{r}_{2/4}\|}, \quad (4.3.3)$$

<sup>1</sup>Fred. Olsen wishes to keep information on the production rope classified, so no further details will be given here.

or equivalently

$$\sin \theta_3 = \frac{\eta_{2_x} - \eta_{4_x}}{\|\mathbf{r}_{2/4}\|}, \quad (4.3.4)$$

where  $\mathbf{r}_{2/4}$  is a straight line from the PTO to the anchor. Using this approximation the rotation matrix can be written as

$$\mathbf{R}(\mathbf{r}_{2/4}) = \frac{1}{\|\mathbf{r}_{2/4}\|} \begin{bmatrix} \eta_{2_z} - \eta_{4_z} & \eta_{2_x} - \eta_{4_x} \\ \eta_{2_x} - \eta_{4_x} & \eta_{2_z} - \eta_{4_z} \end{bmatrix}. \quad (4.3.5)$$

The 2DOF differential equation for the subsea buoy becomes

$$\dot{\boldsymbol{\eta}}_3 = \mathbf{R}(\mathbf{r}_{2/4})\boldsymbol{\nu}_3, \quad (4.3.6)$$

$$\mathbf{M}_{RB_3}\dot{\boldsymbol{\nu}}_3 = \mathbf{F}_{m_3} + \mathbf{F}_{hyd} + \mathbf{F}_{s_3}. \quad (4.3.7)$$

$\mathbf{M}_{RB_3}$  is the rigid body mass matrix,  $\mathbf{F}_{m_3}$  are the forces from the two rope sections,  $\mathbf{F}_{s_3}$  are the static forces due to gravity and buoyancy and  $\mathbf{F}_{hyd_3}$  are the hydrodynamic forces. Here we have neglected the Coriolis forces that arise when the body-fixed frame rotates relative to the earth-fixed frame, a natural consequence of neglecting the pitch dynamics

### Hydrodynamic forces

A simple procedure for evaluating the forces on the subsea buoy can be obtained by combining a procedure recommended by DNV-GL with the theory given by Faltinsen in [18]. Again according to DNV RP-C205 [16] the hydrodynamic force on a small 3-dimensional body at rest affected by waves and current can be approximated as

$$F_i = \rho V 1 + C_{A_i} \dot{v}_i + \frac{1}{2} \rho C_{D_i} S_i v_i |v_i|, \quad (4.3.8)$$

where  $i$  is the force direction,  $V$  is the volume of the object,  $S_i$  is the projected area normal to the force direction, and  $v_i$  is the water particle velocity evaluated at the volumetric centre of the body. We recognise this as a Morison type formulation, which according to Faltinsen [18] can be expanded to include body motion as

$$F_i = \rho V C_{A_i} (\dot{v}_i - \dot{\nu}_i) + \frac{1}{2} \rho C_{D_i} S_i (v_i - \nu_i) |v_i - \nu_i| + \rho V \dot{\nu}_i, \quad (4.3.9)$$

where  $\nu_i$  and  $\dot{\nu}_i$  is the body velocity and acceleration in the force direction. The first and second terms are the added mass force and drag force, which depend on the relative velocity between the body and the water. The last term is the force generated by the undisturbed waves (in hydrodynamic literature referred to as Froude-Krylov forces), and thus does not depend on the body motion.

The hydrodynamic force vector can be written in matrix form as

$$\mathbf{F}_{hyd} = \mathbf{M}_A(\dot{\mathbf{v}} - \dot{\boldsymbol{\nu}}_3) + \mathbf{D}_{drag}(\mathbf{v} - \boldsymbol{\nu}_3)|\mathbf{v} - \boldsymbol{\nu}_3| + \mathbf{M}_{FK}\dot{\mathbf{v}}, \quad (4.3.10)$$

where  $\mathbf{v}$  is the two-dimensional water particle velocity in the body fixed frame.  $\mathbf{M}_A$ ,  $\mathbf{D}_{drag}$  and  $\mathbf{M}_{FK}$  are diagonal matrices representing the added mass, hydrodynamic drag and Froude-Krylov forces, respectively.

### Mooring forces on subsea buoy

The mooring force in global coordinates is given by the tension and angle of the two rope sections as

$$\begin{bmatrix} F_x \\ F_z \end{bmatrix} = F \mathbf{r}_{2/3}^n - F_l \mathbf{r}_{2/3}^n, \quad (4.3.11)$$

where  $F_l$  is the tension of the lower rope. The force vector in local coordinates is

$$\mathbf{F}_{m_3} = \mathbf{R}_3^{-1}(\mathbf{r}_{2/4}) \begin{bmatrix} F_x \\ F_z \end{bmatrix}. \quad (4.3.12)$$

The calculation is simplified by  $\mathbf{R}^{-1} = \mathbf{R}^T$ , since the rotation matrix is skew-symmetric [19].

## 4.3.3 Mooring rope tension

### Mechanical properties

Both ropes are characterized by progressive stiffness and low hysteretic damping. There is uncertainty in the mechanical properties, and to complicate matters further the properties are time-varying. This justifies the use of a simplified linear elastic model similar to the one used for the belts.

Assuming negligible stiffness in compression  $F$  and  $F_l$  can be written on the form

$$F = \begin{cases} E_\epsilon A \epsilon + E_{\dot{\epsilon}} A \dot{\epsilon} & \epsilon > 0 \\ 0 & \epsilon < 0 \end{cases}, \quad (4.3.13)$$

where  $\epsilon$  is the rope elongation,  $E_\epsilon$  is the stiffness modulus and  $A$  is the cross sectional area.  $E_{\dot{\epsilon}}$  is the loss modulus [29], and can be found by estimating the dissipated energy during cyclic loading. Values for  $E_{\dot{\epsilon}}$  were hard to come by. Also, the expression for  $\dot{\epsilon}$  of the production rope (the time derivative of (4.3.17)) becomes computationally intensive. For these reasons the combined damping of the rope sections were included as a linear term  $d_{lin}\nu_2$  acting in the longitudinal direction of the subsea buoy.

### Elongation of lower mooring rope

For the lower rope section the elongation is given by the displacement of the subsea buoy as

$$\epsilon_l = \frac{\|\mathbf{r}_{3/4}\| - l_{l_0}}{l_{l_0}}, \quad (4.3.14)$$

where  $l_{l_0} = \|\boldsymbol{\eta}_{4_0} - \boldsymbol{\eta}_{3_0}\|$  is the unstretched (initial) length of the rope.

### Elongation of production rope

We get a similar equation for the production rope, but now the unstretched length is a function of the winding of the rope;

$$l(\phi_1) = \|\mathbf{r}_{2_0/3_0}\| - r_1 \phi_1, \quad (4.3.15)$$

where  $\|\mathbf{r}_{2_0/3_0}\|$  is the initial rope length. (4.3.15) can also be written

$$l(q_1) = \|\mathbf{r}_{2/3_0}\| - q_1. \quad (4.3.16)$$

The rope elongation is then found as

$$\epsilon = \frac{\|\mathbf{r}_{2/3}\| - l(q_1)}{l(q_1)}. \quad (4.3.17)$$

## 4.4 Implementation and numerical solver

The numerical model consists of the floater, the mooring line and the PTO, which are coupled by the force in the production rope. The system is implemented in SIMULINK [5]. Due to the large range of inertias the model becomes very stiff. Simulations were done using two different solvers implemented in MATLAB; the *ode15s* solver with a relative error tolerance of  $10^{-4}$  and *ode23tb* with a crude relative error tolerance of  $10^{-3}$ . Both solvers are well suited for stiff systems. *ode23tb* was much faster and with no significant reduction in performance.

Parameters of the mooring line and PTO model are given in Appendix C.

## 4.5 Model verification

The model is verified by comparing randomly chosen waves in similar sea states. This allows only for a qualitative comparison between simulations and recorded data. The most characteristic behavior of Lifesaver are the oscillations in the rope velocity. Recorded velocity oscillations are shown in Figure 4.4. Simulated results for a similar wave are shown in Figure 4.5. The simulation model captures the system dynamics sufficiently for

control system development. The simulated oscillations are larger in amplitude and appear to occur more frequently than in the real system. This indicates that the simulation model behaves worse than the real system, in which case it can be considered conservative.

The model should be further verified before it is used as a design tool. This may be done by performing a step response test on Lifesaver in calm water, such that the main excitation is from the generator. The dominant system parameters can then be calculated from the transient response. If the steps in generator force are both positive and negative non-linearities in the system can also be identified.

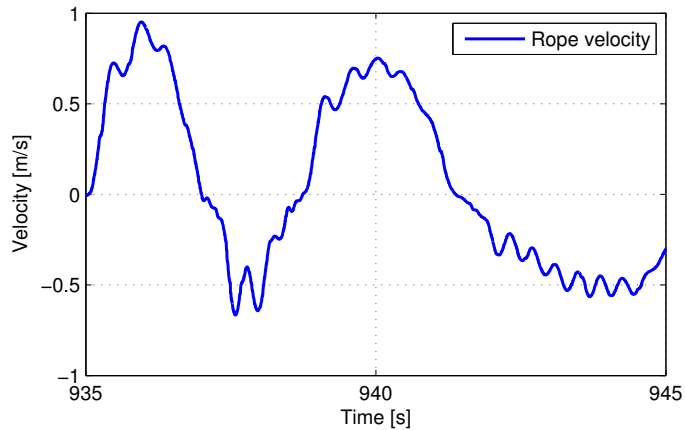


**Figure 4.4:** Characteristic velocity oscillations recorded during testing.

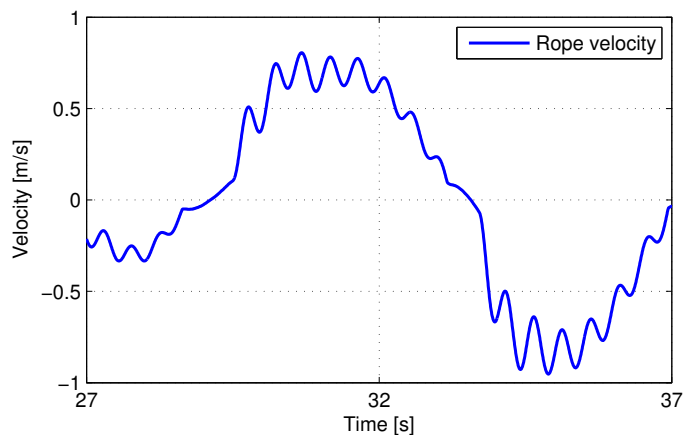


**Figure 4.5:** Characteristic velocity oscillations from simulations. Note; the simulated wave was randomly generated and does not compare to the wave during testing.

# Chapter 5

## System analysis

In this chapter the dominating components of the system dynamics are identified through a frequency analysis and sensitivity analysis. The knowledge gained is then used to develop a Control Plant Model (CPM) for use in control system design.

### 5.1 Linearized model

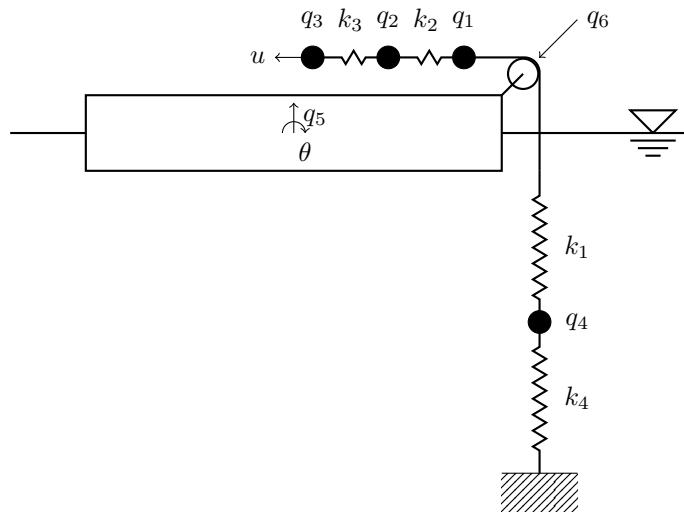


**Figure 5.1:** Linearized model of Lifesaver with a single PTO and mooring line.  $u$  is the generator force.

By restricting the surge motion of both the floater and the subsea buoy and assuming small motions in pitch a linearized model can be developed. The linearized model is shown in Figure 5.1, where the generalized coordinates  $q_1 - q_6$  are defined.  $q_1 - q_3$  correspond

to the generalized coordinates introduced previously.  $q_4$  and  $q_5$  is the heave motion of the subsea buoy and floater respectively.

$q_6 \approx -\|\mathbf{r}_{1/2}\|\theta$  is the motion of the PTO due to pitch rotation, where  $\mathbf{r}_{1/2}$  is the distance from the rotation axis to the PTO, as defined previously. The corresponding inertia is

$$m_6 = I_6\|\mathbf{r}_{1/2}\|^2, \quad (5.1.1)$$

where  $I_6$  is the moment of inertia in pitch. The corresponding stiffness is

$$k_6 = k_\theta\|\mathbf{r}_{1/2}\|^2, \quad (5.1.2)$$

where  $k_\theta$  is the waterplane stiffness in pitch. Further, let  $k_5$  denote the waterplane stiffness in heave.

The PTO, the subsea buoy and the floater are coupled by the force in the production rope, which in the linearized model becomes

$$F = k_1(q_1 - q_2 + q_5 + q_6). \quad (5.1.3)$$

The equation of motion can be written directly as

$$\mathbf{M}\ddot{\mathbf{q}} + \mathbf{D}\dot{\mathbf{q}} + \mathbf{K}\mathbf{q} = \mathbf{u}, \quad (5.1.4)$$

where  $\mathbf{q} = [q_1, \dots, q_6]^T$  and  $\mathbf{u} = [0 \ 0 \ u \ 0 \ 0 \ 0]^T$ .

$\mathbf{M} = \text{diag}(m_1, \dots, m_6)$  is the inertia associated with each degree of freedom. Added mass is included in  $m_4 - m_6$ . The stiffness is found from (5.1.3) and Figure 5.1 as

$$\mathbf{K} = \begin{bmatrix} k_1 + k_2 & -k_2 & 0 & -k_1 & k_1 & k_1 \\ -k_2 & k_2 + k_3 & -k_3 & 0 & 0 & 0 \\ 0 & -k_3 & k_3 & 0 & 0 & 0 \\ -k_1 & 0 & 0 & k_1 & -k_1 & -k_1 \\ k_1 & 0 & 0 & -k_1 & k_1 + k_5 & k_1 \\ k_1 & 0 & 0 & -k_1 & k_1 & k_1 + k_6 \end{bmatrix}. \quad (5.1.5)$$

The linear damping matrix  $\mathbf{D}$  has the same form as  $\mathbf{K}$ , but the values are both uncertain and difficult to evaluate. For  $d_2$  and  $d_3$  the linear damping terms of the numerical model were used. For  $d_5$  and  $d_6$  no linear terms exist, while  $d_1$  and  $d_4$  consists of both the unknown rope damping and the nonlinear damping from the subsea buoy. The unknown damping terms are in any case assumed low such that the dynamic behavior of the system can be sufficiently evaluated without correct values. All parameters used are shown in Table 5.1.

**Table 5.1:** Parameters of the linearized model, with the associated component listed above. The abbreviations are gen.;generator, p.rope; production rope, l. rope; lower rope.

Mass [kg]					
winch	gear	gen.	buoy	heave	pitch
$m_1$	$m_2$	$m_3$	$m_4$	$m_5$	$m_6$
406	450	2235	456	$2.21 \cdot 10^5$	$1.66 \cdot 10^8$

Stiffness [N/m]					
p. rope	1. belt	2. belt	l. rope	heave	pitch
$k_1$	$k_2$	$k_3$	$k_4$	$k_5$	$k_6$
$1.67 \cdot 10^6$	$1.18 \cdot 10^8$	$2.44 \cdot 10^8$	$7.51 \cdot 10^5$	$1.23 \cdot 10^6$	$9.86 \cdot 10^8$

Damping [Nm/s]					
p. rope	1. belt	2. belt	l. rope	heave	pitch
$d_1$	$d_2$	$d_3$	$d_4$	$d_5$	$d_6$
3330	$6.41 \cdot 10^6$	$1.33 \cdot 10^7$	1503	$1.23 \cdot 10^3$	$9.86 \cdot 10^5$

## 5.2 Frequency analysis

The linearized model can be written in state-space form as

$$\begin{bmatrix} \dot{\mathbf{q}} \\ \ddot{\mathbf{q}} \end{bmatrix} = \mathbf{A} \begin{bmatrix} \mathbf{q} \\ \dot{\mathbf{q}} \end{bmatrix} + \mathbf{B}u. \quad (5.2.1)$$

$$(5.2.2)$$

The system matrix  $\mathbf{A}$  is

$$\mathbf{A} = \begin{bmatrix} \mathbf{0}_{6 \times 6} & \mathbf{I}_{6 \times 6} \\ -\mathbf{M}^{-1}\mathbf{K} & -\mathbf{M}^{-1}\mathbf{D} \end{bmatrix}, \quad (5.2.3)$$

where  $\mathbf{I}_{6 \times 6}$  is the identity matrix. The input matrix  $\mathbf{B}$  is

$$\mathbf{B} = [\mathbf{0}_{1 \times 8} \quad 1/m_3 \quad \mathbf{0}_{1 \times 3}]^T. \quad (5.2.4)$$

The frequencies of the system can be found from the eigenvalues of  $\mathbf{A}$  [11]. To find the natural frequencies set  $\mathbf{D} = \mathbf{0}_{6 \times 6}$ <sup>1</sup>.

The natural frequencies are given in Table 5.2, along with the main drivers. It is possible to find the main drivers analytically, e.g. from the individual transfer functions of each degree of freedom or from oscillation modes. Due to the large range of frequencies

<sup>1</sup>The damping parameters are used in the model comparison in section 5.5

this was numerically challenging. Instead an ad hoc procedure was used, where the DOF of interest was isolated by fixing the other DOFs.

The lowest frequencies are related to the heave and pitch motion of the floater. The frequency of approximately 2 Hz is the interesting one. It corresponds to the oscillations recorded during testing, and is the lowest natural frequency of the combined PTO and mooring line. At this frequency the full system,  $q_1 - q_4$ , oscillate together. The frequency is in large caused by the elasticity of the mooring and the combined inertia of the PTO.

11.9 Hz is the natural frequency of the subsea buoy when fixing the PTO and floater. 75.5 Hz is associated with the winch, while 158 Hz is associated with the gearbox.

**Table 5.2:** Natural frequencies of the linearized system, with the associated main drivers.

Frequency [Hz]	0.37	0.39	1.99	11.9	75.5	158
Main driver	heave	pitch	PTO	buoy	winch	gear

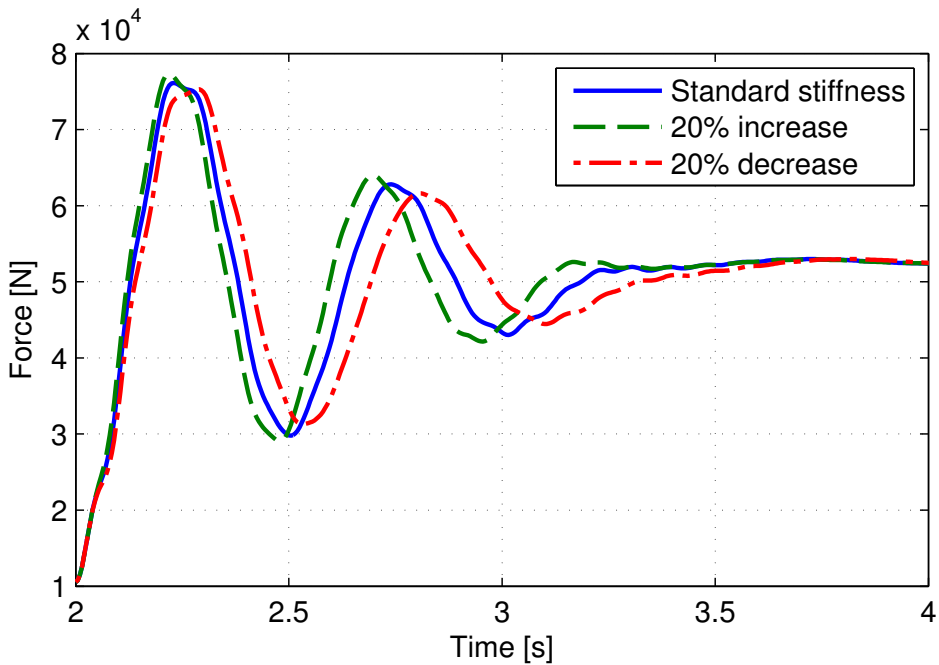


**Figure 5.2:** Step response of rope force for values of  $k_4$ .

### 5.3 Sensitivity analysis

The main uncertainty of the model is related to the mechanical properties of the two rope sections and the hydrodynamic added mass of the subsea buoy. A sensitivity analysis was

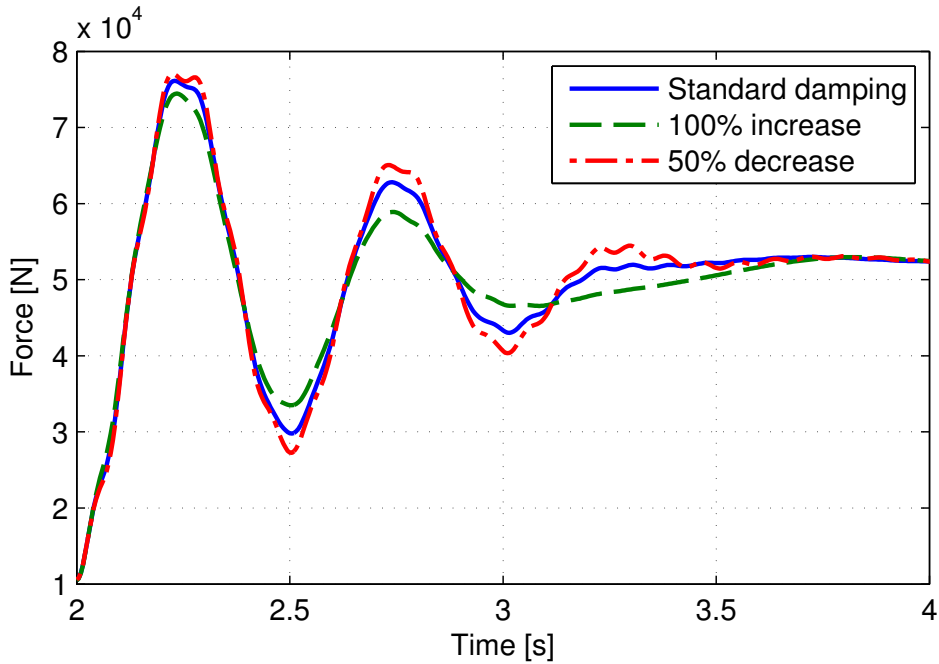


**Figure 5.3:** Step response of rope force for different values of rope damping.

performed by comparing the response in rope force for a step in generator force. Since the main elasticity is found in the lower mooring rope the stiffness sensitivity was assessed by altering  $k_4$ . Results are shown in Figure 5.2 - 5.4. The oscillation frequency is, not surprisingly, sensitive to change in stiffness. Mooring line damping has an effect on the force oscillations. Uncertainty related to the added mass of the subsea buoy does not have a significant impact on the force oscillations.

## 5.4 Control Plant Model

A CPM needs to capture the main dynamics of a process without being overly complicated. From Table 5.1 we note that

$k_6 \gg k_5$  and  $m_6 \gg m_5$ , i.e. the mooring-induced floater motion is much larger in heave than pitch, indicating that the pitch dynamics can be neglected.

$k_3, k_2 \gg k_1, k_4$ , i.e. stiffness of belts are much higher than stiffness of ropes, indicating that the drive train dynamics can be neglected.

$m_3 \gg m_4$ , i.e. the generator inertia alone is much larger than the subsea buoy, indicating that the subsea buoy can be neglected.

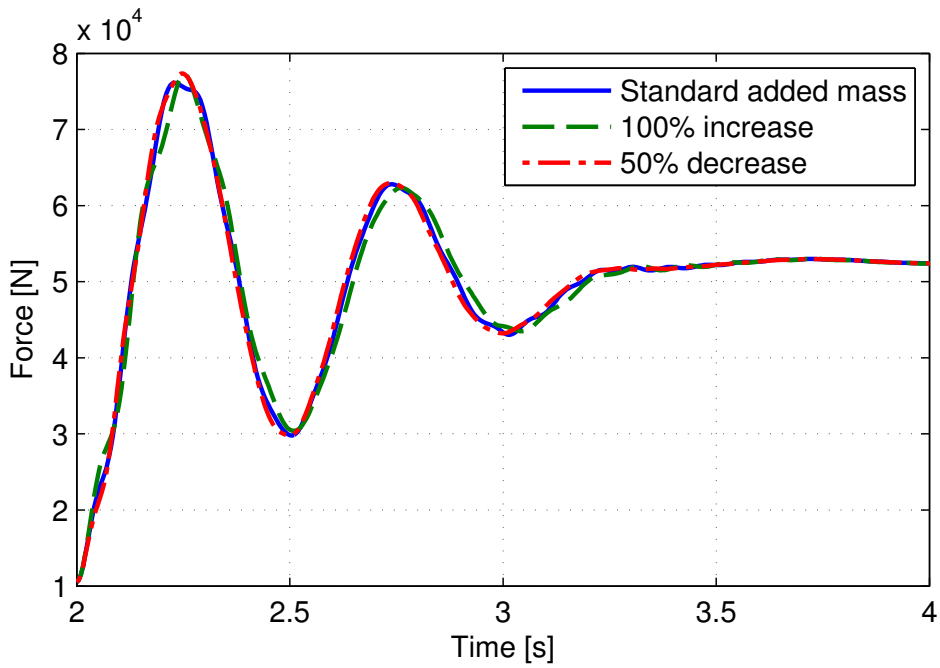


**Figure 5.4:** Step response of rope force for different values of added mass of subsea buoy.

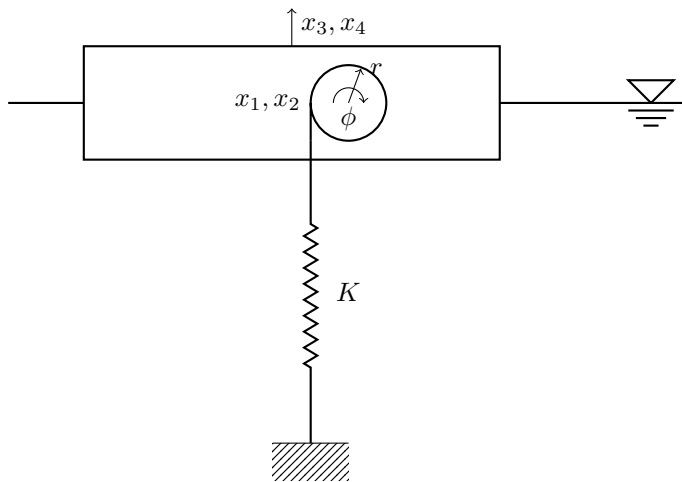


**Figure 5.5:** Illustration of the CPM.

The resulting CPM when neglecting pitch, subsea buoy and the gearbox is shown in Figure 5.5.  $x_1$  is defined as the rope reeling,  $x_2 = \dot{x}_1$  as the rope velocity,  $x_3$  as the vertical

position of the floater and  $x_4 = \dot{x}_3$  as the vertical velocity of the floater.

The combined PTO inertia is

$$M = m_1 + m_2 + m_3 = 3091 \text{ [kg]}. \quad (5.4.1)$$

The equivalent stiffness of the mooring line is

$$K = \left( \frac{1}{k_1} + \frac{1}{k_4} \right)^{-1} = 5.18 \times 10^5 \text{ [N/m]}. \quad (5.4.2)$$

The equation of motion can be written.

$$\begin{bmatrix} M & 0 \\ 0 & m_5 \end{bmatrix} \begin{bmatrix} \dot{x}_2 \\ \dot{x}_4 \end{bmatrix} + \begin{bmatrix} D & 0 \\ 0 & d_5 \end{bmatrix} \begin{bmatrix} x_2 \\ x_4 \end{bmatrix} + \begin{bmatrix} K & K \\ K & k_5 + K \end{bmatrix} \begin{bmatrix} x_1 \\ x_3 \end{bmatrix} = \begin{bmatrix} u \\ 0 \end{bmatrix} \quad (5.4.3)$$

$D = d_v$  is chosen, i.e. the linear friction of the drive train. The mooring line damping, which is uncertain, has thus been omitted. This means we have no terms in the diagonals of the damping matrix.

### 5.4.1 Simplified Control Plant Model

Due to the difference in inertia between floater and PTO  $x_1$  responds much faster to changes in rope force than  $x_3$ . This means that at sufficiently small time scales, approximately smaller than 0.3 seconds, the floater motion can be considered given. Then a simplified CPM with only one DOF is

$$M\dot{x}_2 + Dx_1 + K(x_1 + x_3) = u \quad (5.4.4)$$

where  $x_3$  can be considered an unknown disturbance. The natural frequency of the simplified CPM,

$$F_n = \frac{\sqrt{K/M}}{2\pi} = 2.06 \text{ [Hz]}, \quad (5.4.5)$$

is only  $\approx 3.5\%$  larger than the corresponding frequency of the linearized model. The discrepancy is smaller than the uncertainty of the values.

## 5.5 Comparison of models

A comparison of the three models can be done by plotting the transfer function in a Bode plot [11]. Figure 5.6 shows the transfer function from control input to rope force. The slight discrepancy between the CPMs and the linearized model around the critical frequency of the 2 Hz is due to the subsea buoy, which adds both inertia and damping. The CPMs show very similar response for frequencies above 1 Hz.

Another way to assess the model dynamics is by the step response. The generator force is given a step from 0 to 10 kN. The resulting displacement, as measured at the generator, is shown in Figure 5.7. The dominant oscillations are similar in amplitude and frequency, but the linearised model and CPM also include a low-frequency motion due to motion of the floater.

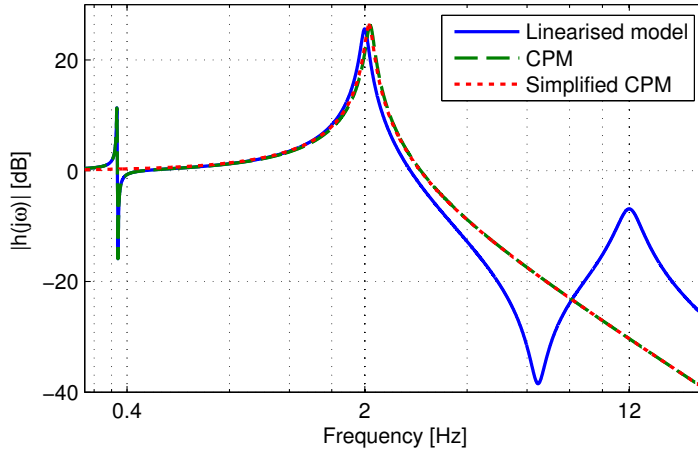


**Figure 5.6:** Bode magnitude plot of the transfer functions from  $u$  to  $F$  of the different models.

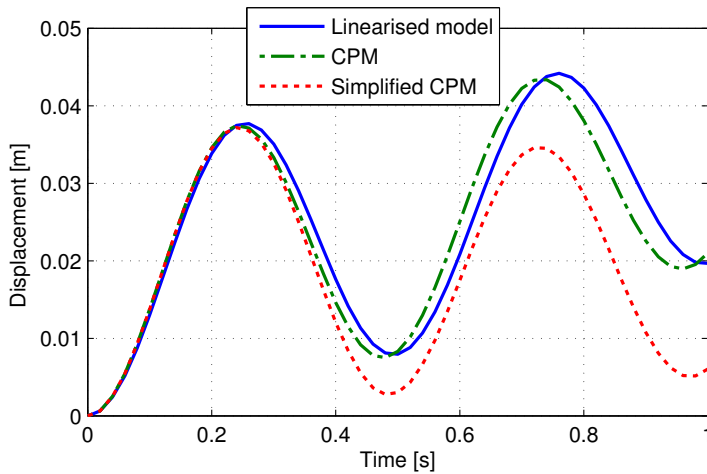


**Figure 5.7:** Response in the generator displacement for a step in generator force from 0 to 10 kN.

# Chapter 6

## Control system development

This chapter starts with the formulation of two state observers. Next a DT CPM is developed to evaluate stability for different control systems. Finally four different control schemes are proposed:

**Reference model:** Mitigates rope force oscillations by limiting the generator force gradient.

**PD feedback:** Dampens oscillations by Proportional-Derivative (PD) feedback of the rope force.

**Hysteretic control:** A control algorithm with the potential of both increasing power output and robustness.

**Extremum seeking:** An optimization algorithm which can be used in combination with any of the aforementioned controllers.

### 6.1 Preliminaries

#### 6.1.1 Reference table

Table 6.1 containing key parameters and definitions used in the control system design is provided as a reference. The states are defined in Figure 5.5.

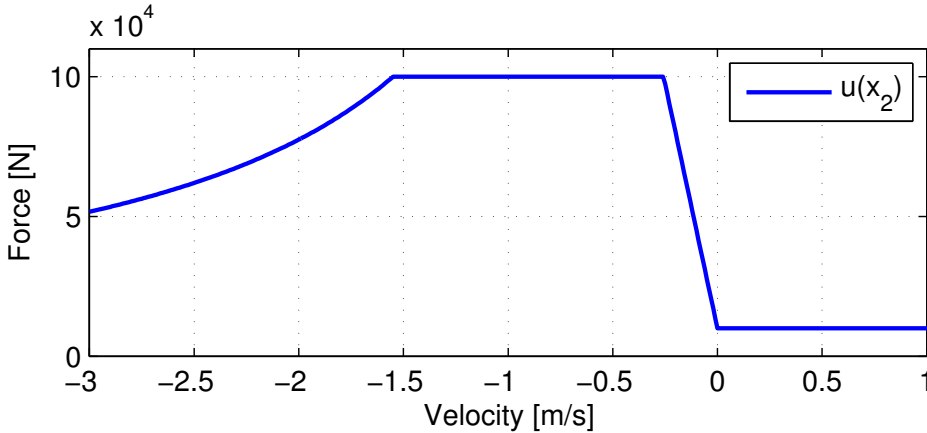
#### 6.1.2 Current control system

Lifesaver operates as a passive converter. The generator force follows the force-velocity relation shown in Figure 6.1. Recall that  $x_2$  is defined positive when reeling in rope, such that negative velocities corresponds with upwards motion. Three operating domains can be identified:

**Damped domain:** The region from approximately  $-0.26 < x_2 < 0$  follows the nominal control law

**Table 6.1:** Key parameters used in control system development.

<b>States</b>	$x_1$	Rope displacement
	$x_2 = \dot{x}_1$	Rope velocity
	$x_3$	PTO vertical position
	$x_4 = \dot{x}_3$	PTO vertical velocity
<b>Output</b>	$F = K(x_1 + x_3)$	Rope force
<b>Input</b>	$u$	Generator force
<b>Measurements</b>	$y_1 = x_1 + v_1$	$v_1$ is measurement error
	$y_2 = x_2 + v_2$	$v_2$ is measurement error
<b>System parameters</b>	$M = 3091$	Drive train inertia [kg]
	$D = 897$	Drive train friction [Ns/m]
	$K = 5.18 \times 10^8$	Rope stiffness [N/m]
	$\omega_n = \sqrt{K/M} \approx 13$	Natural frequency [rad/s]
	$f(u) = f_0 + d_u u$	Nonlinear friction [N]
<b>Control parameters</b>	$B \approx 300 \times 10^3$	Damping coefficient [Ns/m]
	$h = 1/200$	Sampling time [s]

**Figure 6.1:** Generator force  $u$  as a function of velocity  $x_2$ , with  $F_{min} = 10$  kN,  $F_{max} = 100$  kN and  $B = 350$  kNs/m.

$$u = u_{min} - Bx_2, \quad (6.1.1)$$

where  $B = 350$  kNs/m is used in Figure 6.1.

**Undamped domain:** Force saturation occurs at  $u_{min} = 10$  kN to ensure that the rope is kept taut, and at  $u_{max} = 100$  kN which is the mechanical limit of the drive train. When saturated the force is independent of velocity, which results in an undamped system.

**Negatively damped domain:** At -1.55 m/s another saturation mechanism occurs. The generator reaches its power limit and is no longer able to deliver the desired torque. If  $x_2$  continues to decrease  $u$  also decreases, resulting in a negatively damped system.

$B$  should be chosen such that the converted electrical power is maximised. Optimal  $B$  depends on conversion efficiency, system dynamics and sea state. The generator efficiency is shown in Figure 6.2 along with the two saturation mechanisms.  $B = 350 \text{ kNs/m}$  was chosen initially. During testing  $F_{max}$  has been reduced to 50 kN and  $B$  to about 250 kNs/m (different values have been used throughout the test period). For these values force saturation occurs already at  $\approx 0.16 \text{ m/s}$ , while power saturation occurs at  $\approx 3 \text{ m/s}$ .

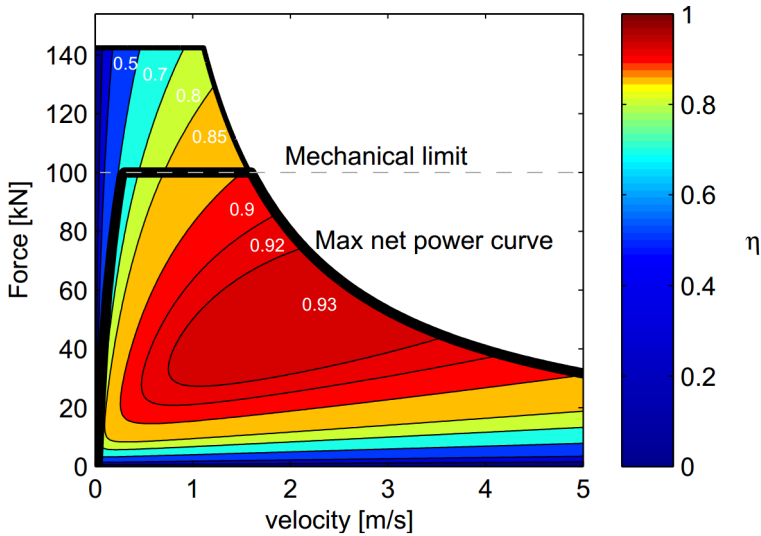


**Figure 6.2:** Efficiency plot for the generator. The thick line corresponds to the force-velocity plot in Figure 6.1. Note: the velocity direction is defined opposite of that used elsewhere in this thesis. Courtesy Fred. Olsen.

### Remark on negatively damped domain

Power saturation has not been properly addressed in this thesis. Obviously negative damping results in unstable behavior. The following update law for  $B$  is proposed to increase robustness when power saturation occurs;

$$B = \frac{u_{min} - u(x_{2,min})}{x_{2,min}}, \quad (6.1.2)$$

where  $x_{2,min}$  is the minimum recorded value of  $x_2$  and  $u(x_{2,min})$  is the force the generator can deliver at  $x_{2,min}$ . This ensures a sufficiently low  $B$  such that power saturation does

not occur before  $x_{2,min}$ , thus avoiding negative damping.  $x_{2,min}$  can be reset for each wave or follow the update law

$$x_{2,min}[k+1] = \begin{cases} x_2[k] & x_2[k] < x_{2,min}[k] \\ (1 - h/T_f)x_{2,min}[k] & x_{2,min}[k] < x_2[k] \end{cases}. \quad (6.1.3)$$

where  $T_f$  is a time constant which decides how fast  $x_{2,min}$  is increased.

### 6.1.3 Implementation

The generator force is set to follow the damping coefficient in the frequency transformer, which operates at several kHz. This is possible since the control law depends only on the velocity such that the generator operates as a pure damper. More sophisticated control systems may have to be imposed at a higher level with lower operating frequency.

### 6.1.4 Sensors

In an attempt to keep costs down the only measurements available for the control system are the rotation and angular velocity of the generator, both of which are measured by an encoder. In the generalized coordinates of the CPM the measurements are  $y_1 = x_1 + v_1$  and  $y_2 = x_2 + v_2$ .

It has not been possible to identify the sensor noise variance, but both measurements are of high quality. The measurements are currently being sampled at a frequency of 200 Hz. This is also the frequency chosen for both the observers and controllers considered in this thesis.

## 6.2 Observers

For control purposes an estimate of the rope force, and in some cases also the motion of the floater, is desired. Two observers are proposed. The first estimates  $F$  from acceleration, and is easy to design and implement. The second, a model-based Kalman filter, is more computationally intensive and time-consuming to implement, but provides better estimates with less delay.

### 6.2.1 Kinematic observer

The rope force can be estimated from the PTO dynamics as

$$\hat{F}[k] = u[k] - M\hat{a}[k] - D\hat{x}_2[k] - f(u[k])\text{sign}(\hat{x}_2[k]), \quad (6.2.1)$$

where  $\hat{a}$  is the estimated acceleration. Since  $\hat{F}$  is estimated using the kinematic relation  $a = \dot{x}_2$  this can be considered a kinematic observer. In the simulation model  $f(u)$  was implemented as Coulomb friction. In the control system it is sufficient to model it as

opposing motion, hence  $f(u[k])\text{sign}(\hat{x}_2[k])$ . Eulers backward difference method [44] yields an explicit expression for  $\hat{a}$ ;

$$\hat{a}[k] = \frac{\hat{x}_2[k] - \hat{x}_2[k-1]}{h}, \quad (6.2.2)$$

where  $h$  is the sampling time. This requires a smooth  $\hat{x}_2$ , which can be obtained by low-pass filtering the measured velocity. One possible choice for filter is the second-order Butterworth filter,

$$F_{lp}(s) = \frac{\omega_c^2}{(s^2 + \sqrt{2}\omega_c s + \omega_c^2)}, \quad (6.2.3)$$

where  $\omega_c$  is the filter cut-off frequency. According to [44] the corresponding discrete filter is constructed by replacing  $s$  with

$$s = \frac{2(z-1)}{h(z+1)}. \quad (6.2.4)$$

$\omega_c$  must be chosen smaller than the Nyquist frequency  $\omega_N = \pi/h$ , and significantly larger than  $\omega_n$ .  $\omega_c = 8 \times 2\pi$  yielded satisfactory results.

## 6.2.2 Model based observer

A more sophisticated observer can be constructed by utilizing the knowledge of the system. The process is adequately described by linear equations, making it suitable for a Kalman filter observer. The Kalman filter can be constructed in many ways depending on how uncertainty and unmodelled forces are included. The CPM illustrated in Figure 5.5 is used for the Kalman filter.

### System equations

The rope force can be written

$$F = K(x_1 + x_3) + b_1, \quad (6.2.5)$$

where  $b_1$  is an unknown time-varying bias that accounts for modelling error and unknown forces. The PTO dynamics can be written

$$\dot{x}_1 = x_2, \quad (6.2.6)$$

$$M\dot{x}_2 = -Dx_2 - F + u - f(u)\text{sign}(x_2). \quad (6.2.7)$$

The floater dynamics can be modelled as

$$\dot{x}_3 = x_4, \quad (6.2.8)$$

$$m_5 \dot{x}_4 = -d_5 x_4 - F + b_2, \quad (6.2.9)$$

where  $m_5$  and  $d_5$  is the inertia and damping in heave.  $b_2$  represents the unmodelled forces. The water plane stiffness is omitted since the instantaneous wave elevation is unknown. The main damping of Lifesaver is from the PTOs, which is difficult to evaluate due to the complex coupled dynamics. As such  $d_5$  can be considered a tuning parameter in the Kalman filter.  $d_5 = 10 \times 10^3$  was used in implementation.

### Bias model

The bias states are modelled as random processes. A first order Gauss-Markov model [13],

$$\dot{b}_i = -\frac{1}{T_{bi}} b_i + w_i, \quad i = 1, 2, \quad (6.2.10)$$

was chosen for both  $b_1$  and  $b_2$ .  $T_{bi}$  is the bias time constant, while  $w_i$  is zero-mean Gaussian white noise.

$b_1$  includes error in the mooring line stiffness and drive train friction, and is probably well described by (6.2.10).  $b_2$ , on the other hand, is dominated by the hydrostatic and hydrodynamic forces, which we know oscillate with the mean wave period. Additional states could be included to better represent the wave forces, but this would add complexity. The proposed model was found to be sufficient.

### State space formulation

We define the state vector as  $\mathbf{x} = [x_1 \ x_2 \ x_3 \ x_4 \ b_1 \ b_2]^T$ . Further we have the measurement vector  $\mathbf{y} = [y_1 \ y_2]$ , measurement noise vector  $\mathbf{v} = [v_1 \ v_2]$  and process noise vector  $\mathbf{w} = [w_1 \ w_2]$ . (6.2.7) is linearized by including the nonlinear term  $f(u)\text{sign}(x_2)$  in the input using  $y_2$  directly in the argument. This yields

$$\mathbf{u} = u - f(u)\text{sign}(y_2). \quad (6.2.11)$$

Since  $y_2$  is measured with high accuracy this is a valid approximation. (6.2.5)-(6.2.11) can be written in matrix form as

$$\dot{\mathbf{x}} = \mathbf{A}\mathbf{x} + \mathbf{B}\mathbf{u} + \mathbf{E}\mathbf{w}, \quad (6.2.12)$$

$$\mathbf{y} = \mathbf{C}\mathbf{x} + \mathbf{v}. \quad (6.2.13)$$

The obtained system is observable, and thus an observer can be constructed to recreate the unmeasured states.

### Observer equations

According to [44] the discrete time Kalman filter equations for an LTI system can be written

$$\hat{\mathbf{x}}[k+1] = \Phi \hat{\mathbf{x}}[k] + \Delta \mathbf{u}[k] + \mathbf{K}[k](\mathbf{y}[k] - \hat{\mathbf{y}}[k]), \quad (6.2.14)$$

$$\hat{\mathbf{y}}[k+1] = \mathbf{C} \hat{\mathbf{x}}[k+1], \quad (6.2.15)$$

where  $\phi$  and  $\Delta$  are the discretized versions of  $\mathbf{A}$  and  $\mathbf{B}$ , respectively. The ZOH discretization method was used in implementation.  $\hat{\mathbf{x}}$  is an estimate of  $\mathbf{x}$ .  $\mathbf{K}[k](\mathbf{y}[k] - \hat{\mathbf{y}}[k])$  is a feedback term which drives  $\hat{\mathbf{y}}$  towards  $\mathbf{y}$ . For a time-invariant system the steady-state Kalman filter gain is found as [13]

$$\mathbf{K}_\infty = \mathbf{X} \mathbf{C} (\mathbf{C} \mathbf{X} \mathbf{C}' + \mathbf{R})^{-1}, \quad (6.2.16)$$

where  $\mathbf{X}$  is the solution of the discrete time Riccati equation;

$$\Phi^T \mathbf{X} \Phi - \mathbf{X} - \Phi^T \mathbf{X} \Delta (\Delta^T \mathbf{X} \Delta + \mathbf{R})^{-1} \Delta^T \mathbf{X} \Phi + \mathbf{Q} = \mathbf{0}. \quad (6.2.17)$$

$\mathbf{R}$  and  $\mathbf{Q}$  are the covariance matrices of the measurement noise  $\mathbf{v}$  and process noise  $\mathbf{w}$ . Assuming uncorrelated noise  $\mathbf{R} = \text{diag}(R_1, R_2)$  and  $\mathbf{Q} = \text{diag}(Q_1, Q_2)$ .

### Rope force and force gradient estimate

The rope force is estimated from (6.2.5) using  $\hat{x}_1$  and  $\hat{x}_3$ . Differentiating (6.2.5) the gradient can be approximated as

$$\hat{F} = K(\hat{x}_2 + \hat{x}_4), \quad (6.2.18)$$

where  $\dot{b}_1$  has been omitted to produce a cleaner estimate.

### Filter tuning

Kalman filter tuning is not trivial. There is a total of six parameters that affect  $\mathbf{K}_\infty$ , which must be tuned interdependently.  $T_{b1}$  and  $T_{b2}$  are a measure of how fast the unmodelled forces vary.

$\mathbf{R}$  represents the measurement uncertainty while  $\mathbf{Q}$  represents the model uncertainty. The generator rotation and velocity are measured with high precision and accuracy, whereas the modelling error is in general large. This gives for a low  $\mathbf{R}$  and high  $\mathbf{Q}$ . However, to produce clean estimates, i.e. for feedback control, more trust must be placed on the model by lowering  $\mathbf{Q}$ .

Tuning was done by trial and error under the following initial assumptions:

$$T_{b2} \approx 5 : b_2 \text{ has a time scale approximately half a wave period.}$$

$T_{b1} \ll T_{b2}$ :  $b_1$  varies significantly faster than  $b_2$ .

$R_2 \ll R_1$ :  $R_2$  must be low such that error in the predicted acceleration leads to update of  $b_1$ . A larger  $R_1$  places less emphasis on  $y_1$  such that the estimates become more robust to errors in  $K$ .

$Q_1 \ll Q_2$ : The unmodelled forces acting on the floater are several orders of magnitude larger than the uncertainty in the PTO model.

During tuning **R** and **Q** deviated far from their physically plausible values. The final parameters are presented in Table 6.2.

**Table 6.2:** Kalman filter gains used in final implementation.

$T_1$	$T_2$	$R_1$	$R_2$	$Q_1$	$Q_2$
1	5	$10^{-7}$	$5 \times 10^{-9}$	1	100

## 6.3 Discrete time CPM

To ensure stability of different control laws the digital implementation must also be considered. This can be done by designing a DT CPM, illustrated in Figure 6.3. The pulse-transfer function  $P(z)$  represents the discrete process dynamics preceded by a digital-to-analog conversion of the control signal.  $C_1(z)$  and  $C_2(z)$  are control laws in z-domain.

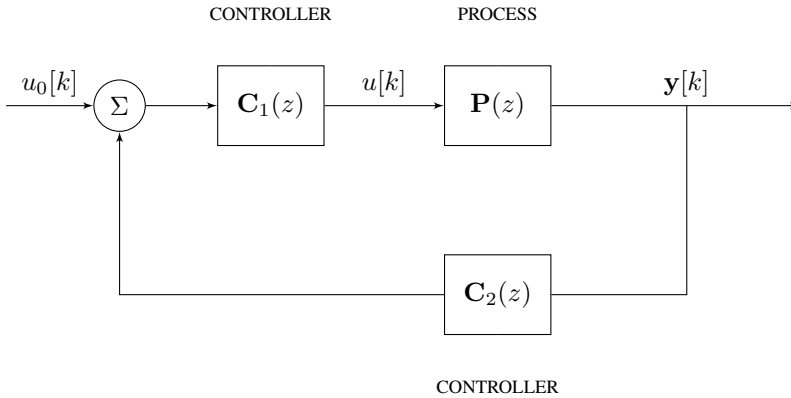


**Figure 6.3:** Discrete time control plant model.

The simplified CPM, which is controllable, is chosen as basis for the DT CPM. For further simplicity friction is omitted. This is considered conservative since damping forces are dissipative, i.e. they remove energy from the system. The Laplace transform of the simplified CPM can be written

$$sx_1(s) = x_2(s), \quad (6.3.1)$$

$$sx_2(s) = \frac{1}{M} (-Kx_1(s) + u(s) + w(s)), \quad (6.3.2)$$

where  $w(s)$  is an unknown disturbance mainly given by  $x_3$ . A block diagram of the control plant model in combined CT-DT with  $C_1(z) = 1$  and  $C_2(z) = -B$  is illustrated in Figure 6.4, where  $x_2$  has been chosen as the process output. This corresponds to the nominal control law currently used.

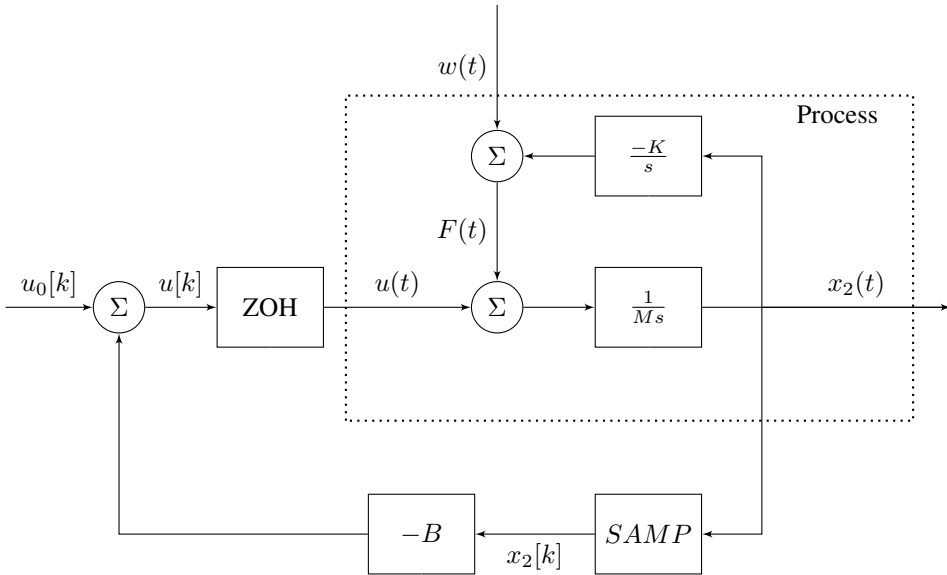


**Figure 6.4:** Control plant model with nominal control law.  $x_1$  is not shown explicitly in the diagram but is part of the inner process loop.

Now the goal is to transform the CT part of the block diagram (the *Process* rectangle) preceded by a ZOH to a DT transfer function  $P(z)$ .  $P(z)$  will then provide the input-output relation between the control input  $u[k]$  and sampled PTO velocity  $x_2[k]$ .

The process transfer function  $p(s)$  is found by inserting (6.3.1) into (6.3.2), which after some rewriting yields

$$\frac{x_2(s)}{u(s)} = p_2(s) = \frac{1}{Ms + Ks^{-1}} = \frac{1}{M} \frac{s}{s^2 + \omega_n^2}, \quad (6.3.3)$$

where we in the last step have used that  $\omega_n^2 = K/M$ . The transfer function of the ZOH is

$$g(s) = \frac{1 - e^{-sh}}{s}. \quad (6.3.4)$$

In time-domain this corresponds to holding the input value constant for a period  $h$ . The discrete transform of the cascade  $g(s)p(s)$  is (according to Table 2.1 in [10])

$$P(z) = \frac{1}{M} \frac{\omega_n^{-1} \sin(\omega_n h)(z-1)}{z^2 - 2 \cos(\omega_n h)z + 1}. \quad (6.3.5)$$

Since  $\omega_n h \approx 13/200 = 0.065$  we have that  $\sin(\omega_n h) \approx \omega_n h$  and  $\cos(\omega_n h) \approx 1$ . (6.3.5) simplifies to the much nicer

$$\begin{aligned} P(z) &= \frac{1}{M} \frac{\omega_n^{-1} \omega h(z-1)}{z^2 - 2z + 1} \\ &= \frac{h}{M} \frac{z-1}{(z-1)^2}. \end{aligned} \quad (6.3.6)$$

$P(z)$  has two real poles at  $z = 1$ , which means it is marginally stable. The marginal stability is due to the fact that the dissipative force  $Dx_2$  has been omitted. Hence we can conclude that the internal dynamics of the real process are stable, in which case  $P(z)$  can be simplified further;

$$P(z) = \frac{h/M}{z-1}, \quad (6.3.7)$$

which covers only the input-output relation. This is the pulse-transfer function that results from setting  $K = 0$  in Figure 6.4, and corresponds to an integrator with gain  $1/M$ . Since  $-Kx_1$  is a stabilizing force doing so will not hide any internal instability.

### 6.3.1 Stability of nominal control law

The closed-loop pulse-transfer function  $H(z)$  of the system shown in Figure 6.4 is found through the following steps;

$$\begin{aligned} H(z) &= \frac{x_2(z)}{u_0(z)} = \frac{P(z)}{P(z)B + 1} \\ &= \frac{\frac{h}{M(z-1)}}{\frac{hB}{M(z-1)} + 1} \\ &= \frac{h/M}{hB/M + z - 1}. \end{aligned} \quad (6.3.8)$$

The stability region is found by setting  $z = \pm 1$ . The solution  $z = 1 \rightarrow B = 0$  corresponds to the undamped domain with  $u_0 = u_{min}$  or  $u_0 = u_{max}$ . It is marginally stable, but again stability can be assumed by considering the effects of  $Dx_2$ .

Setting  $z = -1$  yields  $B = 2M/h$ . This means that the maximum damping that can safely be imposed by the control system is inversely proportional with the sampling rate. This may be a limiting factor when designing more advanced control systems that require

lower sampling rates. For the sampling rate considered in this thesis  $2M/h \approx 1200 \times 10^3$ , which is approximately 4 times the current value of  $B$ .

$B < 0$  corresponds to the negatively damped domain. The resulting system is unstable. This is of course intuitive, but can also be seen from the poles of  $H(z)$ .

## 6.4 Reference model

In steep waves with large accelerations the damped domain may last as short as 0.5 seconds. This excites the PTO dynamics causing the undesirable transient response. A simple way to avoid sudden saturation is by limiting the generator force gradient according to

$$T\dot{u} + u = u_d, \quad (6.4.1)$$

where  $u_d$  is the desired generator force given by the nominal control law. (6.4.1) ensures a feasible transition from the current state to the desired state, and is commonly referred to as a reference model. The reference model is chosen to be of first order to avoid introducing unnecessary delay.

### 6.4.1 Stability in z-domain

Discretizing (6.4.1) using Eulers forward method yields

$$u[k+1] = u[k] + \frac{h}{T}(u_d[k] - u[k]). \quad (6.4.2)$$

The result is both causal and explicit, which means it can be implemented without further modification. The discrete transfer function is found using the forward-shift operator. This yields

$$C_1(z) = \frac{u(z)}{u_d(z)} = \frac{h/T}{z - 1 + h/T}. \quad (6.4.3)$$

The open-loop dynamics, which must be considered since they correspond to the undamped domain, are

$$\begin{aligned} C_1(z)P(z) &= \frac{h/T}{z - 1 + h/T} \frac{h/M}{z - 1} \\ &= \frac{h^2/(TM)}{(z - 1 + h/T)(z - 1)}, \end{aligned} \quad (6.4.4)$$

which is stable for  $T > h/2$ . The closed-loop dynamics are

$$\begin{aligned}
H(z) &= \frac{C_1(z)P(z)}{-C_1(z)P(z)C_2(z) + 1} \\
&= \frac{\frac{h^2/(TM)}{(z-1+h/T)(z-1)}}{\frac{h^2B/(TM)}{(z-1+h/T)(z-1)} + 1} \\
&= \frac{h^2/(TM)}{h^2B/(TM) + (z-1+h/T)(z-1)} \\
&= \frac{h^2/TM}{z^2 - (2-h/T)z + h^2B/(TM) + 1 - h/T}. \tag{6.4.5}
\end{aligned}$$

Inserting  $h = 1/200$ ,  $B = 300 \times 10^3$  and  $M = 3000$  the denominator becomes

$$\text{den} = z^2 - \left(2 - \frac{1}{200T}\right)z + \frac{300}{200^2 \times 3T} + 1 - \frac{1}{200T} \tag{6.4.6}$$

Solving for  $T$  analytically is time-consuming and will not be done. Inserting  $T = 0.1$  yields

$$z^2 - 1.95z + 0.9525 = 0, \tag{6.4.7}$$

with complex roots  $z = 0.975 \pm 0.0433i$ . Since  $\sqrt{0.975^2 + 0.0433^2} = 0.976$  the system is stable, but not by much. Hence a reference model with low  $T$  should be implemented with care.

## 6.4.2 Choice of $T$

The time constant  $T$  is a tuning parameter. For a step in  $u_d$  and assuming ideal implementation it can be interpreted physically as

$$u(t+T) - u(t) = \left(1 - \frac{1}{e}\right)u_d \approx 0.632u_d, \tag{6.4.8}$$

i.e. the time it takes for the generator force to reach 63.2% of the desired value. To avoid exciting a natural frequency  $T > 2\pi/\omega_n$  must be chosen. A large  $T$  means production loss since the generator force deviates from the desired force. The step response of the system for different  $T$  are shown in Figure 6.5.  $T = 0.2$  yields 17 % overshoot, while  $T = 0.4$  yields 8 % overshoot. Both are a significant decrease from the system with no reference model.

## 6.5 Feedback control of rope force

Feedback control can be used to improve tracking of a desired rope force given by

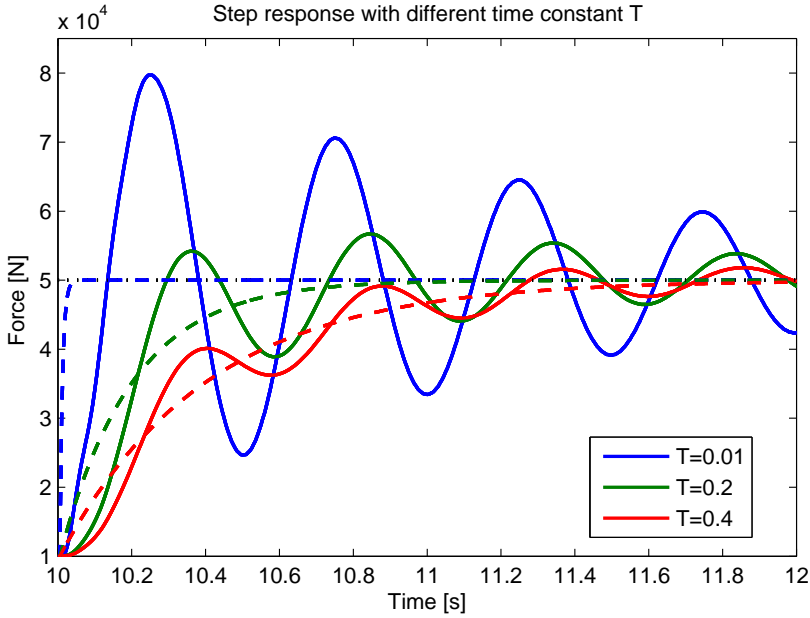


**Figure 6.5:**  $F$  (solid) and  $u$  (dashed) for a step in  $u_d$  from 10-50 kN, with first order reference model  $T\dot{u} + u = u_d$ .

$$F_d = \begin{cases} F_{min}, & 0 < x_2 \\ F_{min} - Bx_2 & -x_{2,sat} < x_2 < 0 \\ F_{max} & x_2 < -x_{2,sat}, \end{cases} \quad (6.5.1)$$

where  $x_{2,sat} = (F_{max} - F_{min})/(-Bx_2)$ . A force balance equation of the PTO dynamics can be written

$$F = u - M\dot{x}_2 - Dx_2 + f(u)\text{sign}(x_2). \quad (6.5.2)$$

Inserting  $u = F_d$ , as is the case for the current control system, yields the rope force error

$$\bar{F} = F - F_d = -M\dot{x}_2 - Dx_2 + f(u)\text{sign}(x_2). \quad (6.5.3)$$

The aim of feedback control is thus to cancel the inertial and dissipative forces of the PTO dynamics, which will inevitably lead to a reduction in stability.

### 6.5.1 Feedback using kinematic observer

A proportional feedback control law using estimates from the kinematic observer is

$$u[k] = F_d[k] - k_P(F_d[k] - \hat{F}[k]). \quad (6.5.4)$$

Inserting (6.2.1) for  $\hat{F}$  yields

$$u[k] = F_d[k] + \frac{k_P}{1 + k_P}(M\hat{a}[k] + D\hat{x}_2[k] + f(u[k])\text{sign}(\hat{x}_2[k])). \quad (6.5.5)$$

The expression can be made explicit by replacing  $f(u[k])$  with  $f(F_d[k])$ .  $M\hat{a}[k]$  corresponds to acceleration feedback, which was explored in [30] and found to be difficult to implement. The two last terms can be considered friction compensation [44], and should be straight-forward to implement.

## 6.5.2 Feedback using model based observer

The Kalman filter provides estimates of  $F$  and  $\dot{F}$  of sufficient quality for PD feedback. By also including derivative feedback both performance and robustness is increased significantly. The PD control law can be formulated as

$$u[k] = F_d[k] + K_p(F_d[k] - \hat{F}[k]) + K_d(\dot{F}_d[k] - \dot{\hat{F}}[k]). \quad (6.5.6)$$

$\dot{F}_d$  can be provided by a reference model  $\dot{F}_d = (F_r - F_d)/T$ , where  $F_r$  is now given by (6.5.1). In general  $\dot{F}_d[k]$  is unknown, in which case it is omitted.

### Error dynamics

Stability in the z-domain is shown in Appendix D assuming perfect estimates and no disturbance ( $x_3 = x_4 = 0$ ). However, this was found to be more of theoretical interest. The estimates are far from perfect, and the assumption of no disturbance does not hold. Instead robustness must be ensured through careful implementation. To gain a better understanding of how PD feedback affects the system the error dynamics will be derived in continuous time. Neglecting friction the force balance equation of the PTO can be written

$$M\ddot{x}_1 + K(x_1 + x_3) = u. \quad (6.5.7)$$

For simplicity we assume that  $F_d$  and  $\dot{F}_d$  are known and independent of  $x_2$ . For the special case of  $x_3 = \dot{x}_3 = 0$  the rope force becomes  $F = Kx_1$ . It follows that  $F_d = Kx_{1,d}$ . (6.5.6) can now be written as

$$u = Kx_{1,d} + K_p(Kx_{1,d} - Kx_1) + K_dK(\dot{x}_{1,d} - \dot{x}_1). \quad (6.5.8)$$

Inserting (6.5.8) into (6.5.7) we obtain the stable error dynamics

$$\frac{M}{1+K_p}\ddot{x}_1 + \frac{K_d K}{1+K_p}\dot{x}_1 + K\bar{x}_1 = 0, \quad (6.5.9)$$

from which it is clear that the proportional term removes mass from the system. The natural frequency of the closed-loop system becomes

$$\omega_{nPD} = \sqrt{\frac{K(1+K_p)}{M}} = \omega_n \sqrt{1+K_p}. \quad (6.5.10)$$

### Choice of $K_p$ and $K_d$

A natural upper bound is  $K_p = 1$ , which compensates  $\bar{F}$  exactly.  $K_d$  can be found from

$$\begin{aligned} K_d &= \frac{1+K_p}{K} 2\zeta \sqrt{\frac{MK}{1+K_p}} \\ &= 2\zeta(1+K_p)^{1/2} \omega_n^{-1}, \end{aligned} \quad (6.5.11)$$

by specifying the relative damping ratio  $\zeta$ .  $K_p = 1$  and  $\zeta = 1$  yields  $K_d \approx 0.21$ .

## 6.6 Hysteretic controller

The Kalman filter separates the wave-frequency floater motion from the high-frequency rope motion. This enables control strategies that require knowledge of the phase. One such strategy will be explored. The strategy is inspired by the "bang-bang" control scheme proposed by Hoskins and Nichols in [24]<sup>1</sup>, and modified for use on Lifesaver.

For resistive loading in combination with a reference model  $B$  and  $T$  must be tuned such that the performance is robust for the steepest waves. For less steep waves this limits the power output unnecessarily.

Instead of following the nominal control law from  $u_{min}$  to  $u_{max}$  it may be more efficient to bring the rope force to its mechanical limit in a controlled manner independent of wave steepness. The following control algorithm, illustrated in Figure 6.6, is proposed in combination with a reference model:

**Initial phase:** When at wave trough  $u_d = u_{max}$ .

**Damped phase:** After  $t_{delay}$  seconds switch to  $u_d = u_{min} - Bx_2$ .

**Down phase:** When wave crest is reached  $u_d = u_{min}$  until wave trough.

The wave crest and wave troughs are identified from the sign of  $x_4$ . A reference model ensures smooth transition from  $u$  to  $u_d$ . The control algorithm brings  $u$  to  $u_{max}$  also for waves that normally would not saturate. This means it is not suited for low sea states.

<sup>1</sup>The controller was discussed in Section 2.2.1

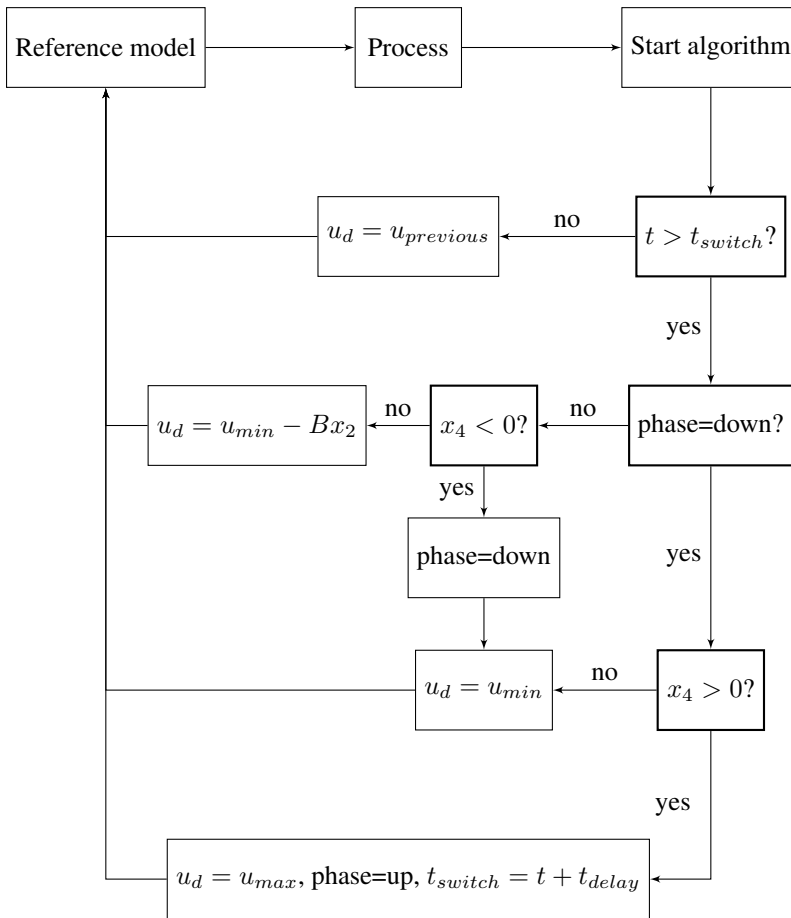


**Figure 6.6:** Algorithm for hysteretic controller. Logic operations are marked by bold rectangles. The rest are declarations.

## 6.7 Real-time optimization

Let  $B^*$  denote the value of  $B$  that maximizes power output.  $B^*$  is unknown and time-varying. Extremum seeking can be used to find  $B^*$  without requiring prior knowledge of the sea state or process dynamics. The method does not require a model of the plant, an important distinction from many other adaptive control methods [9]. This makes it suitable for complex processes such as the one at hand.

In very general terms, the method finds the extreme value (minima or maxima) of a performance function by introducing small perturbations in the control settings and measuring the change in output. The algorithm is, in fact, rather intuitive. If the performance increases the control parameter changes in the direction of the perturbation.

Stability of extremum seeking for general nonlinear dynamic systems has been proven by Krstic and Wang [27]. There exists several variations of extremum seeking. The method

implemented for use in this paper, illustrated in Figure 6.7, is described below.

**Performance function:** The process output  $J$  must be convex in the input parameter  $B$  such that an extremum exists [22]. To maximize the average power output a natural choice for  $J$  is simply the low-pass filtered electrical power. The filter  $F(s)$  must filter out the power fluctuations due to variations in the incoming waves. This means that the time scale of the filter should span several waves. A second order lowpass filter,

$$F(s) = \frac{1}{T_F^2 s^2 + 2T_F s + 1} \quad (6.7.1)$$

with  $T_F = 60$  was used in simulations.

**Perturbation signal:** A perturbation is applied to  $B$  to get an implicit estimate of the gradient of  $J$ . The perturbation can be periodic or stochastic, as long as it has zero mean to avoid bias. The perturbation must be large enough to produce a measurable change in  $J$ , while the frequency must be chosen lower than the process dynamics, which are given by  $F(s)$ . A sinusoidal perturbation,

$$B(t) = B_0(t) + a \sin(\omega t), \quad (6.7.2)$$

with  $\omega = 2\pi/180$  and  $a = 5 \times 10^3$  was used. Different values for  $B_0$  were used.

**High-pass filter:** The gradient of  $J$  is found by removing the stationary part with a high pass filter

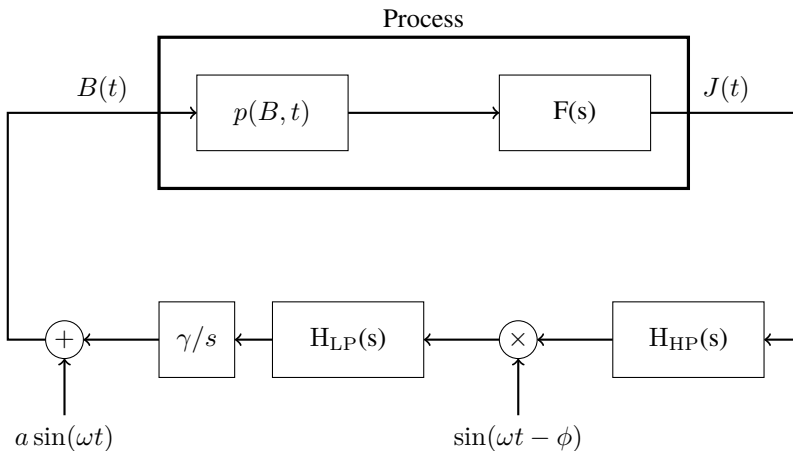


**Figure 6.7:** Extremum seeking scheme used on Lifesaver to drive the performance function  $J(t)$  towards its maximum.  $p(B, t)$  denotes the unknown process dynamics.

$$H_{HP}(s) = \frac{T_{HP}s}{T_{HP}s + 1}. \quad (6.7.3)$$

Variations in  $J$  due to the perturbation signal must be allowed pass. This means  $T_{HP} > \pi\omega$  must be chosen.  $T_{HP} = 160$  was used.

**Demodulation signal:** The variations in  $J$  are multiplied with  $\sin(\omega t - \phi)$  to drive  $B$  towards  $B^*$ .  $\phi$  is chosen such that the demodulation signal is in phase with variations in  $J$  due to perturbations in  $B$ . The delay was found experimentally to be approximately 20 seconds, in which case  $\phi = 20\omega$ .

**Lowpass filter:** The lowpass filter,

$$H_{LP}(s) = \frac{1}{T_{LP}s + 1}, \quad (6.7.4)$$

is not strictly necessary, but serves to remove wave-frequency oscillations in  $J$  without introducing additional phase lag before the demodulation signal. The oscillations occur due to the high peak-to-average power ratio during a wave cycle.

**Integrator:** To find the positive gradient  $\gamma$  must be positive. To avoid fluctuations in  $B_0$  the short term variations must be dominated by the perturbation signal. This means that  $\gamma$  must be chosen sufficiently low such that the integrator works at the slowest time scale.  $\gamma$  was found by trial and error. Since the average electric power varies significantly with wave height and period a single value of  $\gamma$  that works well for all sea states was not found. This may be overcome by choosing a performance function that is relatively independent of incoming wave power, e.g. the average electric power divided by the estimated incoming wave power. This is similar to what was done by Hals et al in [22].

**Table 6.3:** Parameters used in extremum seeking.

$\omega$	$\mathbf{a}$	$T_F$	$T_{HP}$	$T_{LP}$	$\phi$	$\gamma$
$2\pi/180$	$5 \times 10^3$	60	160	20	$20\omega$	1

# Chapter 7

## Results and discussion

### 7.1 Observer performance

The observers were tested on real data recorded on Lifesaver. Since neither the true rope force nor true floater motion is known performance can only be evaluated qualitatively.

#### 7.1.1 Comparison of observers

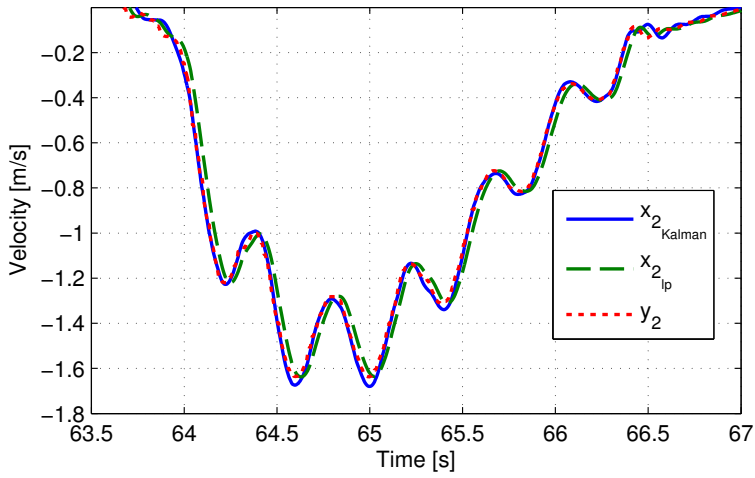
Figure 7.1 compares  $y_2$  and  $\hat{x}_2$  using the Kalman filter and the kinematic observer. Subscript  $lp$  is used for the kinematic observer.  $y_2$  can be assumed to be very close to the correct value.  $\hat{x}_{2lp}$  is phase-shifted, as one would expect.  $\hat{x}_{2Kalman}$  is in phase with  $y_2$ , but deviates at local extrema.

Figure 7.2 compares  $\hat{F}$  using the Kalman filter and the low-pass filter. The Kalman filter produces a cleaner estimate than the low-pass filter. Since  $\hat{x}_{2Kalman}$  is in phase with  $y_2$  it can be assumed that  $\hat{F}_{Kalman}$  is also in phase with  $F$ .

The kinematic observer does not provide estimates of sufficient quality for feedback control. To ensure stability of pure proportional feedback  $k_p$  must be set very low, which limits the effect. This is mainly due to the estimation delay introduced by the low-pass filter. The kinematic observer can however be used as a supervisor to ensure that the rope force stays within acceptable limits by tuning of the control parameters.  $u_{max}$ ,  $u_{min}$ ,  $B$  and  $T$  (if a reference model is used) are all control parameters that can be updated real-time to obtain desired robustness for the prevailing sea state.

#### 7.1.2 Additional Kalman filter estimates

The Kalman filter outputs two additional estimates;  $\hat{x}_4$  and  $\dot{\hat{F}}$ . Figure 7.3 compares  $\hat{x}_4$  with  $\hat{x}_2$ . Included in the plot is also the floater motion estimated by fusion of GPS and IMU (accelerometer) measurements. The accuracy of this estimate is not high enough for this to be considered the true value, but it does give an indication of the smoothness of the floater motion.



**Figure 7.1:** Estimates of  $x_2$  from Kalman filter and kinematic observer.  $y_2$  is recorded rope velocity.

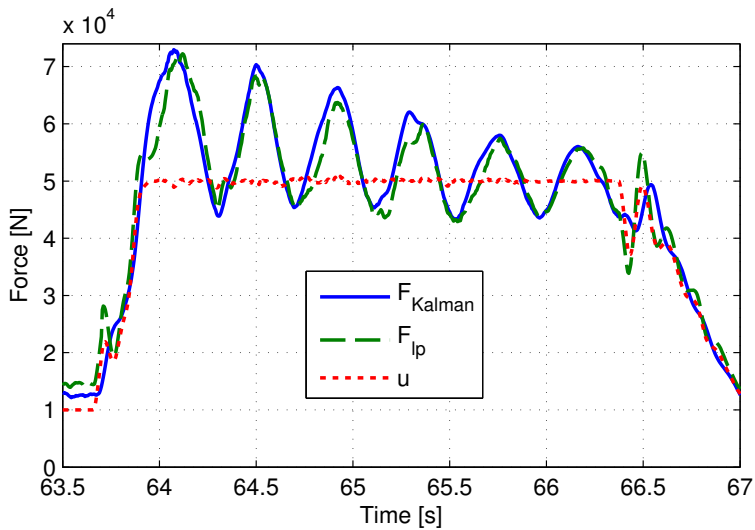


**Figure 7.2:** Rope force estimated with Kalman filter and kinematic observer.  $u$  is generator force.

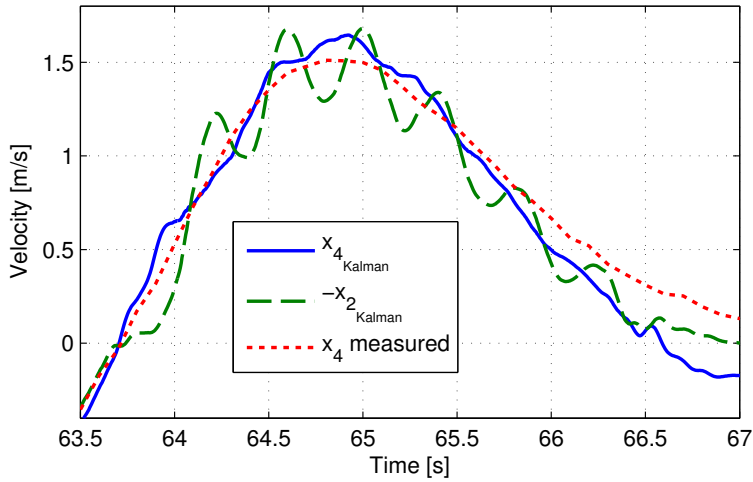


**Figure 7.3:**  $\hat{x}_4$  estimated by the Kalman filter.  $x_4$  measured is the floater motion estimated by fusion of GPS and IMU measurements.

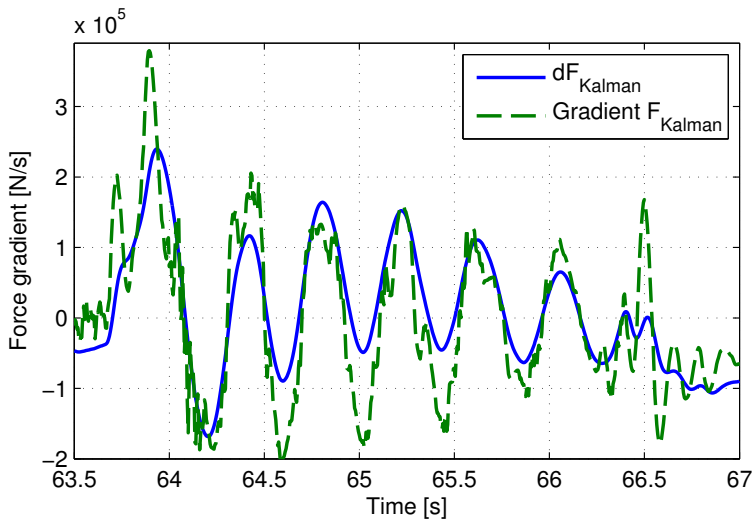


**Figure 7.4:**  $\hat{F}$  estimated by the Kalman filter ( $dF_{Kalman}$ ).  $Gradient F_{Kalman}$  is the derivative of  $\hat{F}$  calculated numerically.

$\dot{\hat{F}} = K(\hat{x}_2 + \hat{x}_4)$  is shown in figure 7.4 along with the gradient of  $\hat{F}$  (calculated numerically). The Kalman filter produces a clean estimate of  $\dot{\hat{F}}$  which is well suited for feedback control.

Notice that  $\hat{x}_4$  does not oscillate in the same way as  $\hat{x}_2$ . The Kalman filter may not produce an accurate estimate of the floater velocity, but it is able to separate wave induced motion from the motion due to elongation of the mooring line. The high-frequency velocity oscillations can be damped by tracking of  $\hat{x}_4$ , thus limiting inertial forces. In fact, by looking at the expression for  $\dot{\hat{F}}$ , this is what is done with the derivative term of the PD feedback.

## 7.2 Controller performance

Performance of five different controllers were compared for a sea state  $H_s = 2.75$  m.,  $T_p = 12$  s. The controllers and control parameters were:

**Current controller**

**Reference model:**  $T = 0.2$ .

**PD feedback:**  $k_p = 1, k_d = 0.1$ .

**PD feedback/reference model:**  $k_p = 1, k_d = 0.2, T = 0.2$ .

**Hysteretic controller:**  $t_{delay} = 1, T = 0.2$ .

$B = 250$  kNs/m,  $u_{min} = 10$  kN and  $u_{max} = 50$  kN were used for all controllers.  $k_d$  was set lower for the pure PD feedback controller since  $\dot{F}_d$  is not available without a reference model. Robustness of the hysteretic controller will be evaluated separately. Additional plots from the case study are found in Appendix A.

### 7.2.1 Robustness

Rope force for a selected wave is compared in Figure 8.1, while generator force is compared in Figure 8.2. The current control law shows significant oscillations and also has an incident of slack in the mooring line between 37 and 38 seconds. The reference model effectively reduces force peaks and should be easy to implement. It reduces oscillation amplitude but does not dampen them.

The PD feedback controller is effective in dampening oscillations, but has a larger initial overshoot than the reference model. The combination of PD feedback and reference model removes oscillations and significantly reduces the initial overshoot when saturation occurs.

The performance of PD feedback depends largely on the quality of estimates. If estimates are poor the system may become unstable. For this reason PD feedback should be implemented with care, and  $K_p$  and  $K_d$  may have to be set lower than the values used in simulation. Robustness to modelling error should be verified by altering the model parameters used in simulations.

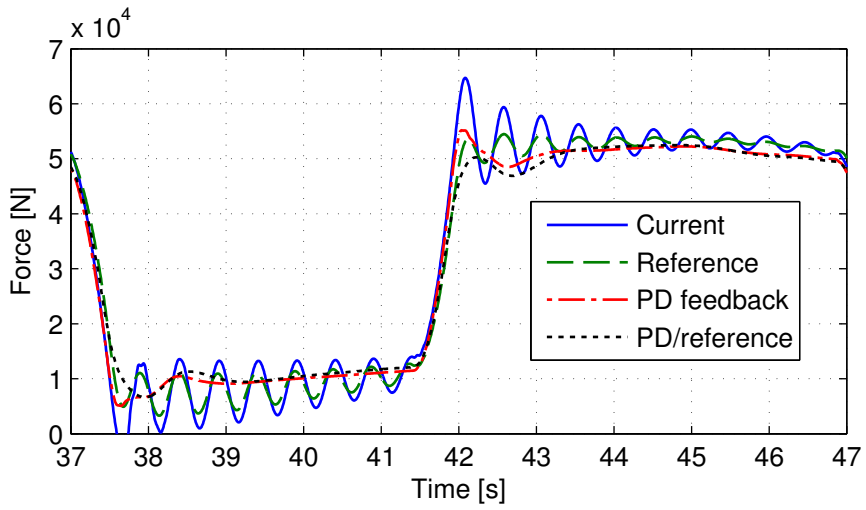


**Figure 7.5:** Rope force for a selected wave with four different controllers.

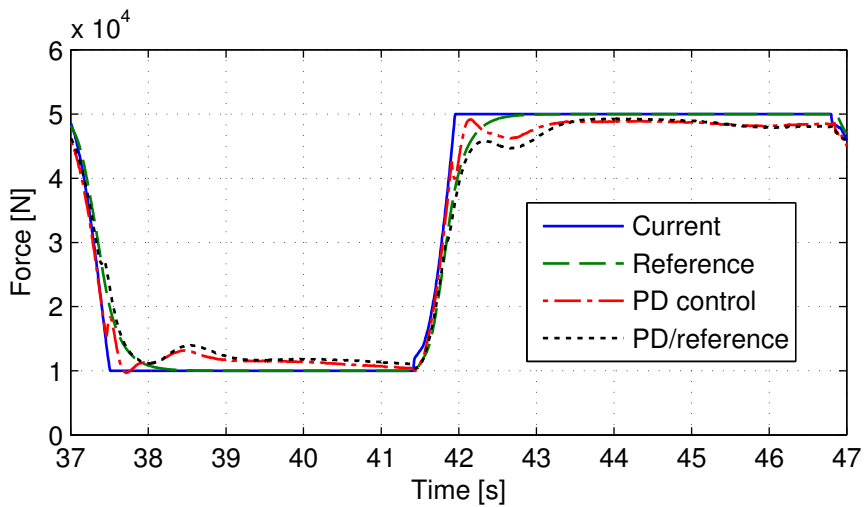


**Figure 7.6:** Generator force for a selected wave with four different controllers.

## 7.2.2 Power output

Generator power of the different controllers are shown in Figure 8.3. Average power output of the short simulation considered in the controller comparison are shown in Table 7.1<sup>1</sup>. 60 seconds is not enough for a conclusion to be drawn, but in any case direct comparison using same  $B$  and saturation limits is not relevant. The proposed controllers deviate from the nominal control law, and will inevitably lead to a reduction in power output if the same  $B$  and saturation limits are used. However, the new controllers allow for less conservative settings, which of course leads to an increase in power output.

**Table 7.1:** Average power output [kW] during 60 seconds.

Current	Reference	PD feedback	PD/reference	Hysteretic
6.73	6.54	6.14	5.92	6.14

## 7.2.3 Hysteretic controller

Performance of the hysteretic controller is shown in Figure 8.7. The algorithm appears to be robust. Some chattering of  $u_d$  occurs near wave crests (see additional plots in Appendix A), but since  $u$  is low-pass filtered through the reference model this is not considered a concern. It can also be avoided by additional hysteresis.

The peak rope forces are independent of wave steepness and depend only on the choice of  $T$ . This means the force limits can be sustained simply by deciding  $T$ . PD feedback may be used to remove the oscillations. The algorithm still needs some improvement. Currently the power output is low. This is partly due to the fact that it occasionally wrongfully identifies a wave trough, as happened at the 50 second mark in Figure 6.6. However, it does show that phase control is possible using the estimates from the Kalman filter.

## 7.3 Extremum seeking

Extremum seeking was tested for regular waves where a time-independent optimum  $J$  exists. The same  $B$  was used for all PTOs. Due to coupled dynamics multi-parameter extremum seeking [9] must be implemented in order to individually tune  $B$  for each PTO.

The algorithm had largest effect for sea states where  $u$  did not saturate. For this reason  $u_{max} = 100$  kN was used. Results for a steep wave  $H = 1.5$  m.,  $T = 6.8$  s. are shown in Figure 7.9, while results for a benign wave  $H = 1.5$  m.,  $T = 12$  s. is shown in Figure 7.10.  $B_0 = 250$  kNs/m was chosen for the first, and  $B_0 = 350$  kNs/m for the second. The adaptation rate was limited by the high peak-to-average power ratio. Convergence was not achieved during the 60 minutes of simulation after the algorithm was switched on<sup>2</sup>. However, the two tests show that the algorithm does indeed increase power output.

The adaptation rate is expected to be even lower in irregular seas. Still, it may be fast enough to track a time-varying optimum due to changes in sea state.

<sup>1</sup>The simulations were short due to time-constraints and a computationally intensive model.

<sup>2</sup>Simulation length was limited due to computational constraints.

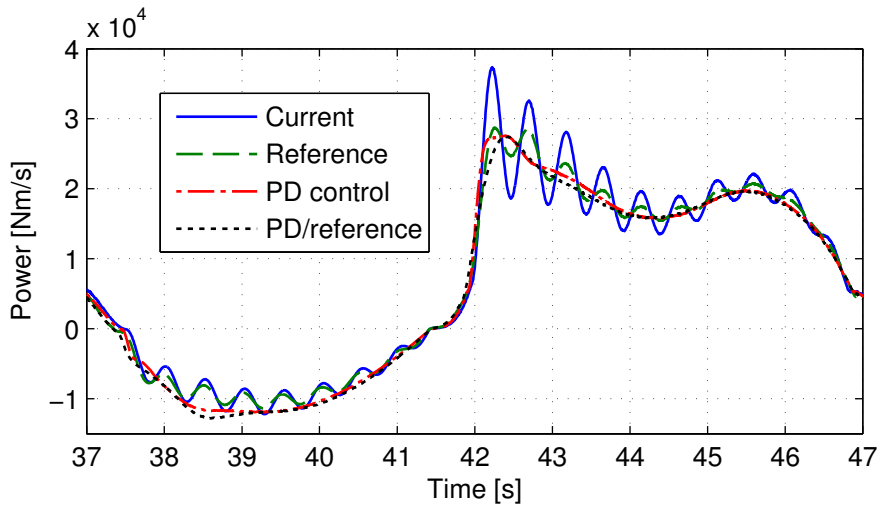


**Figure 7.7:** Generator power for a selected wave with four different controllers.

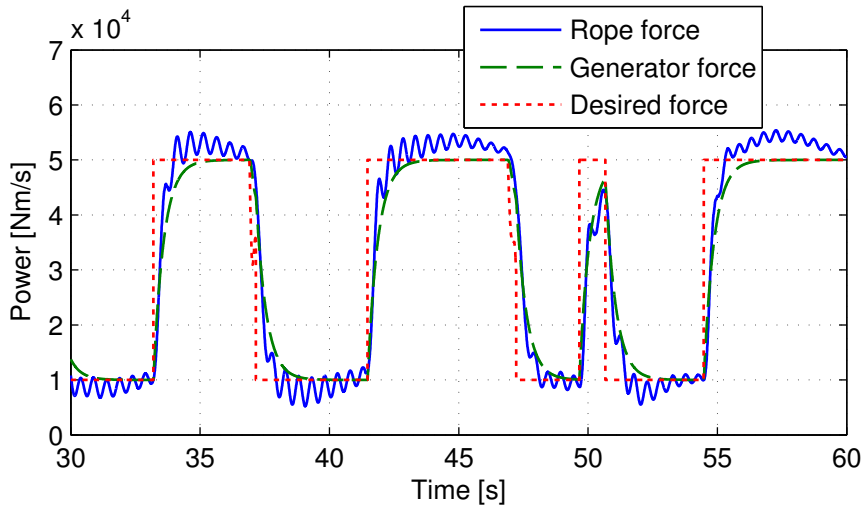


**Figure 7.8:** Rope force, generator force and desired force with the hysteretic controller.

The increase in power output is closely linked to how convex  $J$  is in  $B$ , and how much  $B^*$  depends on sea state. If  $B^*$  is relatively constant for a wide range of sea states, and  $J$  is relatively constant for a wide range of  $B$ , the benefit from extremum seeking will be low. For the steep wave (Figure 7.9) the increase in  $J$  is less than two percent. For the benign wave (Figure 7.10) the increase is almost eight percent.

Figure 7.11 is included to show how the algorithm behaves when convergence is achieved. Unfortunately there was a mistake in the generator efficiency such that  $B^*$  is lower and more defined compared to Figure 7.9.

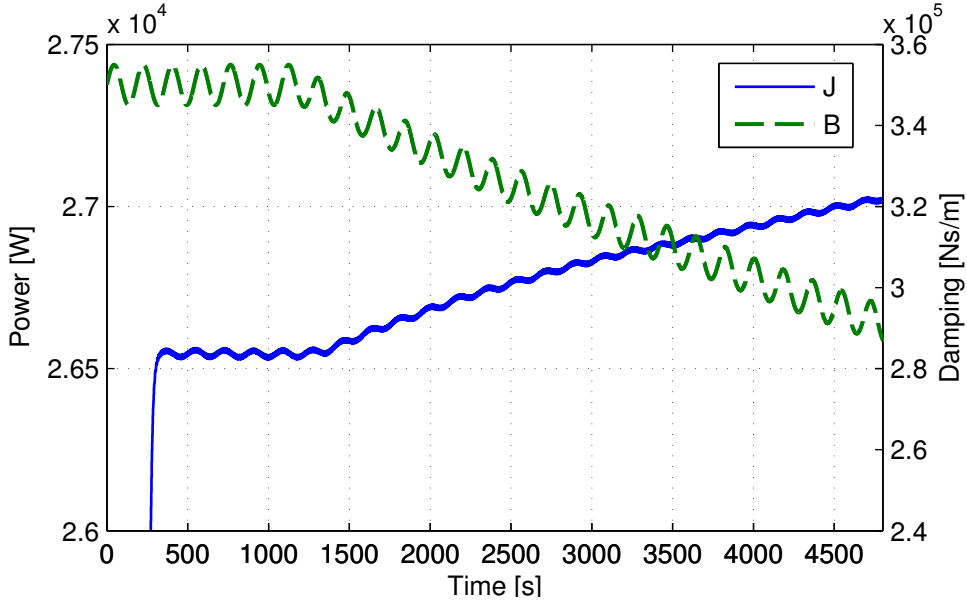


**Figure 7.9:** Normalized output function  $J$  and damping coefficient  $B$  for a regular wave  $H = 1.5$  m.,  $T = 6.8$  s. ES algorithm is switched on after 1200 seconds due to transients in  $H_{HP}$ . Wave-frequency oscillations in  $J$  have been removed for clarity in plot.

## 7.4 Recommendations for future design

Although this thesis is mainly concerned with the control system, it is clear that the unwanted behavior also can be mitigated by altering the design. The transient response of the system is given by the stiffness, inertia and damping. Below is a discussion of how these parameters affect the system, and how they can be altered.

**Stiffness:** Increasing the stiffness will move  $F_n$  away from the wave frequencies, making the system less sensitive to fast changes in the generator force. The main elasticity is found in the lower mooring rope. In the future a stiffer rope should be considered.

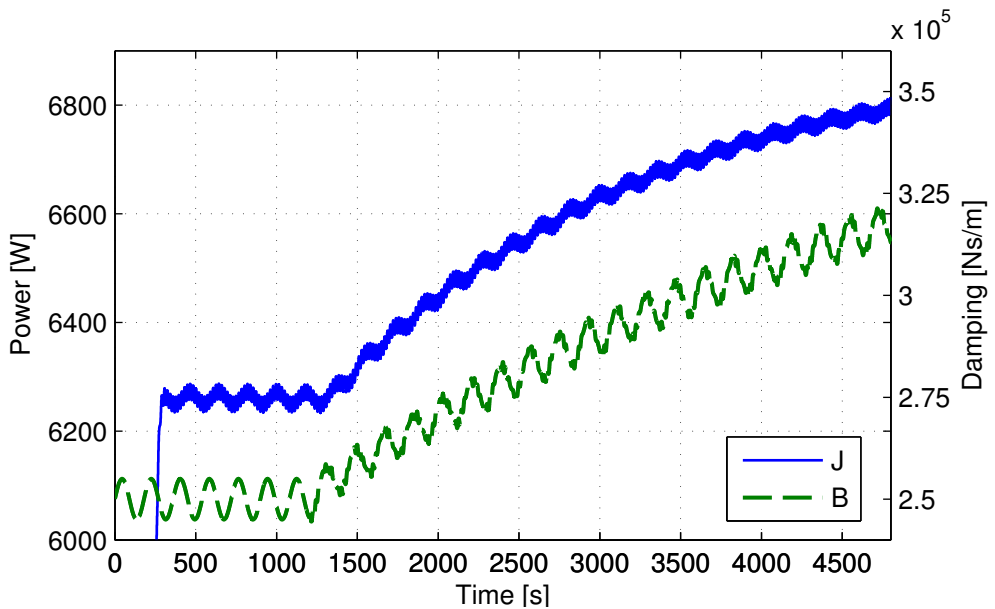


**Figure 7.10:** Output function  $J$  and damping coefficient  $B$  for a regular wave  $H = 1.5$  m.,  $T = 12$  s. ES algorithm is switched on after 1200 seconds due to transients in  $H_{HP}$ . Wave-frequency oscillations in  $J$  have been removed for clarity in plot.

**Inertia:** Lowering the drive train inertia will also reduce  $F_n$ , which will affect the system in the same way as increased stiffness. A decrease in inertia will also change the magnitude of force oscillations. However, reducing the inertia is difficult due to the large gear ratio required from winch to generator, and the required structural strength.

**Damping:** Increased damping will of course reduce the transient response. Increasing the drive train damping is not an option since it will lead to a production loss. However, damping may be included anywhere along the mooring line. The most cost-effective option is probably increasing the viscous damping of the subsea buoy, e.g. by increasing the surface roughness or surface area. This will also increase the hydrodynamic forces due to current and waves. The implications of this should be assessed beforehand.

In the future Lifesaver may be installed at deeper waters. An assessment of this is included in Appendix B.

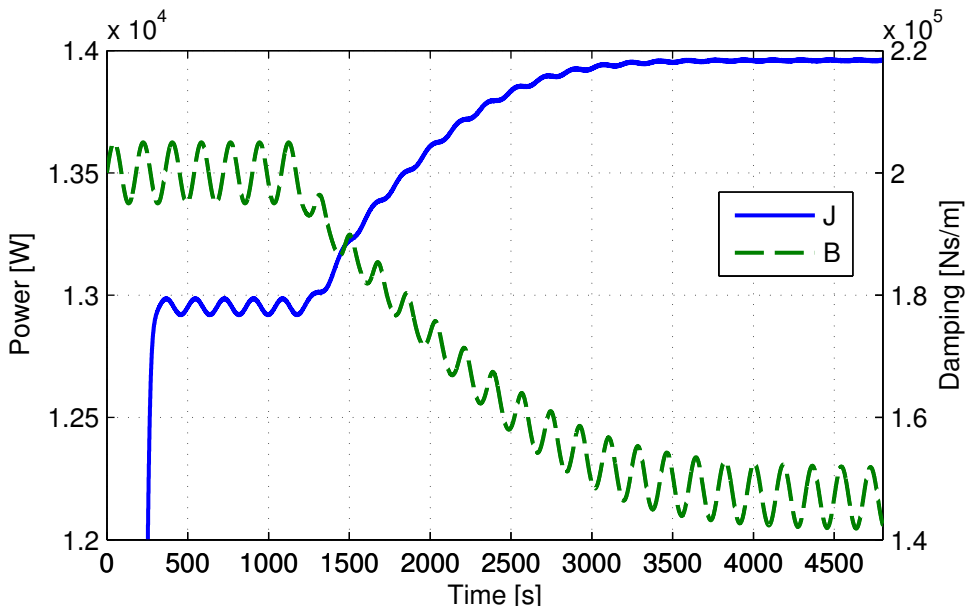


**Figure 7.11:** Output function  $J$  and damping coefficient  $B$  for a regular wave  $H = 1.5$  m.,  $T = 6.8$  s. ES algorithm is switched on after 1200 seconds due to transients in  $H_{HP}$ . Wave-frequency oscillations in  $J$  have been removed for clarity in plot. Note; wrong parameters were used for the generator efficiency.

# Chapter 8

## Conclusion and future work

### 8.1 Conclusion

**Analysis:** The force oscillations are identified as the transient response due to sudden saturation of the generator force. The main elasticity is found in the mooring line while the dominating inertia is the combined inertia of the PTO. It is possible to mitigate the oscillations by altering the design, but this may be difficult and costly.

**Observers:** In the author's opinion the biggest achievement of this thesis is the Kalman filter. It enables the use of several more advanced control algorithms, including PD feedback and phase control. The kinematic observer is easier to implement and may be used indirectly to ensure that the rope force stays within acceptable limits.

**Sampling time:** Due to the large  $B$  needed for efficient energy conversion the operating frequency of the control system must be sufficiently low.

**Reference model:** Limiting the generator force gradient is the easiest way to limit force oscillations. A first order reference model is well suited for this. The reference model does not rely on state feedback, which makes it robust and straight-forward to implement.

**Feedback control:** PD feedback in combination with a reference model removes both oscillations and the initial overshoot after saturation. Using this controller the saturation limits may be chosen close to the mechanical limit of the drive train. Since PD feedback cancels inertial and dissipative forces it must be implemented with care. Error or delay in estimations may result in unstable behaviour.

**Hysteretic control:** Phase control is an interesting topic that should be explored further. The proposed hysteretic controller behaves in a predictable and robust manner. With further improvement it may also increase power output.

**Optimization:** Real-time optimization using extremum seeking is possible, but the effect may be limited.

## 8.2 Recommendations for future work

**Model verification:** The model should be further verified by experimental testing on Lifesaver. A step response test is believed to be well suited, as the system dynamics can be identified from the transient response. Such an experiment also has high repeatability, making it more robust to external disturbances.

**Controller testing:** Robustness of the proposed controllers should be further verified by simulations.

**Increase damping of subsea buoy:** The possibilities for limiting oscillations by increasing the damping of the subsea buoy should be further explored.

**Augmented Kalman filter:** The proposed Kalman filter can be augmented with a damped harmonic oscillator that represents the wave excitation. This should improve the prediction capabilities.

**Impedance control:** Using Kalman filter estimates as input impedance control schemes may be possible to implement. Tracking the floater velocity in an inner loop and the desired force in an outer loop is a robust control procedure that may limit force oscillations.

**Multi-parameter extremum seeking:** Individual tuning of  $B$  may increase the power output. Extremum seeking can also be used to optimise the rope force in the wind-in phase.

**Phase control in low seas:** Power output can be increased by improving the oscillation phase of the floater such that the peak velocities are closer to the peak excitation forces. In low sea states this may be achieved by active tuning of  $B$ . The neural fuzzy-logic controller proposed by Schoen et al [37] may be suitable for this purpose.

# Bibliography

- [1] (2011). Renewables global status report 2011. Technical report, Renewable Energy Policy Network for the 21st Century.
- [2] (2013). IPCC Fifth Assessment report: The Physical Science Basis. Technical report, Intergovernmental Panel on Climate Change, IPCC.
- [3] (2013). MATLAB R2013b, The Mathworks Inc.
- [4] (2013). Renewables global status report 2013. Technical report, Renewable Energy Policy Network for the 21st Century.
- [5] (2013). SIMULINK R2013b, The Mathworks Inc.
- [6] (2014). IPCC Fifth Assessment report: Mitigation of Climate Change. Technical report, Intergovernmental Panel on Climate Change, IPCC.
- [7] (Visited 7/6 2014). [yearbook.enerdata.net](http://yearbook.enerdata.net).
- [8] Aamo, O. and T. Fossen (2001). Finite element modelling of moored vessels. *Mathematical and Computer Modelling of Dynamical Systems* 7(1), 47–75.
- [9] Ariyur, K. B. and M. Krstic (2003). *Real-time optimization by extremum-seeking control*. John Wiley & Sons.
- [10] Åström, K. J. and B. Wittenmark (2011). *Computer-controlled systems: theory and design*. Courier Dover Publications.
- [11] Balchen, J. G., T. Andresen, and B. A. F. A. Foss (2004). *Reguleringsteknikk*, Volume 5. Tapir.
- [12] Bjerke, I. K., E. Hjetland, G. Tjensvoll, and J. Sjolte (2011). Experiences from field testing with the bolt wave energy converter. In *European Wave and Tidal Energy Conference (EWTEC11)*, Tech. Rep.
- [13] Brown, R. G., P. Y. Hwang, et al. (1992). *Introduction to random signals and applied Kalman filtering*, Volume 3. John Wiley & Sons New York.

- [14] Chen, Q., Y. Li, Z. Yang, J. E. Seem, and J. Creaby (2010). Self-optimizing robust control of wind power generation with doubly-fed induction generator. In *ASME 2010 Dynamic Systems and Control Conference*, pp. 929–936. American Society of Mechanical Engineers.
- [15] Clément, A., P. McCullen, A. Falcão, A. Fiorentino, F. Gardner, K. Hammarlund, G. Lemonis, T. Lewis, K. Nielsen, S. Petroncini, et al. (2002). Wave energy in europe: current status and perspectives. *Renewable and sustainable energy reviews* 6(5), 405–431.
- [16] DNV-GL (2010). DNV-RP-C205.
- [17] Falnes, J. (2002). Ocean waves and oscillating systems. *Ocean Waves and Oscillating Systems*, by Johannes Falnes, pp. 286. ISBN 0521782112. Cambridge, UK: Cambridge University Press, April 2002. 1.
- [18] Faltinsen, O. M. (1990). *Sea Loads on Ships and Ocean Structures*. Norwegian University of Science and Technology: Cambridge University Press.
- [19] Fossen, T. I. (2011). *Handbook of Marine Craft Hydrodynamics and Motion Control*. Norwegian University of Science and Technology: John Wiley & Sons Inc.
- [20] Hagerman, G. (1992). Wave energy resource and economic assessment for the state of hawaii. *Prepared by SEASUN Power Systems for the Department of Business, Economic Development, and Tourism, Final Report*.
- [21] Hals, J. (2010). *Modelling and phase control of wave-energy converters*. Ph. D. thesis, Ph. D. dissertation, Department of Marine Technology, Norwegian University of Science and Technology, Trondheim.
- [22] Hals, J., J. Falnes, and T. Moan (2011). A comparison of selected strategies for adaptive control of wave energy converters. *Journal of Offshore Mechanics and Arctic Engineering* 133(3), 031101.
- [23] Haszeldine, R. S. (2009). Carbon capture and storage: how green can black be? *Science* 325(5948), 1647–1652.
- [24] Hoskin, R. and N. Nichols (1986). Optimal strategies for phase control of wave energy devices. In *Utilization of Ocean Waves—Wave to Energy Conversion*, pp. 184–199. ASCE.
- [25] J. Sjolte, I. Bjerke, G. T. and M. Molinas (2013). Summary of performance after one year of operation with the lifesaver wave energy converter system. *Submitted to the European Wave and Tidal Energy Conference (EWTEC13)*.
- [26] Khalil, H. K. (2000). *Nonlinear Systems*. Michigan State University: Pearson Education Internatiol.
- [27] Krstić, M. and H.-H. Wang (2000). Stability of extremum seeking feedback for general nonlinear dynamic systems. *Automatica* 36(4), 595–601.

- 
- [28] Leira, B. J., S. Fang, and M. Blanke (2011). Vertical position control for top tensioned riser with active heave compensator. In *ASME 2011 30th International Conference on Ocean, Offshore and Arctic Engineering*, pp. 549–558. American Society of Mechanical Engineers.
- [29] Macioce, P. (2003). Viscoelastic damping 101. *Sound and Vibration 1*.
- [30] Marley, M. H. (2014). Modelling and control of a wave energy converter.
- [31] McCormick, M. E. (2013). *Ocean wave energy conversion*. Courier Dover Publications.
- [32] Mork, G., S. Barstow, A. Kabuth, and M. T. Pontes (2010). Assessing the global wave energy potential. In *ASME 2010 29th International Conference on Ocean, Offshore and Arctic Engineering*, pp. 447–454. American Society of Mechanical Engineers.
- [33] Newman, J. N. (1977). *Marine hydrodynamics*. MIT press.
- [34] Rustad, A. M. (2007). *Modelling and control of top tensioned risers*. Ph. D. thesis, Norwegian University of Science and Technology.
- [35] Sagatun, S. I., T. I. Fossen, and K.-P. Lindegaard (2001). Inertance control of underwater installations. In *Proceedings of the 5th IFAC Conference on Control Application in Marine Systems (CAMS'01)*.
- [36] Sandvik, C. M. (2012). Wave-to-wire model of the wave energy converter bolt2: control and power extraction with an all-electric power take-off system.
- [37] Schoen, M. P., J. Hals, and T. Moan (2008). Robust control of heaving wave energy devices in irregular waves. In *Control and Automation, 2008 16th Mediterranean Conference on*, pp. 779–784. IEEE.
- [38] Schoen, M. P., J. Hals, and T. Moan (2011). Wave prediction and robust control of heaving wave energy devices for irregular waves. *Energy Conversion, IEEE Transactions on 26(2)*, 627–638.
- [39] Shields, M. A. and A. I. Payne (2014). Marine renewable energy technology and environmental interactions.
- [40] Sjolte, J., I. Bjerke, E. Hjetland, and G. Tjensvoll (2011). All-electric wave energy power take off generator optimized by high overspeed. In *Proceedings of the 9th European Wave and Tidal Energy Conference, Southampton, UK*, pp. 5–9.
- [41] Sjolte, J., C. M. Sandvik, E. Tedeschi, and M. Molinas (2013). Exploring the potential for increased production from the wave energy converter lifesaver by reactive control. *Energies 6(8)*, 3706–3733.
- [42] Sjolte, J., G. Tjensvoll, and M. Molinas (2012). All-electric wave energy converter connected in array with common dc-link for improved power quality. In *Power Electronics for Distributed Generation Systems (PEDG), 2012 3rd IEEE International Symposium on*, pp. 431–436. IEEE.

- [43] Skaare, B. and O. Egeland (2006). Parallel force/position crane control in marine operations. *Oceanic Engineering, IEEE Journal of* 31(3), 599–613.
- [44] Sørensen, A. (2011). Marine control systems-propulsion and motion control of ships and ocean structures. *lecture notes, Norwegian University of Science and Technology, Department of Marine Technology.*
- [45] Taghipour, R., T. Perez, and T. Moan (2008). Hybrid frequency–time domain models for dynamic response analysis of marine structures. *Ocean Engineering* 35(7), 685–705.
- [46] Teske, S., O. Schaefer, A. Zervos, J. Beranek, and S. Tunmore (2008). *Energy [r] evolution: a sustainable global energy outlook.*
- [47] Yang, Z., Y. Li, and J. E. Seem (2013). Maximizing wind farm energy capture via nested-loop extremum seeking control. In *ASME 2013 Dynamic Systems and Control Conference*, pp. V003T49A005–V003T49A005. American Society of Mechanical Engineers.

# Appendix A

## Comparison of controllers

Additional plots from case study with  $H_s = 2.75$  m. and  $T_p = 12$  s.

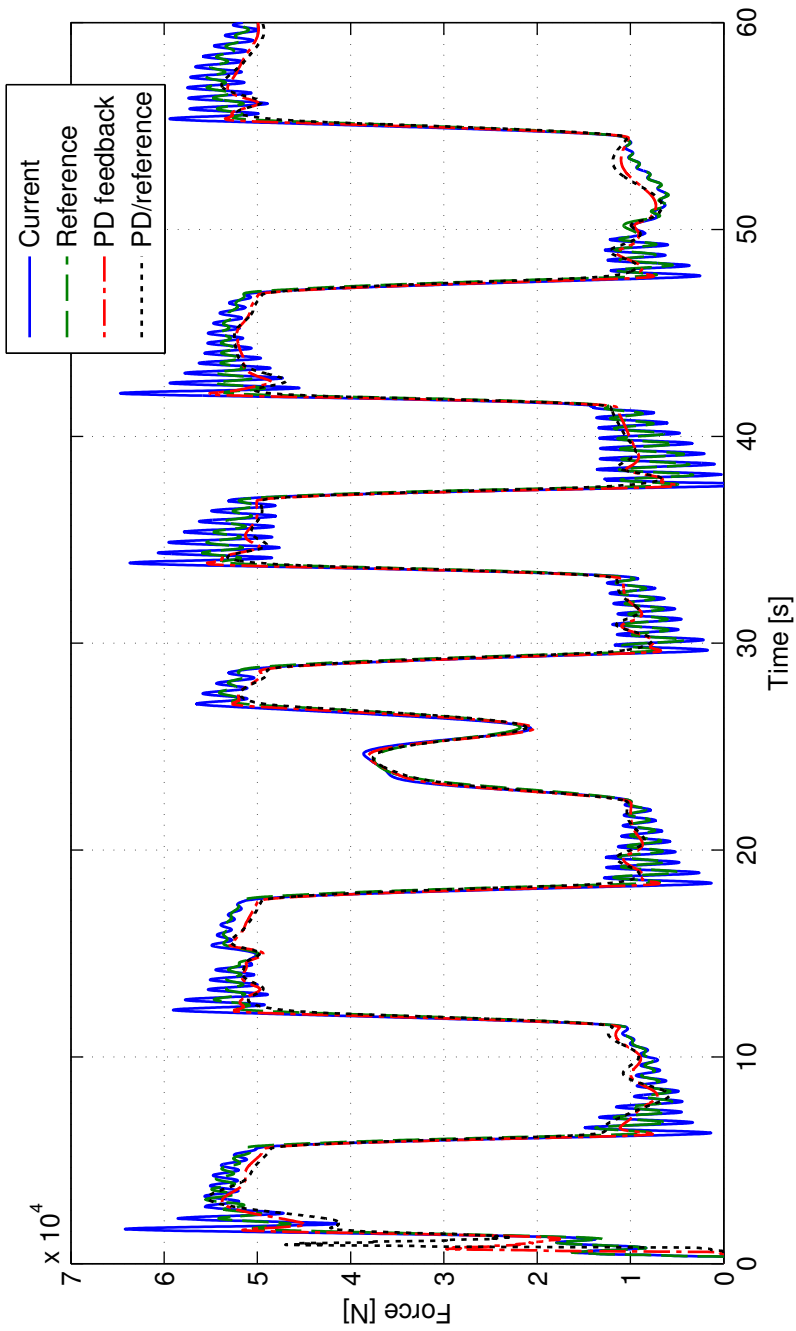


**Figure 8.1:** Rope force for with four different controllers.

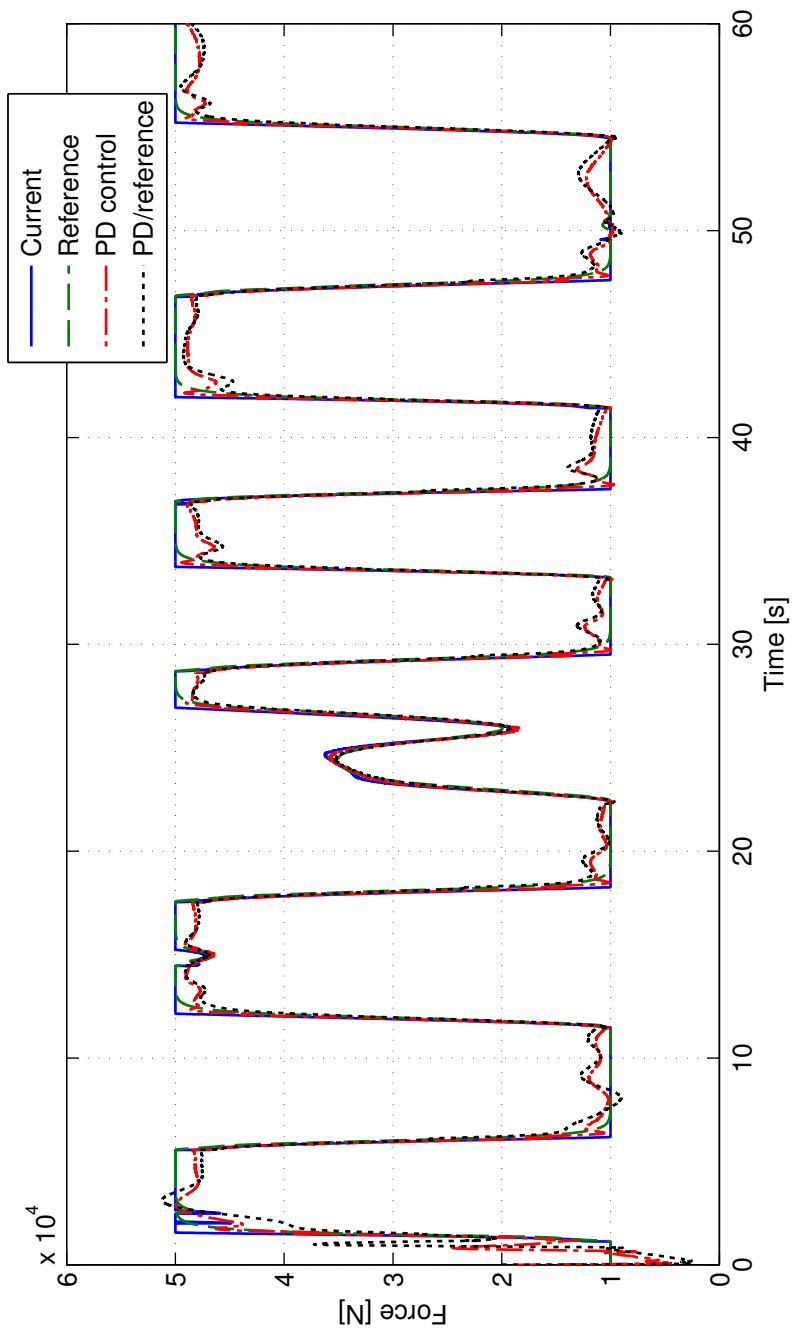
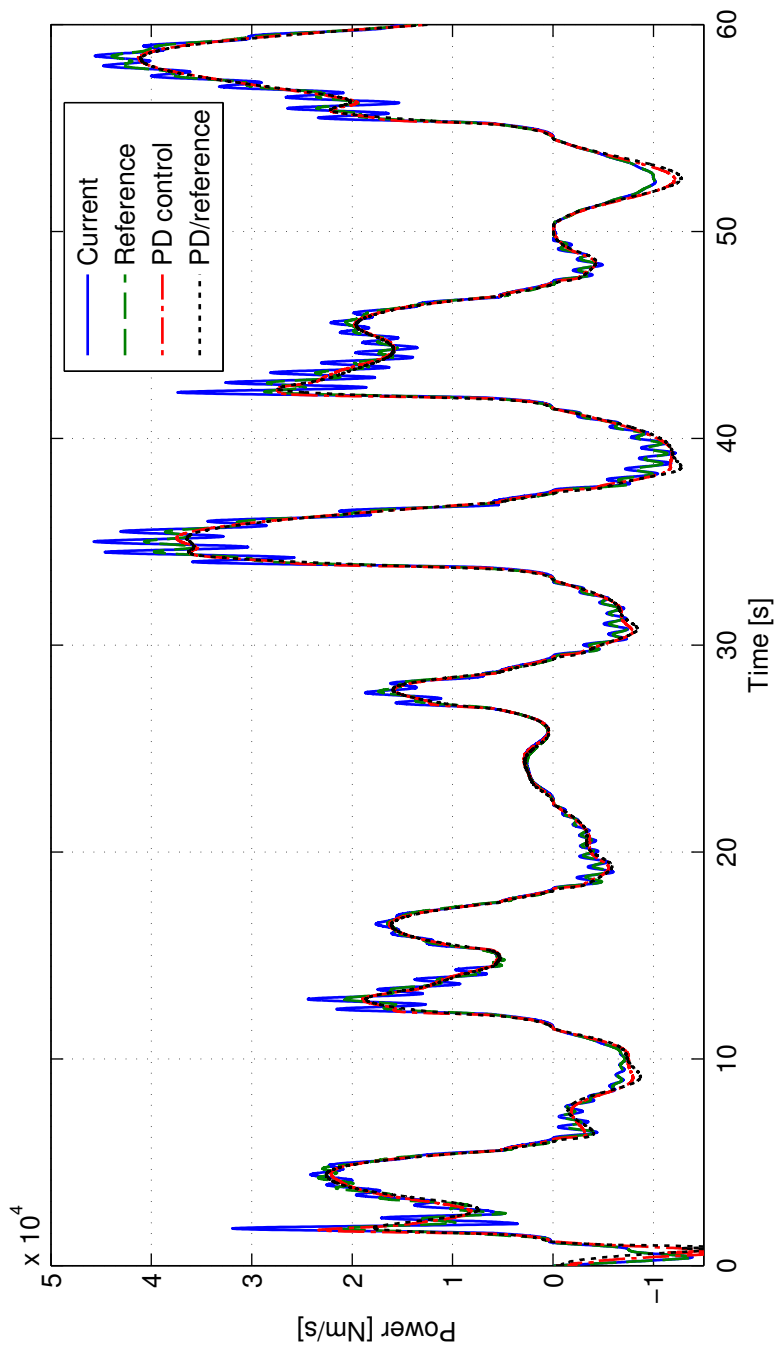
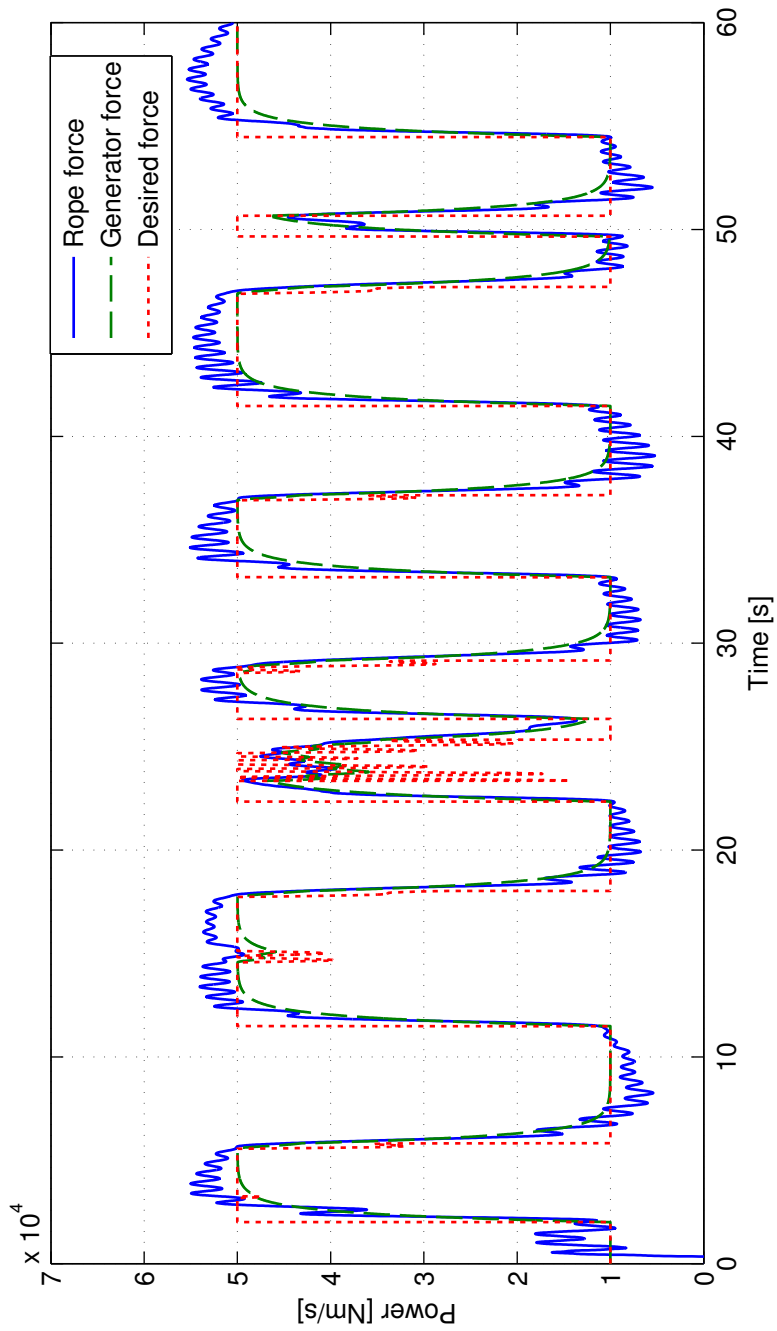


Figure 8.2: Generator force with four different controllers.



**Figure 8.3:** Generator power with four different controllers.



**Figure 8.4:** Rope force, generator force and desired force with the hysteretic controller.

# Appendix B

## Effects of increased water depth

Case study with varying values of  $T$  for the reference model and varying depth. Elastic modulus and cross-sectional area of ropes and submergence of subsea buoy is kept constant. Increasing  $T$  reduces oscillations. Increasing depth reduces stiffness which leads to reduced oscillation frequency. Reduced frequency means the PTO is less excited by fast changes in generator force. Reduced stiffness means more motion of the subsea buoy, which increases damping. For these reasons the oscillation amplitude does not differ significantly. However, elasticity of mooring leads to production loss. If Lifesaver is installed at deeper waters a thicker rope should be considered such that the resulting stiffness is similar or higher than at the current location. Note; scale of plot with 100 m. water depth differs from the others.

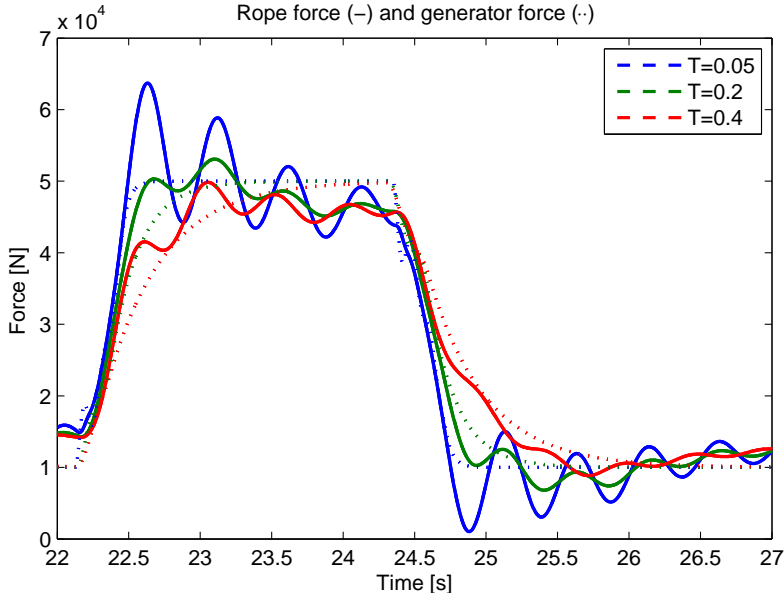


**Figure 8.5:** Rope force (solid) and generator force (dashed) with different values of  $T$  and 50 m. water depth.

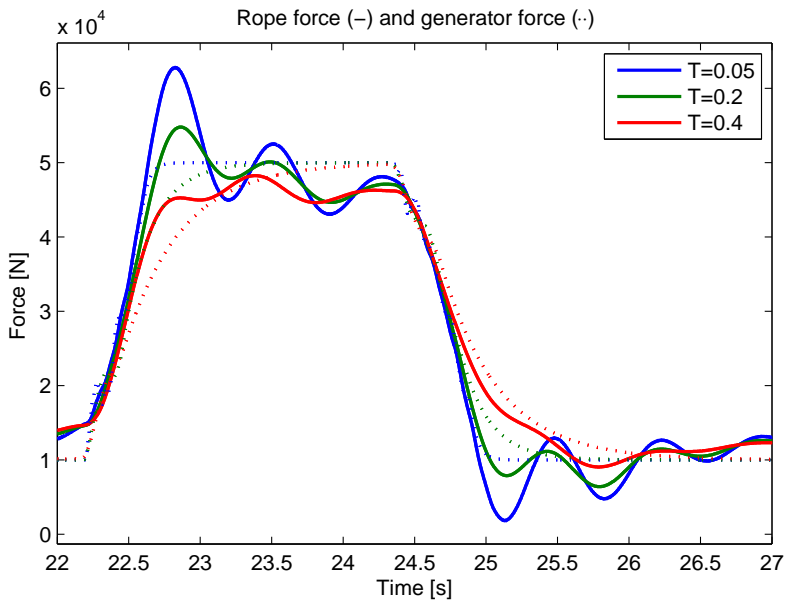


**Figure 8.6:** Rope force (solid) and generator force (dashed) with different values of  $T$  and 100 m. water depth.

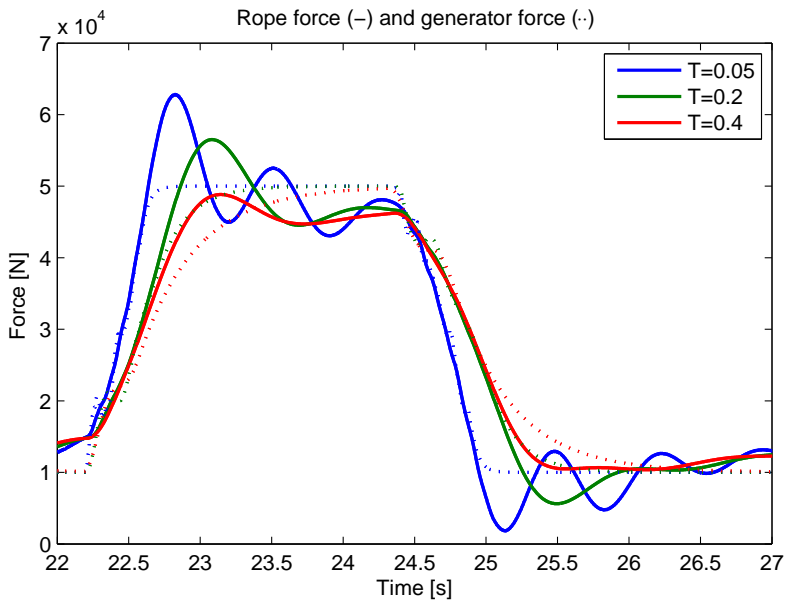


**Figure 8.7:** Rope force (solid) and generator force (dashed) with different values of  $T$  and 200 m. water depth.

# Appendix C

## Numerical model

The floater model is classified. Numerical values of the PTO and mooring line model developed in this thesis are presented below. The PTO and mooring line model can be implemented in any model that simulates the motion of  $\eta_2$ .

## Generalized PTO model

$$\mathbf{I}_q \ddot{\mathbf{q}} + \mathbf{D}_q \dot{\mathbf{q}} + \mathbf{K}_q \mathbf{q} = \boldsymbol{\tau}_q.$$

$$\mathbf{I}_q = 10^3 \times \text{diag}(0.4062, 0.4500, 2.2347)$$

$$\mathbf{D}_q = 10^6 \times \begin{bmatrix} 6.4051 & -6.4051 & 0 \\ -6.4051 & 19.668 & -13.263 \\ 0 & -13.263 & 13.263 \end{bmatrix} + 299.3 \times \begin{bmatrix} 1 & 0 & 0 \\ 0 & 1 & 0 \\ 0 & 0 & 1 \end{bmatrix}$$

$$\mathbf{K}_q = 10^8 \times \begin{bmatrix} 1.1798 & -1.1798 & 0 \\ -1.1798 & 3.6228 & -2.4430 \\ 0 & -2.4430 & 2.4430 \end{bmatrix}$$

$$\boldsymbol{\tau}_q = [-F \quad 0 \quad u_{eff}]^T$$

$$u_{eff} = u - (1001 + 0.0358u) \tanh(100q_3)$$

## Subsea buoy model

$$\dot{\boldsymbol{\eta}}_3 = \mathbf{R}(\mathbf{r}_{2/4}) \boldsymbol{\nu}_3$$

$$\mathbf{M}_{RB_3} \dot{\boldsymbol{\nu}}_3 = -\mathbf{D}_m \boldsymbol{\nu}_3 + \mathbf{F}_{m_3} + \mathbf{F}_{hyd} + \mathbf{F}_{s_3}.$$

$$\mathbf{F}_{hyd} = \mathbf{M}_A (\dot{\mathbf{v}} - \dot{\boldsymbol{\nu}}_3) + \mathbf{D}_{drag} (\mathbf{v} - \boldsymbol{\nu}_3) |\mathbf{v} - \boldsymbol{\nu}_3| + \mathbf{M}_{FK} \dot{\mathbf{v}},$$

$$\begin{aligned}\mathbf{F}_{s_3} &= \mathbf{R}^T(\mathbf{r}_{2/4})[0 \quad 2188]^T \\ \mathbf{M}_{\mathbf{RB}_3} &= \text{diag}(217, 217) \\ \mathbf{M}_{\mathbf{A}} &= \text{diag}(285.2, 238.9) \\ \mathbf{M}_{\mathbf{FK}} &= \text{diag}(440, 440) \\ \mathbf{D}_{\text{drag}} &= \text{diag}(358.75, 197.3) \\ \mathbf{D}_{\mathbf{m}} &= \text{diag}(0, 4000)\end{aligned}$$

$\mathbf{D}_{\mathbf{m}}$  represents mooring line damping acting on subsea buoy.

### Lower rope model

$$\begin{aligned}F_l &= \max\left(26.3 \times 10^6 \frac{\|\mathbf{r}_{3/4}\| - 35}{35}, 0\right) \\ \boldsymbol{\eta}_4 &= [0 \quad -50]^T\end{aligned}$$

### Production rope model

$$F = \max\left(25 \times 10^6 \frac{\|\mathbf{r}_{2/3}\| - 15 + q_1}{15 - q_1}, 0\right)$$

# Appendix D

## PD feedback in z-domain

In section 6.5 we showed that PD control, in particular the proportional term, will reduce stability. Since the DT CPM is not exact, and the feedback is on estimated rather than exact states, stable poles of the pulse-transfer function is not sufficient to indicate stability. Instead stability must be ensured by simulations and careful implementation. The rather lengthy calculations will, however, show how stability can be ensured in the z-domain for proportional-derivative control.

When  $\dot{F}_d$  is unknown the PD feedback control law is

$$u[k] = F_d[k] + K_p(F_d[k] - \hat{F}[k]) - K_d(\dot{\hat{F}}[k]).$$

Assuming perfect estimates and no disturbances ( $x_3 = x_4 = 0$ );

$$\hat{F}[k] = Kx_1[k],$$

$$\dot{\hat{F}}[k] = Kx_2[k].$$

The DT CPM developed in section 6.3 outputs  $x_2$  and can not be used for the PD feedback controller. Let  $p_{x_1}(s)$  denote the transfer function from  $u(s)$  to  $x_1(s)$ .  $p_{x_1}(s)$  can be found from  $p(s)$  (the transfer function from  $u$  to  $x_2$  of section 6.3);

$$p_{x_1}(s) = \frac{p(s)}{s} = \frac{1}{K} \frac{\omega^2}{s^2 + \omega^2} \quad (8.2.1)$$

The cascade  $g(s)p_{x_1}(s)$  is found from Table 2.1 in [10] as;

$$P_{x_1}(z) = \frac{1}{K} \frac{(1 - \cos(\omega h))(z + 1)}{z^2 - 2\cos(\omega h)z + 1}$$

The relation between  $x_2[k]$  and  $x_1[k]$  can be written

$$x_1[k] = x_1[k - 1] + \frac{h}{2}(x_2[k] + x_2[k - 1]) \quad (8.2.2)$$

where the trapezoidal (Tustin) method is used to ensure a stable mapping ( $[k]$  instead of  $[k + 1]$  on the right-hand is chosen to ensure a causal expression). Applying the backward shift operator yields

$$\begin{aligned}zx_1[k] - x_1[k] &= \frac{h}{2}(zx_2[k] + x_2[k]) \\2x_1(z - 1) &= hx_2(z + 1) \\ \frac{x_2}{x_1} &= \frac{2(z - 1)}{h(z + 1)}\end{aligned}\tag{8.2.3}$$

The control law can now be expressed solely as a function of  $x_1$ . In the damped domain we get;

$$u[k] = (1 + K_p)u_{min}[k] - \left\{ K_p K + (B(1 + k_p) + K_d K) \frac{2(z - 1)}{h(z + 1)} \right\} x_1[k] \tag{8.2.4}$$

The curly brackets is  $C_2(z)$ , i.e. the pulse-transfer function of the feedback controller. In addition we have a gain  $(1 + k_p)$  of the input. The closed-loop dynamics are

$$H(z) = \frac{x_1(z)}{u_{min}(z)} = (1 + k_p) \frac{P_{x_1}(z)}{-C_2(z)P_{x_1}(z) + 1} \tag{8.2.5}$$

The poles of  $H(z)$  are found numerically using the symbolic maths toolbox implemented in MATLAB [3]. Inserting  $h = 1/200$ ,  $\omega = 13$ ,  $K_p = 1$ ,  $K_d = 0.1$ ,  $B = 300 \times 10^3$  and  $K = 5.2 \times 10^5$  yields  $z = 0.992$  and  $z = 0.057$ . For the undamped domain  $B = 0$  the poles are  $z = 0.955 \pm 0.08$ .